2006-09

Time-frequency, bi-frequency detector analysis of noise technology radar

Heuschel, Eugene R.

Monterey, California. Naval Postgraduate School

NAVAL POSTGRADUATE SCHOOL

MONTEREY, CALIFORNIA

THESIS

TIME-FREQUENCY, BI-FREQUENCY DETECTION ANALYSIS OF NOISE TECHNOLOGY RADAR

by

Eugene R. Heuschel III

September 2006

Thesis Advisor: Phillip E. Pace

Approved for public release; distribution is unlimited

THIS PAGE INTENTIONALLY LEFT BLANK

REPORT DOCUMENTATION PAGE			Form Approved OMB No. 0704-0188
Public reporting burden for this collection of information is estimated to average 1 hour per response, including the time for reviewing instruction, searching existing data sources, gathering and maintaining the data needed, and completing and reviewing the collection of information. Send comments regarding this burden estimate or any other aspect of this collection of information, including suggestions for reducing this burden, to Washington headquarters Services, Directorate for Information Operations and Reports, 1215 Jefferson Davis Highway, Suite 1204, Arlington, VA 22202-4302, and to the Office of Management and Budget, Paperwork Reduction Project (0704-0188) Washington DC 20503.			
1. AGENCY USE ONLY ***(Leave blank)***	**2. REPORT DATE** September 2006	**3. REPORT TYPE AND DATES COVERED** Master's Thesis	
4. TITLE AND SUBTITLE: Time-Frequency, Bi-Frequency Detection Analysis of Noise Technology Radar		**5. FUNDING NUMBERS**	
6. AUTHOR(S) Eugene R. Heuschel III			
7. PERFORMING ORGANIZATION NAME(S) AND ADDRESS(ES) Center for Joint Services Electronic Warfare Naval Postgraduate School, Code EC Monterey, CA 93943-5000		**8. PERFORMING ORGANIZATION REPORT NUMBER**	
9. SPONSORING /MONITORING AGENCY NAME(S) AND ADDRESS(ES) Office of Naval Research, Code 313 Arlington, VA		**10. SPONSORING/MONITORING AGENCY REPORT NUMBER**	
11. SUPPLEMENTARY NOTES The views expressed in this thesis are those of the author and do not reflect the official policy or position of the Department of Defense or the U.S. Government.			
12a. DISTRIBUTION / AVAILABILITY STATEMENT Approved for public release; distribution is unlimited		**12b. DISTRIBUTION CODE** A	

13. ABSTRACT (maximum 200 words)

Enemy integrated air defense systems (IADS) using low probability of intercept (LPI) emitters can cause significant problems for suppression of enemy air defense (SEAD) techniques. New threat emitter configurations using low-power random noise modulation have a significant processing gain unavailable to non-cooperative intercept receivers. Consequently, the detection of these emitters can not be accomplished with conventional intercept receiver detection methods.

This thesis examines the use of time-frequency, bi-frequency signal detection techniques to identify the parameters of the four types of continuous waveform noise radar recently reported. These include: (a) random noise, (b) noise plus frequency modulation continuous wave (FMCW), (c) noise FMCW plus sine and (d) random binary phase modulation. Quadrature mirror filtering for wavelet decomposition is used to investigate the four types of noise signals in order to extract the signal parameters. The FFT accumulation method for estimating the spectral correlation density function is also used to examine the cyclostationary bi-frequency properties of the waveforms. In addition, the periodic autocorrelation function and periodic ambiguity function are studied to determine the waveform properties in the delay-Doppler offset domain. Results show that non-cooperative intercept receivers can increase their processing gain using these types of signal processing techniques providing a more efficient response time to the threat.

14. SUBJECT TERMS Random noise radar, Non-cooperative intercept, Time-frequency, Bi-frequency, Signal processing, Waveform detection, Periodic ambiguity function, Random signal radar, Low probability of intercept, QMFB, Cyclostationary, Noise technology radar,	**15. NUMBER OF PAGES** 124
	16. PRICE CODE

17. SECURITY CLASSIFICATION OF REPORT	**18. SECURITY CLASSIFICATION OF THIS PAGE**	**19. SECURITY CLASSIFICATION OF ABSTRACT**	**20. LIMITATION OF ABSTRACT**
Unclassified	Unclassified	Unclassified	UL

NSN 7540-01-280-5500

Standard Form 298 (Rev. 2-89)
Prescribed by ANSI Std. 239-18

THIS PAGE INTENTIONALLY LEFT BLANK

Approved for public release; distribution is unlimited

TIME-FREQUENCY, BI-FREQUENCY DETECTION ANALYSIS OF NOISE TECHNOLOGY RADAR

Eugene R. Heuschel III
Major, United States Air Force
B.S., Temple University, 1988
B.A., University of Maryland, 1993

Submitted in partial fulfillment of the
requirements for the degree of

MASTER OF SCIENCE IN ELECTRICAL ENGINEERING

from the

NAVAL POSTGRADUATE SCHOOL
September 2006

Author: Eugene R. Heuschel III

Approved by: Phillip E. Pace
Thesis Advisor

David C. Jenn
Second Reader

Jeffrey B. Knorr,
Chairman, Department of Electrical and Computer Engineering

THIS PAGE INTENTIONALLY LEFT BLANK

ABSTRACT

Enemy integrated air defense systems (IADS) using low probability of intercept (LPI) emitters can cause significant problems for suppression of enemy air defense (SEAD) techniques. New threat emitter configurations using low-power random noise modulation have a significant processing gain unavailable to non-cooperative intercept receivers. Consequently, the detection of these emitters can not be accomplished with conventional intercept receiver detection methods.

This thesis examines the use of time-frequency, bi-frequency signal detection techniques to identify the parameters of the four types of continuous waveform noise radar recently reported. These include: (a) random noise, (b) noise plus frequency modulation continuous wave (FMCW), (c) noise FMCW plus sine and (d) random binary phase modulation. Quadrature mirror filtering for wavelet decomposition is used to investigate the four types of noise signals in order to extract the signal parameters. The FFT accumulation method for estimating the spectral correlation density function is also used to examine the cyclostationary bi-frequency properties of the waveforms. In addition, the periodic autocorrelation function and periodic ambiguity function are studied to determine the waveform properties in the delay-Doppler offset domain. Results show that non-cooperative intercept receivers can increase their processing gain using these types of signal processing techniques providing a more efficient response time to the threat.

THIS PAGE INTENTIONALLY LEFT BLANK

TABLE OF CONTENTS

THIS PAGE INTENTIONALLY LEFT BLANK

LIST OF FIGURES

LIST OF TABLES

THIS PAGE INTENTIONALLY LEFT BLANK

ACKNOWLEDGMENTS

I would like to thank the following people who have contributed significantly to the development of this work:

Dr. Phillip E. Pace from the Naval Postgraduate School for concept development, refinement, and enlightenment of future developments in noise technology radar, specifically random noise radar (RNR).

Dr. Ram Narayanan from The Pennsylvania State University for his time in sharing the leading RNR developments and clarification on other worldwide research efforts. His energy and interest in implementation are distinguished.

Mr. Shrawan Surrender from The Pennsylvania State University for assistance and teamwork in MATLAB programming.

Dr. Ben Fitzpatrick from The Loyola-Marymount University for initial MATLAB insight and development of concepts making the code a bit more flexible.

Mrs. Melissa M. Heuschel for her selfless patience and support while this research and development effort endured, often conflicting with family events.

This work was supported by the U. S. Office of Naval Research, ONR Code-313, Arlington, VA. Much thanks to Dr. Peter Craig for his support of this effort.

THIS PAGE INTENTIONALLY LEFT BLANK

EXECUTIVE SUMMARY

Noise technology radar[1] follows a paradigm shift in the radar and electronic warfare community. The evolution is extraordinary. Characterizing that paradigm shift is to go from megawatt transmission of modulated electromagnetic energy to milliwatt "background" noise, is as significant as the development of digital receivers.

As often seen in electronic warfare, new technology spawns new countermeasures. This leapfrogging seems endless and is further accelerated by the advent of digital technology and software receivers. Several advancements have been made around the world to develop noise radar technology. For example, Mr. Sune Axelsson in Sweden has devised processing improvements to expedite signal processing times. Dr Liu Guosui in China has explored different techniques in the generation of random signal radar to enhance channel isolation, many of which he says can be expected on the battlefield. Dr. Ram Narayanan in the United States has developed a model of broadcasting simple Gaussian noise and has suggested improvements for more practical applications.

The approach of this thesis is to examine the various random noise modulations used by the LPI emitter and explore the processing tools available to the intercept receiver. Simulations in MATLAB are done to characterize the different modulation techniques and intercept receiver strategies.

This research effort looked at random noise radar (RNR) and random signal radar (RSR) techniques making up this category of Low Probability of Intercept (LPI) radar. The approach is to model the noise radar transmitter technology in MATLAB and compare the key waveform parameters, such as the periodic autocorrelation and periodic ambiguity response. The output of each

[1] Noise Technology Radar combines all of the concepts being developed using the noise as a transmission medium. The two major classes include Random Noise Radar (RNR) and Random Signal Radar (RSR).

model is the in-phase and quadrature components of the noise waveforms at the output of the non-cooperative intercept receiver's analog to digital converter. The digitized low-power random noise modulations are then processed through two intercept receiver analysis tools designed to extract the signal parameters. These analysis tools consist of time-frequency and bi-frequency transforms necessary for signal detection and parameter extraction. From this, conclusions are made regarding the capabilities of these signal processing techniques to extract the threat emitter parameters.

Most of the research in noise technology radar has been to realize a working methodology and implementing a prototype. Thus, this effort advances the state of our understanding in countermeasures against anyone using this noise technology radar. With the development of solid state microwave technology and very-large-scale-integration (VLSI), RNR concepts have come more to the forefront of field applications. Most forms of RNR use a replica of the original transmitted noise waveform to correlate the target return signal. To determine the target distance, RNR uses the power difference between the two correlated signals. Doppler measurements can also be made using this waveform.

There is a distinction between RNR and RSR. RNR transmits white Gaussian noise while RSR uses a frequency modulated continuous waveform (FMCW) to modulate a bandlimited noise source. Another form of RSR uses a FMCW modulated noise with an additional sine wave. In addition, random phase modulation of a carrier frequency is also included as an RSR technique [12].

In summary, this thesis examines the four types of noise technology radar waveforms. In addition, the use of a non-cooperative intercept receiver using time-frequency and bi-frequency signal processing techniques is examined in order to quantify the ability of the receiver to detect noise technology radar systems and extract the transmitted waveform parameters.

I. INTRODUCTION

A. DETECTABILITY OF NOISE TECHNOLOGY RADAR

Enemy integrated air defense systems (IADS) that use low probability of intercept (LPI) emitters can cause significant problems for suppression of enemy air defense (SEAD) techniques. New threat emitter configurations that use for example, low-power random noise modulation, have a significant processing gain that is unavailable to friendly intercept receivers. Consequently, the detection of these types of emitters can not be accomplished with conventional intercept receivers.

Consistent with the classic leapfrog in radar technology development, a solution is needed to detect noise technology emitters and field this technique in the shortest time possible. One approach would be through unmanned systems as they are well suited for the reconnaissance mission and live in a culture of rapid development and fielding.

The main effort of this thesis is to examine the various random noise modulations that can be used by an LPI emitter and quantify the ability to detect these modulations and extract the waveform parameters. Simulations in MATLAB are done to characterize the different noise modulation emitter designs. Simulations in MATLAB are also done to determine the performance of an intercept receiver in its ability to detect these noise signals using time-frequency and bi-frequency techniques.

B. PRINCIPAL CONTRIBUTIONS

1. Literature Search

The first step in this thesis involved a literature search to investigate the various types of low-power random noise modulation, also known as noise technology radar [1]; followed by an investigation into who was conducting this development. For example in [2], Mr. Ralf Stephan and Mr. Heinrich Loele at the Radio Frequency and Microwave Technology Institute, Technical University of

Ilmenau, Germany, explored pulse compression using random phase codes for medical applications. Another well-publicized approach comes from Mr. Sune Axelsson from Sweden in [3], who explored several variables such as high-speed analog to digital conversion techniques. He proposes using digital antenna beam forming and low-bit analog-to-digital converter (ADC) hardware to measure target approach angle. Mr. Axelsson's approach however is similar to Dr. Ram Narayanan's RNR concepts initially developed at the University of Nebraska [4]. Thus, modeling this approach was not accomplished, but a fair amount of explanation exists for Mr. Axelsson's work in Appendix A – Other Worldwide Efforts in RNR. For direction finding, Dr. Ram Narayanan uses the RNR monopulse as an effective architecture for angle estimation. This work is illustrated in [5]. Several others in Germany, Italy, and Singapore have attempted RNR generation or have used similar UWB techniques in other fields such as medicine – all with varying degrees of success. Appendix A also addresses these efforts.

The result of the literature research was a familiarization with noise technology radar and its two major groupings. The leading architectures found fell into two main groups: random signal radar (RSR) and random noise radar (RNR). Other architectures involved varying design parameters. In one of the most prominent forms of noise technology, RNR, a microwave noise source is used as the transmitted energy signal for target detection [1]. In its simplest form, the RNR receivers use a basic correlation between a delayed copy (reference) of the transmitted random white noise and the radar return. By adjusting the delay of the reference signal to identify the correlation peak, one can extract the round trip time to the target, and subsequently the target's range [5]. Another leading form of noise technology, RSR, uses a noise source that is modulated by a frequency modulated continuous waveform (FMCW). In addition, another form of RSR uses an FMCW plus sine wave. A random phase modulated carrier frequency is also considered a RSR [1].

2. Narayanan Interview

Approaching various researchers of RNR became most fruitful with an interview with Dr. Ram Narayanan from The Pennsylvania State University. Dr. Narayanan's approach to noise technology radar comes in the form of RNR, which uses a microwave noise source as a broadcast signal [6]. This approach is the simplest and most promising in terms of LPI. After the interview and extensive email traffic, the principles of RNR were defined and the specific application of Dr. Narayanan's approach was clarified [4]. This discussion centered on the further understanding of RNR principles, clarification of worldwide efforts, application to future military systems, and modeling techniques. This effort extensively helped illuminate this approach to noise technology and understand its potential. Much was gained from this experience to include several follow-on efforts planned with presentations to the space acquisitions community, use of government radar range testing facilities, future studies, and a potential small business programming effort.

3. Analysis Approach

The basic approach taken in this research was to model the transmitter techniques used in the RNR, RSR noise radar architectures found in the literature. Then from the intercept receiver's perspective, the waveform is captured and digitized at the intermediate frequency resulting in the in-phase and quadrature-phase components of the received "noise." An electronic intelligence (ELINT) receiver is then considered in order to detect and identify the signal modulation parameters, such as noise bandwidth, modulation bandwidth, modulation period and the width of the random phase subcodes. To do this, the ELINT receiver processes the intercepted signals using time-frequency and bi-frequency signal processing techniques. To illustrate the capability of these types of techniques, plots are shown illustrating the signal characteristics that are recovered. From these results, conclusions are made.

The contributions of this thesis have not been found in the open literature. The significance of this thesis is the simulation of the LPI noise technology radar

signals (using MATLAB) along with the digital receiver and processing techniques for counter-LPI. In doing so, this thesis provided the opportunity to study the various trade-offs that are involved not only in the intercept receiver design but also in the development of noise technology radar. A designer can also pursue new concepts for their particular application, whether it is civilian or military. Military designers may want to find a new approach to LPI, counter-LPI strategies. Civilian designers may be struggling with the electromagnetic compatibility tradeoffs of a crowded radio frequency spectrum [7]. Thus by this approach, both communities can benefit.

4. Modeling

The noise radar transmitter models are developed in stages starting with the basic microwave noise modulation used in RNR, then moving to the three more complex RSR techniques. To gauge the model accuracy, the interim results are plotted at significant steps in the transmitter design. Once the model worked properly, another look was made to characterize the transmitted signal using additional functions. The periodic autocorrelation (PACF) and periodic ambiguity function (PAF) were used to compare the noise radar receiver performance characteristics.

From the intercept receiver perspective, time-frequency and bi-frequency signal processing techniques were examined. Initial considerations included the Wigner-Ville distribution, Choi-Williams, cyclostationary analysis, and the use of Quadrature Mirror Filter Banks (QMFB). Ultimately, the QMFB and the cyclostationary analysis were chosen and each intercepted noise technology waveform was compared using these techniques. When analyzing each intercepted noise technology waveform, different layers of the QMFB analysis revealed various types of information about the intercepted noise waveform in time and frequency including the identification of which type of noise technology is being intercepted. The cyclostationary analysis is especially useful for non-cooperative intercept receivers and has many advantages to detect and identify LPI signals due to its interference rejection capabilities. Cyclostationary analysis

was used to examine the cycle-frequency characteristics of the noise modulation [8]. This type of analysis also reveals information such as noise bandwidth, carrier frequency, phase subcode widths in addition to the type of noise modulation being intercepted. It was found that the cyclostationary analysis gives good insight when examining the RSR type of waveforms [8].

In the refinement of the tools and the concepts, exploratory efforts were made into the effects of phase, amplitude, frequency, filtering, application of noise, effects of complex or real noise, and randomness of phase, to name a few. None of these efforts affected the primary design, but were helpful in understanding the architecture and validity of the model. Comments to these efforts are made throughout the thesis.

With consideration to all of the models, certain generalities apply. The first of which is bandwidth. Bandwidth is used to specify a range resolution [9, 4]. Thus, a respectable 0.5 m range resolution is gained from a 300 MHz wide noise bandwidth, following [4]:

$$\Delta R = \frac{c}{2B} \tag{1}$$

where c is the speed of light and B is the signal bandwidth. To be efficient, all filters used within the transmitter models were developed in the Filter Design & Analysis tool in MATLAB. To illustrate the effect of bandwidth, two noise bandwidth cases were developed. Specifically the 100 MHz wide noise, between 300-400 MHz, and the 300 MHz wide noise between 200-500 MHz were built. The second generality is to verify the ultra-wideband (UWB) requirement, which is the case in all four models. For example, if a *B* = 300 MHz signal has a bandwidth greater than 25% of the carrier frequency f_c = 350 MHz, then it is considered a UWB waveform. As another consistency throughout the models the final code output is the in-phase and quadrature-phase components from the ADC. These are pulled from the real and imaginary portions of the complex signal. This data is then passed to the time-frequency and bi-frequency tools for analysis. In the next section, the concept of LPI is discussed with RNR and RSR; a sub-category of this type of emitter.

C. LOW PROBABILITY OF INTERCEPT RADAR

1. Characteristics

A typical definition broadly describes the LPI radar as radar that uses low power, low antenna pattern sidelobes, wide bandwidth, and pulse compression to reduce the probability of being intercepted by a non-cooperative intercept receiver. Limited transmission time or frequency "camouflage" among atmospheric attenuation effects are also common techniques [8]. To achieve some of these characteristics, different techniques are used. For example, the modulated continuous wave (CW) signal has a low transmit power compared to the high peak power of digital pulse radar, yet with similar detection performance [8]. With antennas used in LPI, the antenna pattern may follow a pencil beam or fan beam with strong illumination taper to mitigate the sidelobes [8]. Finally, a wide signal bandwidth (depending on the application) is common and can be implemented in a variety of ways.

Fundamental to LPI radar is the application of pulse compression as applied to a CW waveform. General architectures used by LPI radar fall into four types: frequency modulation, phase modulation, a hybrid of both, and noise radar [8]. An example of a frequency modulation LPI waveform is the FMCW radar. The processing gain (or time bandwidth product) of the radar depends upon the selection of the modulation period t_m and the modulation bandwidth ΔF as [8]:

$$PG = t_m \Delta F \tag{2}$$

LPI radar that phase modulate a CW waveform have a different processing gain and is giving by the code period T multiplied by the inverse of the subcode period t_b as:

$$PG = T\left(\frac{1}{t_b}\right) = N_c \tag{3}$$

where N_c is the number of subcodes [8]. That is, the processing gain is directly dependent on the number of subcodes used.

For both frequency and phase modulated LPI radar, a key characteristic is the coding with a reference signal. There are many forms of LPI signaling

including FMCW, polyphase coding (including Barker polyphase codes), frequency shift keying, and hybrids of phase or frequency modulation. Applications have been developed for altimeters, landing systems, surveillance, fire control, terrain avoidance, targeting, target acquisition, or practically any other radar application. The FMCW signal is particularly effective for search-and-track radar [8]. These techniques are becoming more prevalent with digital signal processing and the development of digital radar [8]. The fourth category, noise technology radar, is the subject of this thesis.

2. Evolution of Intercept Receivers to Noise Technology

As technology develops more capabilities in the digital arena, the digital receiver will dominate future electronic warfare. The “strength” of the receiver is in the speed of the analog-to-digital converters (ADCs) with capabilities coming from the postdetection signal processing. To extract the frequency information, the spectrum analyzer processes the downconverted incoming signal. With the heterodyne approach to downconversion, the bandpass filter, local oscillator, and mixer are in series to convert the incoming signal first to an intermediate frequency (IF), then to a baseband. At baseband, the receiver is looking for the in-phase and quadrature (I/Q) components from the phase and/or frequency modulated incoming LPI signal [8]. The Doppler shift information will also be contained in the I/Q components as the frequency translation will preserve the phase differences [10]. Thus, the digital receiver generates the I/Q components from the intercepted RNR, RSR waveforms. The data is then strobed to the signal processor where time-frequency and bi-frequency routines are used to extract the waveform characteristics.

With the evolution of digital radios, radar, processing speeds, and memory size, digital radio frequency (RF) memories can be used to record emissions and sophisticated software can increase processing gain. The digital radio frequency memory (DRFM) can capture radiated emissions for processing by the intercept receiver. The DRFM is often used with a bandpass filter to focus on the expected frequency range and a local oscillator may be tuned to search within

the pass band. As the signals are digitized, parallel processed, and reconstituted, the double sideband DRFM produces the phase of the captured signal using both an in-phase and quadrature channel [11]. This is why the digital processing components (I/Q) from the captured signal are presented to the time-frequency and bi-frequency analysis tools.

D. RANDOM *SIGNAL* RADAR VS. RANDOM *NOISE* RADAR

1. Terminology

Much terminology exists as new technology emerges from the labs and into the working environment. Terms such as UWB, RNR, and RSR often get interchanged with the newcomer. To clarify, the term “random noise radar” (RNR) is defined as transmitting microwave noise that is not modulated. In contrast, “random signal radar” (RSR) uses random noise that is modulated [12]. For the immediate future and this thesis, RNR and RSR fall into the general category of noise technology radar [1].

Now that UWB radar has been developed and fielded, it is helpful to use the UWB guidelines. These guidelines are that as the fractional bandwidth of the radar is greater than 0.25 with no assignment to center frequency of the time-bandwidth product [12]. Although defined, many still combine principles of UWB in modeling of RNR [4]. As with technology, our descriptive language will emerge with time.

2. Random Noise Radar

RNR uses a microwave noise source as a transmitted energy signal for target detection and typical radar functions [1]. In its simplest form, the RNR receivers use a basic correlation between a delayed random white noise source

signal, and a radar return. By adjusting the delay of the source signal to identify the correlation peak, one can extract the round trip time to the target, and subsequent target range [5].

Characteristically, RNR has the distinct advantages of suppressing range ambiguities, excellent range resolution (wideband), low range sidelobes, and high electronic protection capabilities due to its LPI nature [1]. This is not without a price. One of the challenges RNR faces is the long processing time needed for integrating and smoothing the processed data. At this early stage, these challenges limit their use in high-speed tracking, immediate threat warning, and target detection in aircraft [5]. Even with these temporary drawbacks, the advantages of large bandwidth and increased average power characteristics, RNR can be used in surveillance, altimetry, collision avoidance, foliage penetration, and sub-surface profiling.

3. Random Signal Radar

The types of RSR that exist include: Noise FMCW radar, Sine Plus Noise FMCW radar, Noise FMCW Fuse System, Random Position Pulse Radar, Random Binary Phase-Coded (RBPC) CW Radar, and Random Pulse Radar [1]. Three of these technologies (Noise FMCW, Sine Plus Noise FMCW, and RBPC CW) were explored and modeled due to their usefulness and the availability of open source information.

In contrast to RNR, RSR uses a signal modulated by a lower frequency noise source, as a transmitted energy signal for target detection and typical radar functions [1]. RSR has its advantages with an ideal “thumbtack” periodic ambiguity function, excellent range and Doppler resolution, and high electronic protection capabilities [1].

To simulate the emitters, the paper in reference [1] was reviewed for coding each of the three models. Initially, Guosui et al composed the Noise FMCW and explored its advantages and shortcomings. Next, the team added a sine wave (single tone) to overcome the effects of “leakage”. This adds to the

isolation between the transmit and receive channels. This design is called the Sine Plus Noise FMCW. It has limitations in the ability to detect high-velocity targets and long range targets. Therefore, a new design is in order, namely the RBPC CW radar [1].

Dr. Guosui and his team introduced several types of RSR in their research. Initially, correlation RSR used the delayed source signal as a reference to correlate with the target return. When the return signal is correlated, the peak of the correlation indicates the distance to the target, the delay of the reference signal determines the distance to the target, and the Doppler filter output bins determine the target velocity. In another approach Guosui et al discuss the Spectrum Analysis RSR as another means to measure target distance after the return and source signal correlation. This technique reveals the target distance by measuring the modulation frequency from the correlation with a spectrum analyzer [8].

The RSR challenges include measuring Doppler accurately, detecting long range targets, “leakage” or isolation between transmit and receive channels, and large ambiguity sidelobes. From these limitations, different architectures are proposed and explained throughout the thesis [1]. Another challenge RSR faces is the long processing time needed for integrating and correlating the target return. This limits their use in high-speed tracking or immediate threat warning or target detection in aircraft [5].

E. OVERVIEW OF THE THESIS

This thesis is grouped into two primary sections: (1) the discussion of LPI noise technology radar and (2) the investigation of non-cooperative intercept receiver signal processing strategies to identify the noise characteristics from the intercepted waveform. Figure 1 below illustrates the flow of the thesis. The effort was first to design and build the software models for each of the four noise technology architectures. Then the periodic ambiguity analysis was performed to examine at the performance of the emitter. Following this, the signal processing

models and analysis were developed from the perspective of the non-cooperative intercept receiver. Finally, results were rolled up into the conclusion chapter.

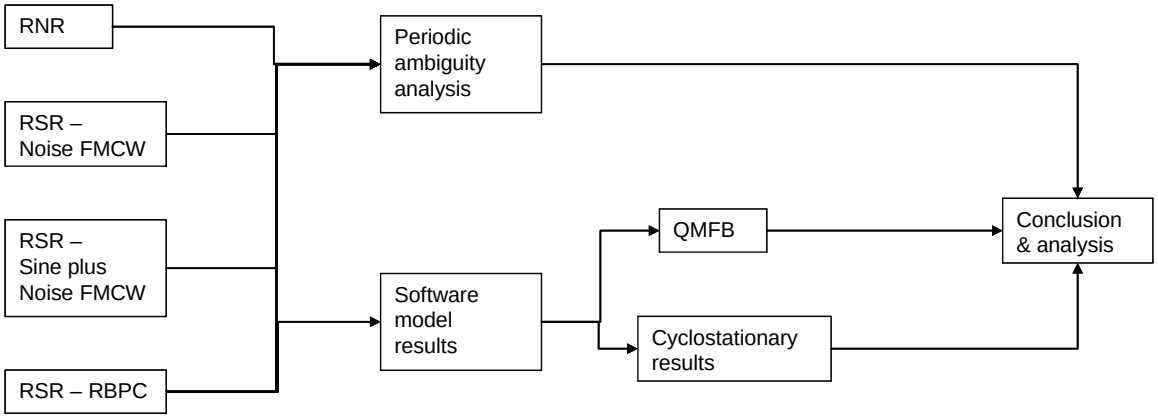

Figure 1. Thesis Flow.

Figure 2 below shows the future intercept receiver on board an unmanned aerial vehicle (UAV) intercepting the LPI emitter that uses noise technology radar. In the past, conventional receivers could not distinguish noise technology radar from the background noise. Now the received signal (Noise FMCW) appears nicely as shown on the left. To the conventional intercept receiver, the noise FMCW waveform, (or any of the other noise technology waveforms) appear as noise; as shown on the right.

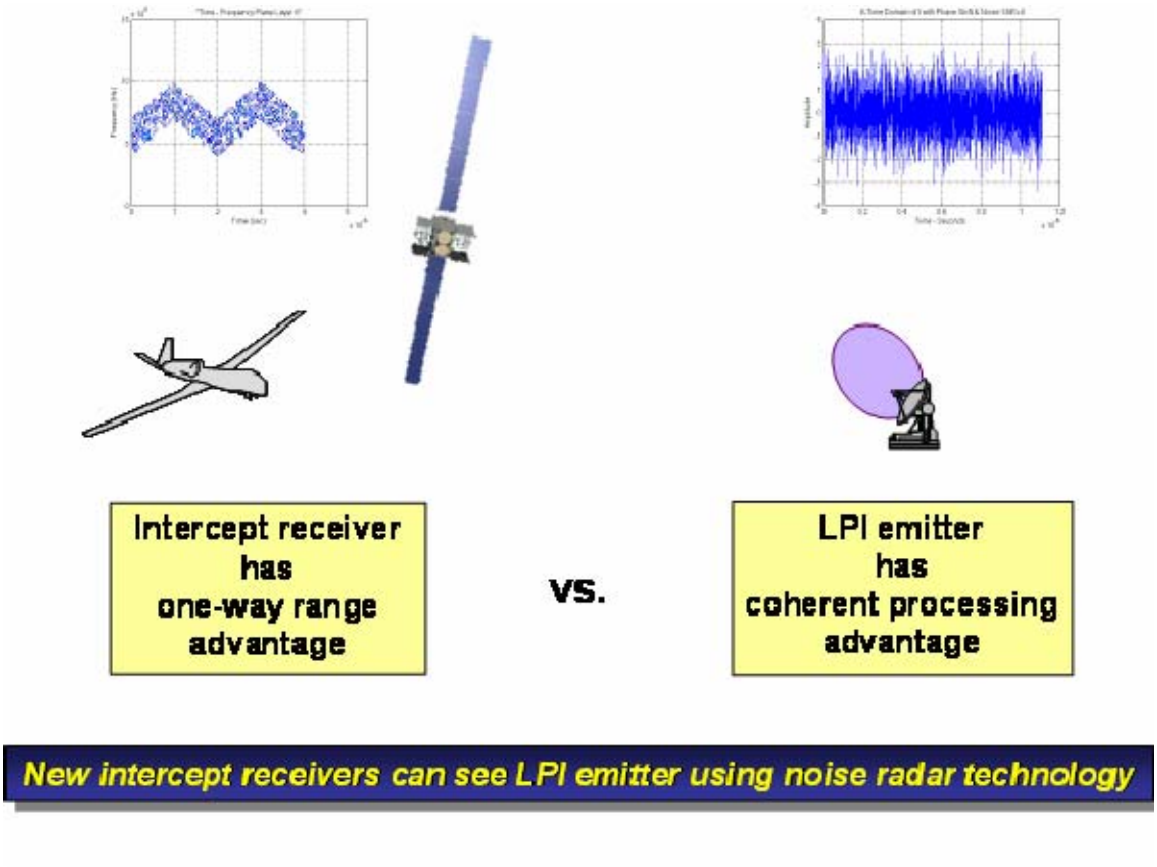

Figure 2. Intercept Receiver versus LPI Noise Emitter.

Chapter II – Noise Technology Radar Architectures contrasts the work of two leading open-source researchers. The analysis tools for the emitter consist of concepts, which apply to both architectures – the periodic ambiguity function, periodic autocorrelation function, and the power spectral density function. This is followed with an in depth discussion of each architecture. The RNR section discusses the emitter as modeled in this thesis. It discusses some of the math behind the technology, and the periodic ambiguity quick-look. The RSR section is presented in the same manner for each of three leading RSR architectures. Reasons for design decisions are explained.

Chapter III – Intercept Receiver Detection Results explains the two signal processing algorithms used for detecting the noise technology waveforms. It shows the performance results for all the noise technology radar illustrated up to this point.

Chapter IV – Conclusions brings together the surprising results in the detection of signal characteristics from LPI radar using noise technology. Also highlighted is the lack of analysis in the open source literature for intercepting noise technology radar. As history shows, as a new technology appears, new tactics also appear to counter the original advantages. This is a new technology, which is growing rapidly. The reader may entertain the application to unmanned aerial systems. To address findings outside of the scope of the thesis, yet relevant and related, two appendices highlight other worldwide efforts in noise technology and capabilities in the modeling tools. In summary, the Conclusion chapter resubmits the main arguments with supporting computational results.

THIS PAGE INTENTIONALLY LEFT BLANK

II. NOISE TECHNOLOGY RADAR ARCHITECTURES

The noise technology radar techniques and models are presented in this section. For convenience of the reader, the PACF and PAF are discussed first.

A. PERIODIC AMBIGUITY ANALYSIS

Periodic ambiguity analysis helps us understand range/velocity measurement accuracy, target resolution, and the response to clutter for a CW radar receiver. Certain periodic ambiguity measurements can be used for this analysis, namely the periodic autocorrelation function (PACF) and the periodic ambiguity function (PAF).

The PACF is helpful in identifying characteristics of a typical (periodic) CW signal. Consider for example a CW phase coded signal, the magnitude of the PACF is:

$$R(rt_b) = \frac{1}{N_c}\sum_{n=1}^{N_c} u(n)u^*(n+r) \tag{4}$$

where r is the delay, t_b is the subcode duration of the phase codes, N_c is the number of phase codes, $u^*(n+r)$ is the stored reference function, and $n = \pm 0, 1, 2, \ldots$ etc, and $u(n)$ is the received signal's complex envelope also given as

$$u(t) = u(t+nT) \tag{5}$$

with T equal to the code period $T = N_c t_b$ in seconds. In the results, the PACF is presented with the ACF for comparison.

The PAF can be used to illustrate the magnitude of a matched filter for the coherent CW signal. The PAF is also used to demonstrate the correlation of the received signal to the delayed version of the original transmitted signal [8]. For the results in this thesis, the number of delayed copies of the reference signal used in the correlation is N = 1. Increasing this number helps reduce the sidelobes that are present.

The PAF is given as:

$$\left|\chi_{NT}(\tau,\nu)\right| = \left|\frac{1}{NT}\int_{0}^{NT} u(t-\tau)u^{*}(t)e^{j2\pi\nu t}dt\right| \tag{6}$$

where τ is the offset or delay and the delay rate of change is represented by the Doppler shift ν. The PAF for N periods is related to the single-period ambiguity function by a universal relationship as:

$$\left|\chi_{NT}(\tau,\nu)\right| = \left|\chi_{T}(\tau,\nu)\left|\frac{\sin(N\pi\nu T)}{N\sin(\pi\nu T)}\right|\right| \tag{7}$$

where

$$\left|\chi_{T}(\tau,\nu)\right| = \frac{1}{T}\left|\int_{0}^{T} u(t-\tau)u^{*}(t)e^{j2\pi\nu t}dt\right| \tag{8}$$

is the single period ambiguity function. Thus the PAF has main lobes at $\nu T = 0, \pm 1, \pm 2...$ [8]. The receiver is matched to an expected delay at a certain Doppler frequency. When delay and Doppler shift are present, the receiver response is revealed in the ambiguity analysis. In the periodic ambiguity plots the emitter performance is displayed as a function of the time delay (τ) and Doppler shift (ν).

B. MODEL GENERALITIES

1. Model Outline

Since two leading theories appear in the open literature, this thesis will look at the RNR model proposed by Dr. Ram Narayanan from The Pennsylvania State University and the RSR models proposed by Dr. Liu Guosui from the Nanjing University of Sciences & Technology, China.

The beginning and end of all four software models are similar. At the beginning, the initial variables are common and identified as the common variables. At the end of each model, the plotting and saving functions are practically the same. In the middle portion of each model, the unique code to that particular design is found. Any variation to these areas will be explained in the respective section.

2. Common Variables

Starting the design was the selection of transmit frequency. For ease of design, the initial 350 MHz carrier frequency was chosen to be consistent with typical UHF search radar. At this frequency, there are very slight weather effects on the mission of long range surveillance and short range acquisition [13]. Taking another view, one can also consider the 350 MHz carrier frequency as the local oscillator (LO) or intermediate frequency (IF) signal; downconverted to 1/10th of the transmitted signal in the S band (~3.5 GHz)[2].

Although configured for 350 MHz, the models can be modified for any frequency range, including frequencies meeting the UWB definition[3]. The carrier frequency, or LO/IF signal, dictates the sampling frequency of 3 GHz to avoid aliasing from the carrier frequency (Nyquist interference). Subsequent signal pass/stop band filters were built around these parameters.

The emitter's receiver bandwidth of 300 MHz was selected to give a large bandwidth about an expected carrier frequency to capture enough of the intercepted signal and for range resolution preferences. A receiver bandwidth of 100 MHz was also run for comparison. Note, these models assume an intercept receiver has no *a priori* knowledge of the transmitted noise waveform.

The observation interval is worthy of mention here as a variable of design. The observation interval is the time interval that the intercept receiver has to look at the emitter. This duration is later used to quantify the time period to produce the number of samples for noise generation and timing. The combination of the sampling frequency and observation interval provided the number of samples for processing of the intercepted signal. Any observation interval can be used. There is no relationship between the observation interval and sampling frequency, except to determine the number of samples used, based on the equation [4]:

$$nsamples = i_o * f_s \tag{9}$$

[2] Any frequency can be chosen for IF, but typically the IF is 10% of the carrier frequency [4].

[3] UWB is defined as waveforms that have instantaneous fractional bandwidths greater than 25% with respect to the center frequency [12].

where i_o is the observation interval desired in seconds and f_s is the sampling frequency in Hz. For example, 4 μsec * 3 GHz = 12000 samples.

Another design factor chosen was the transmit noise power level of –40 dB. When higher values were chosen (e.g. 0 dB), the amplitude of the noise signal increased above the level for a normal thermal noise floor. This would defeat the advantages of LPI, thus was not deemed realistic.

After the user inputs are queried, the code produces a bandlimited white Gaussian noise using the "wgn" function in MATLAB. Selecting the noise as either real or complex was another consideration. Complex Gaussian noise was used as referenced by Axelsson's work [14]. From experimentation with the code, there were no noticeable effects from using either real or complex noise. Selection of the noise bandwidth depends on the desired range resolution. In [15], Narayanan used 1-2 GHz for penetration through the soil in mine detection [4]. To keep the examples simple, two noise bandwidths are shown in this analysis for comparison purposes: 100 MHz and 300 MHz.

Completing the processing, the final section of the model captures the I/Q components of the signal for further time-frequency processing. *These I & Q vectors must be row vectors for proper execution in MATLAB.* Additional variables are added as the models develop and will be explained in their respective sections.

3. Filter Design

Common FIR bandpass filters are built using the Filter Design & Analysis (FDA) tool in MATLAB's Signal Processing toolbox. In the form of a graphical user interface (GUI), this application creates the filter coefficients needed for signal processing. With the FDA tool, the user can specify cutoff frequencies, filter types, and frequency pass ranges, avoiding the trial and error approach using the radar code. In this thesis, the filters limit the bandwidth of the noise signal before transmission. The 100 MHz filter band passed the signal from 300-400 MHz, while the 300 MHz filter band passed the signal from 200-500 MHz. If

the bandwidth or sampling frequency is altered, the designer must modify the FIR filters used to band limit the noise. Further explanation of the FDA tool is included in Appendix B – Details of the FDA Tool.

4. Emitter Output: I and Q

Since a digital transmitted signal is modeled, the processing goal is realized with in-phase and quadrature components of the intercepted signal from the ADC in the intercept receiver. The "I" and "Q" variables are prepared in various methods explained in each section.

At the end of the computational run, the user is queried to save the I/Q data in an intuitive file structure. After being rounded to the nearest integer, the parameters are saved in the filename and saved in the working directory with a positive input from the user. The data is then ready for analysis and plotting with the time-frequency and bi-frequency tools for potential signal characteristic recovery.

5. PACF, PAF, and PSD Plotting Overview

The left hand axis ($\nu * N_c$) represents the normalized Doppler offset, while the right hand axis τ / t_b represents the normalized delay offset. The z axis $\left|\chi(\tau,\nu)\right|$ represents the magnitude of the receiver's periodic ambiguity function. For the RSR random binary phase coded waveform, the plot axes are a function of the code period (T), the number of phase codes (N_c), and the number of code periods used by the correlation receiver (N). The PAF main lobe is observed on the delay axis at every $N_c * bsc$, where N_c is the number of phase codes and bsc is the number of samples per subcode width [8]. For the RNR the code period is the observation interval (the noise is continuously transmitted) and the code repeats on the delay axis at integer multiples of the number of samples in the observation interval. For the two remaining RSR waveforms (noise FMCW and noise FMCW plus sine) the triangular code period is $2t_m$ and the code

repeats every $2 f_s t_m$ samples on the delay axis. This data was generated using the "ambfn7.m" file and the "paf_preprocess.m" preprocessing file provided in the LPIToolbox in [8]. In the pre-processing GUI, several parameters need to be set and are explained in the respective analysis section.

6. Frequency Modulated Continuous Wave Generation

Guosui et al [1] make reference to the linear frequency modulation in their design. For noise FMCW and noise FMCW plus sine RSR models, the generation of the FMCW signal is the same. Initially two extra variables are added for the linear frequency modulating ramp functions. These variables are modulation bandwidth ΔF and the modulation period t_m. To realize this, the FMCW signal is first generated, followed by the multiplication with the noise waveform. This is represented partially in the MATLAB code as:

```
% TRIANGULAR FMCW GENERATION
% sI1 is the In-Phase (I) transmitted signal for the up-ramp (without noise)
% sI2 is the In-Phase (I) transmitted signal for the down-ramp (without noise)
  sI1 = A*cos(2*pi*((f-deltaF/2).*t + deltaF/(2*tm).*t.^2));
  sI2 = A*cos(2*pi*((f+deltaF/2).*t - deltaF/(2*tm).*t.^2));
```

The quadrature components of the triangular waveform (FMCW) are prepared in a similar manner, simply shifted 90 degrees, by use of the sine function. After the two I & Q components are combined, noise modulation (multiplication) is realized with multiplying by the complex white Gaussian noise. Finally, the real and imaginary parts can be extracted for time-frequency processing.

C. RANDOM NOISE RADAR

1. Theory of Operation

The primary function of the Narayanan RNR model is to detect the target range and Doppler frequency. In this approach [15], Mr. Muhammad Dawood and Dr. Ram Narayanan generated RNR with a noise source with a Gaussian amplitude distribution and average power output of 0 dBm (1 mW) in the 1-2 GHz

range. The major advantage of this technique is to capture the Doppler frequency of a moving target, through the use of heterodyne correlation techniques [14].

Referencing Figure 3 below, the transmitted noise is between 1 to 2 GHz. The first bandpass filter (BPF) is centered at 1.5 GHz with a bandwidth of 1 GHz. The power divider (PD1) splits the signal into two parts; one part to be transmitted after a 100W amplifier while the second part is split off for later correlation with the receive signal, via a fixed delay line (DL1) and the variable delay line (DL2). The variable delay line can be programmed for delays from 0 to 19.968 μs in 0.156 ns steps. To provide a reference signal for later correlation, MXR1 up-converts the lower sideband of a 160 MHz phase-locked oscillator and combines this with the reference source noise signal. An oscillator of 160 MHz is a common and inexpensive component readily available commercially [14]. MXR2 combines the 1-2 GHz return signal with the delayed replica of the source signal and the resultant signal is now centered on and filtered around 160 MHz at the IF BPF. Continuing on, the received signal of interest continues down the PD3 (power divider 3), which splits into a logarithmic amplifier to capture the amplitude, and an I/Q detector to capture the in-phase and quadrature components for time-frequency and bi-frequency analysis described later.

Worthy of mention in Figure 3 below are a few points on the Doppler resolution. The Doppler return from the slow-moving target will show up at roughly 50 Hz about the carrier frequency, when using 1.5 GHz. Seeking to isolate and keep this Doppler information, the model uses a low-pass filter at, e.g., 100 MHz. This filtering also dispenses of undesirable harmonics of the 160 MHz LO frequency [4]. This filtering results in focusing on the Doppler information using the RNR.

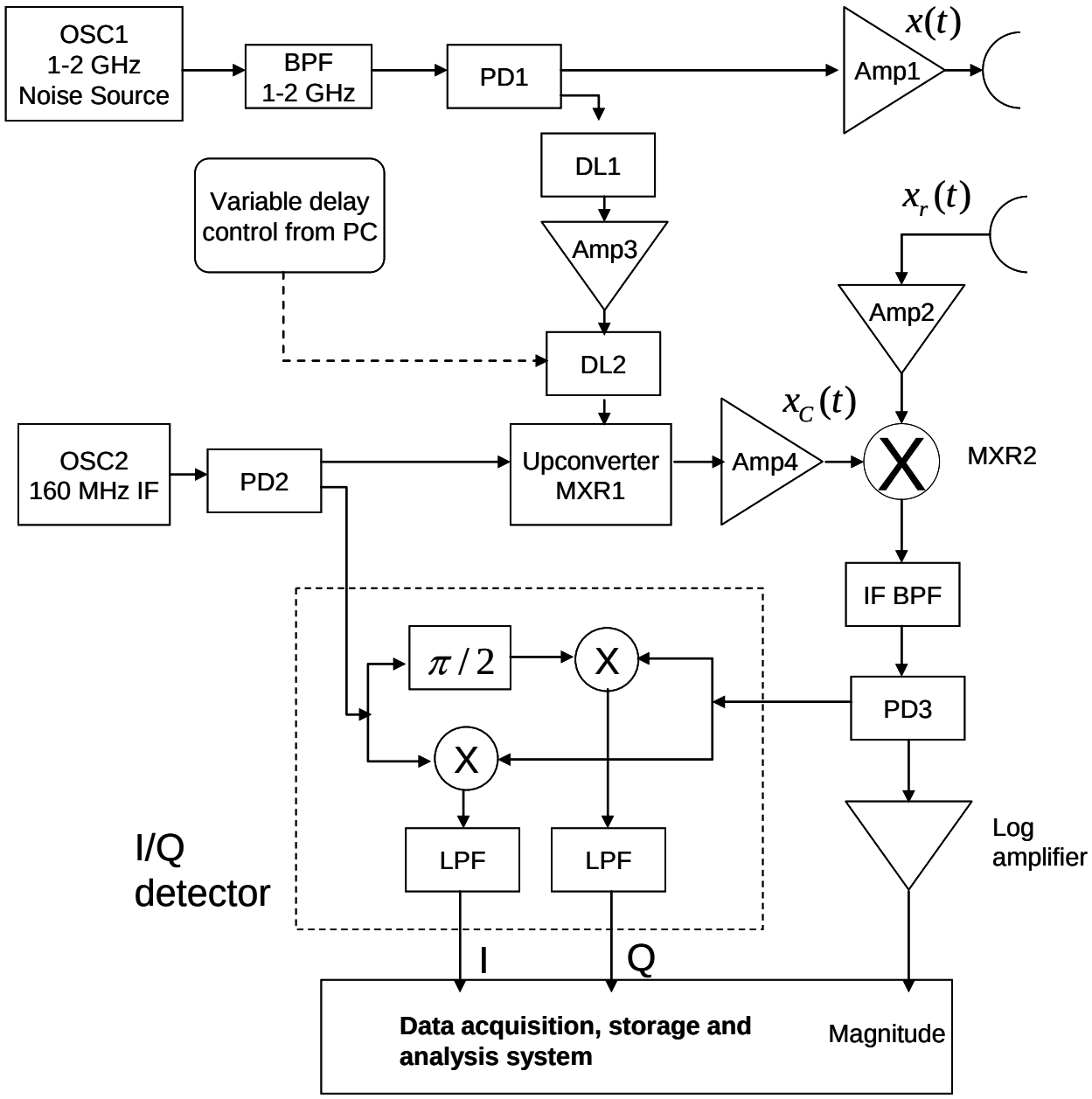

Figure 3. Block Diagram – Complete Random Noise Radar [After 13].

2. Overview and Transmitter Block Diagram

The RNR architecture by Dr. Ram Narayanan uses a random microwave noise source that is bandlimited and amplified [6]. This thesis models the transmitter portion of the radar and uses the detected and digitized data for the input to the intercept receiver signal processing. Without loss of generality, this thesis models the transmitted noise has a bandwidth $B = 300$ MHz to lay between 200 MHz and 500 MHz. Figure 4 below illustrates the configuration of the transmitter.

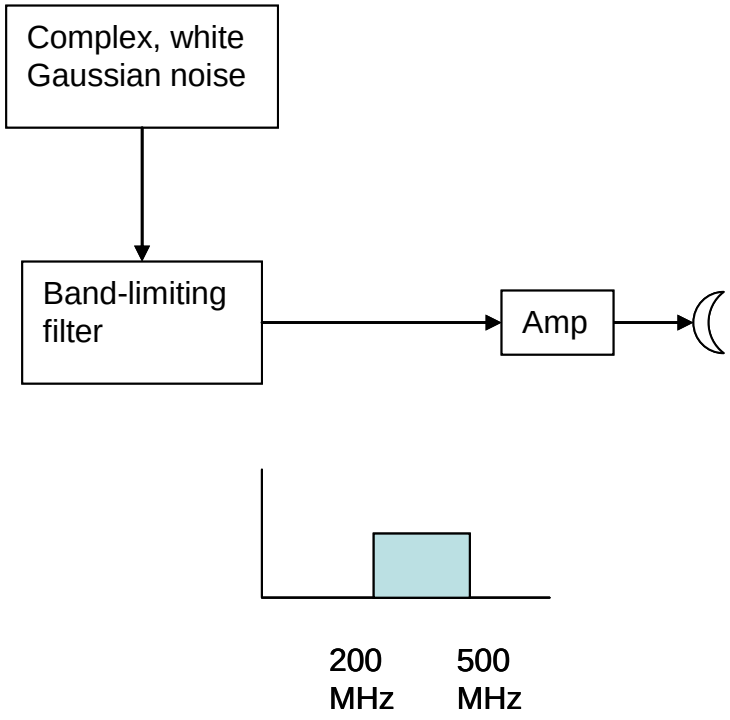

Figure 4. Block Diagram – Transmitter of the Random Noise Radar.

3. Mathematical Description

The mathematical description for the complete emitter design is given in [6]. The transmitted signal (bandpass process) is expressed as:

$$X(t) = X_c(t)\cos(2\pi f_o t) - X_s(t)\sin(2\pi f_o t) \qquad (10)$$

where $X(t)$ is the Gaussian noise process centered at $2\pi f_o$, with a bandwidth B, and $2\pi f_o > \frac{B}{2}$. For the received signal back at the radar, it can be shown that:

$$X_r(t) = X_c^{'}(t)\cos\{\omega_o[(1+\alpha)t - \tau_o]\} - X_s^{'}(t)\sin\{\omega_o[(1+\alpha)t - \tau_o]\} \qquad (11)$$

where the target at a distance R will have a delay of $\tau_o = \frac{2R}{c}$ and be moving with a radial velocity v_o giving a delay $\tau_o - \alpha t$ and $\alpha \sim \frac{2v_o}{c}$.

4. Model Development and Results

The MATLAB code was initially adopted from Dr. Ram Narayanan's work with Mr. Dawood in [6]. However, extensive modification has taken place. The design uses a random, white Gaussian noise signal, which is bandlimited.

Using the baseline variables of the carrier frequency, bandwidth, amplitude, and noise power level, the code was run to ultimately produce the in-phase and quadrature components for the time-frequency and bi-frequency processing. Various plots were produced along the path shown in the block diagram. Figure 5 illustrates the white Gaussian noise and Figure 6 illustrates the bandlimiting of this emitted signal.

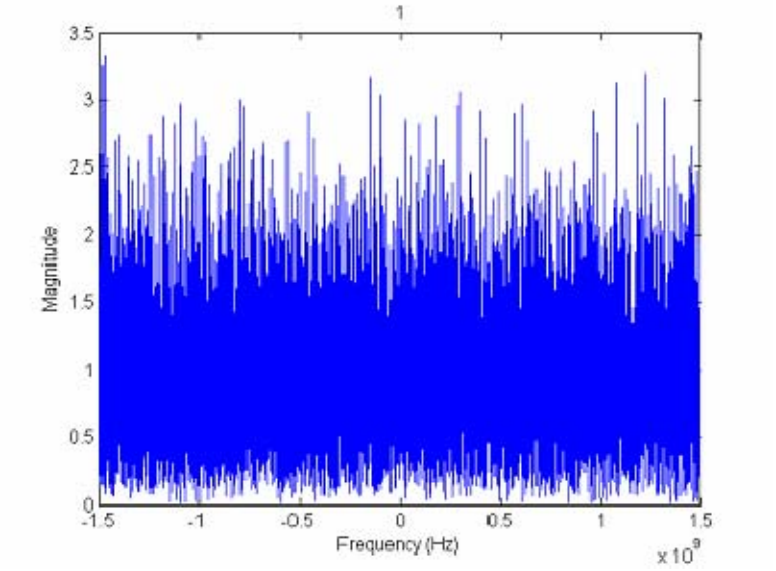

Figure 5. Wideband Microwave Noise Signal.

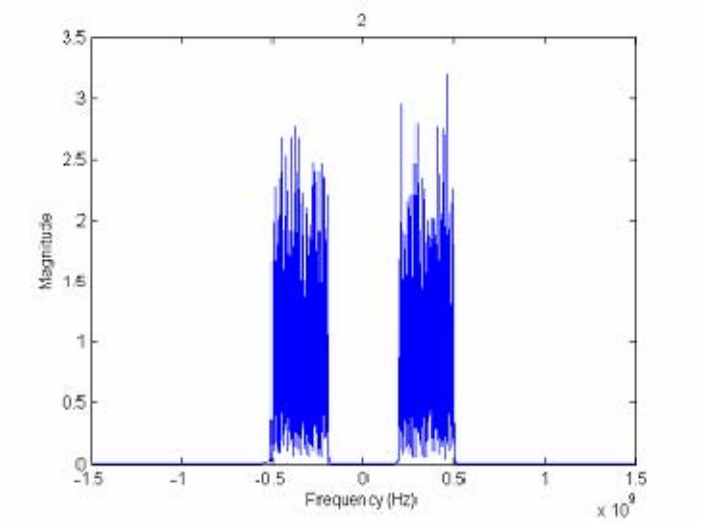

Figure 6. Bandlimited Microwave Noise Signal, f_c = 350 MHz, 300 MHz.

Here the bandlimiting filters pass the noise signal between 200-500 MHz. The frequency scale reflects the intercept receiver ADC sampling frequency of 3 GHz.

A key performance element is the bandwidth. For good range resolution, clutter discrimination, and LPI, the noise signal needs to spread the energy over

a large modulation bandwidth. In this thesis, the noise bandwidth was chosen to be 300 MHz to provide a range resolution of 0.5 meters, following:

$$\Delta R = \frac{c}{2B} \tag{12}$$

where B is the signal bandwidth and c is the speed of light.

5. Receiver Periodic Ambiguity Results

The emitter's Doppler processing fidelity, range resolution, and response to clutter can be identified with the PACF and the PAF [8]. To begin the processing, certain inputs were made to the PAF generation process described in Appendix B [8]. Pre-processing parameters chosen for the PAF generation are shown in Table 1 below:

Frequency-modulated signal	Option 2
Periods used to include N:	1
Sampling frequency used f_s (Hz):	3×10^{9}
Carrier frequency f_c (Hz):	350×10^{6}
Modulation period (s):	1×10^{-6}

Table 1. PAF Pre-processing Parameters – RNR.

Examining the basic characteristics, the RNR model produced the following results about the transmitted noise signal. Figure 7 shows the amplitude and phase versus the delay offset axis τ / t_b (normalized by the subcode period which in this case is the sampling period $1/f_s$).

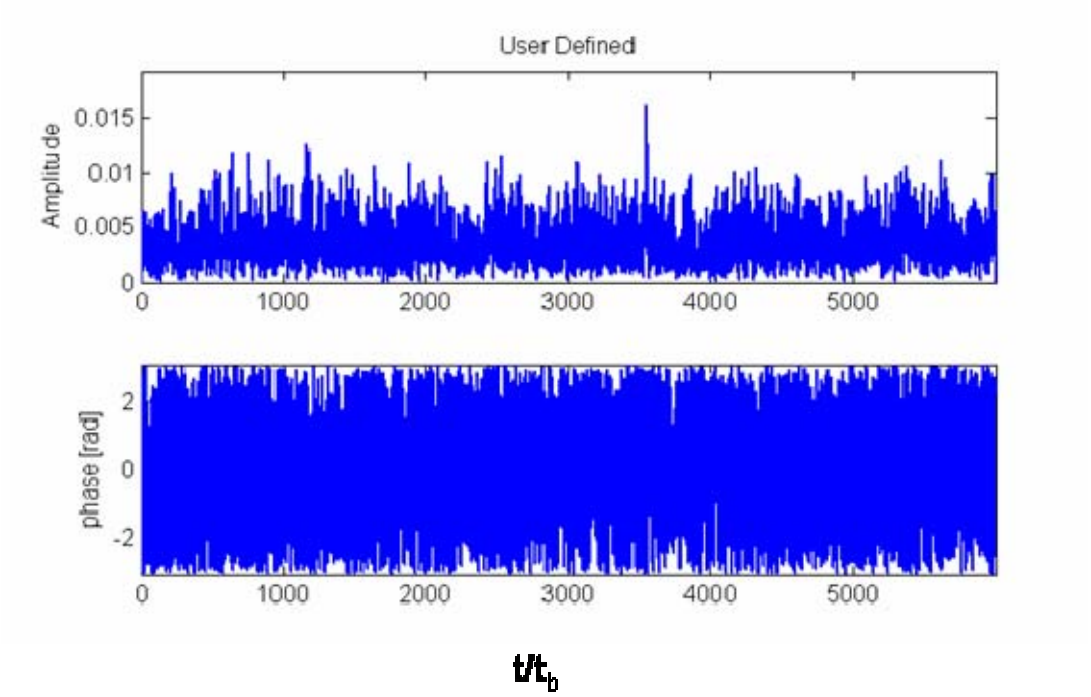

Figure 7. RNR – Transmitted Signal Parameters.

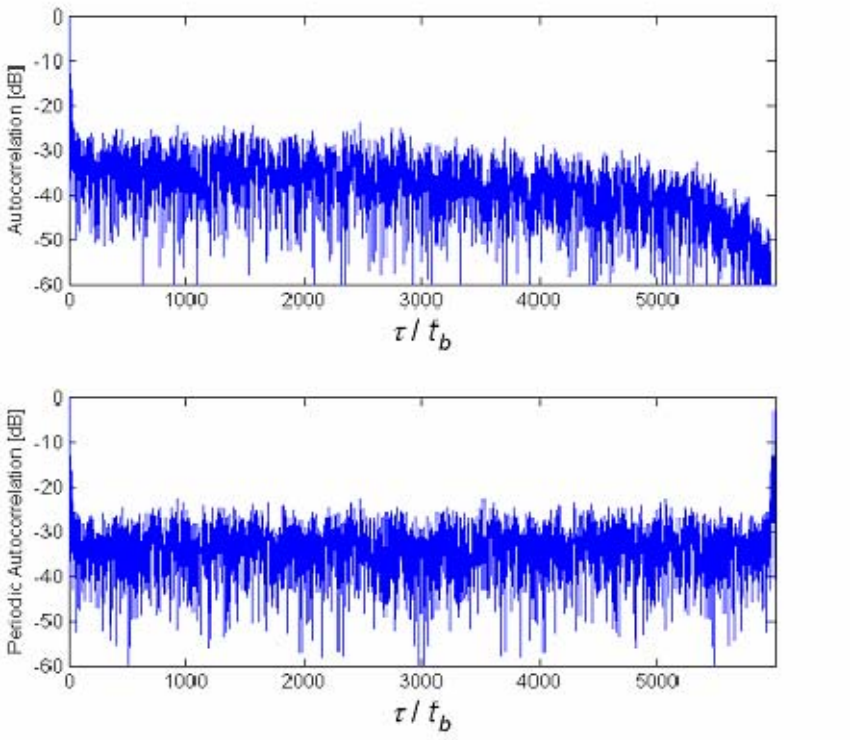

Figure 8. RNR – ACF & PACF Results.

Discernable from the ACF (top), the peak sidelobes appear at approximately –12 dB down from the main lobe. On the PACF (bottom), one can tell the side lobes are also –12 dB. Figure 9 illustrates the PAF where the peak sidelobes are observable.

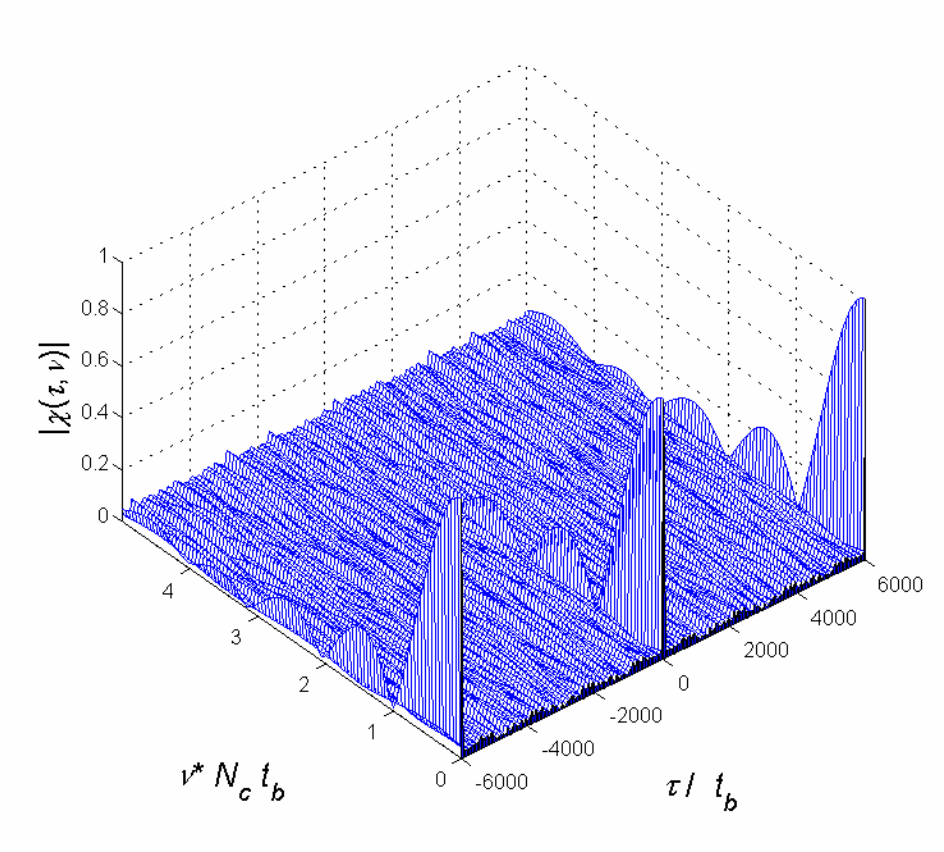

Figure 9. RNR – Periodic Ambiguity Function.

Along the delay offset axis, the scale is normalized by the subcode period t_b. The code repeats at intervals of the code period multiplied by the sampling frequency. In this case, the PAF repeats at every 6000 points (2 µsec * 3 GHz). Note that the zero Doppler cut of the PAF is the PACF shown in Figure 8. The sidelobes on the delay axis are noticeable, but small compared to the magnitude of the mainlobe. On the normalized Doppler axis, the sidelobes are significant (~0.25). Thus, this radar is expected to have challenges with the range

resolution, Doppler processing, and its response to clutter. Increasing the number of reference codes *N* used for the correlation process can reduce the sidelobes. Windowing of the reference function in the receiver also helps to reduce the sidelobes.

D. RANDOM SIGNAL RADAR – NOISE FMCW

As in typical continuous wave radar, leakage (isolation) between transmit and receive antennas can affect long range detection performance due to the degraded sensitivity that results. Although this thesis is focused on the source of transmission, the complete receiver design is included here to gain a better understanding of this noise technology. The following radar designs attempt to progressively mitigate this CW leakage and illustrate the research ongoing with Dr. Guosui.

1. Theory of Operation

In the noise FMCW approach, a white Gaussian noise source is linearly frequency modulated by an FMCW waveform. Figure 10 is shown to illustrate the full receiver architecture and follows from [16]. The return-source correlation takes place in the receiver's front-end mixer. After the mixer, the beat frequency starts with a certain frequency at zero range and gradually increases to reflect the increase in range. At long range, the mixer output beat frequency represents the range to the target. Optimized filters pass either the target signal with some noncorrelation signal or strictly the noncorrelation signal. The power detectors detect the signal envelope and a difference amplifier selects the correct channel to determine the target distance.

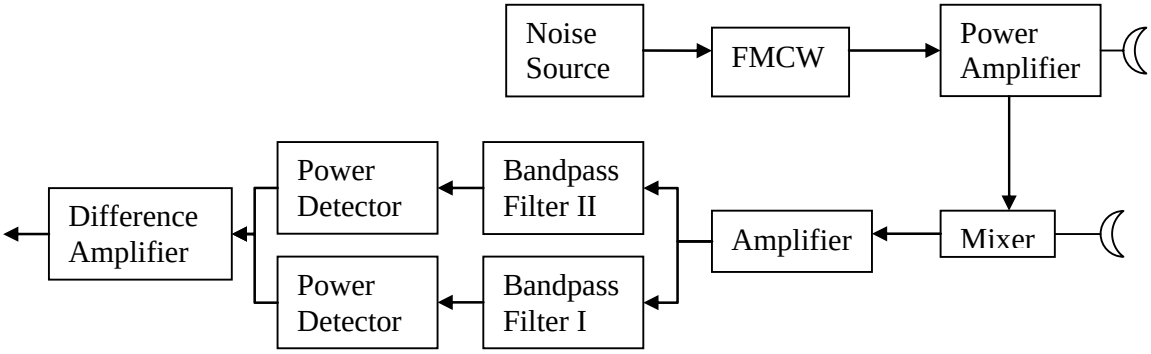

Figure 10. Block Diagram – Complete Noise FMCW Radar [After 16].

The inability to measure target speed due to a sawtooth triangular waveform, detect long range targets, and the significant leakage (isolation) between transmit and receive channels are limitations of this current Noise FMCW radar implementation. To suppress CW leakage, the addition of another frequency has been implemented with the Sine Plus Noise FMCW radar [16].

2. Overview and Transmitter Block Diagram

Figure 11 shows a detailed block diagram of the noise FMCW transmitter that uses a triangular FMCW waveform (target range and speed). With our approach, a microwave noise generator first produces a wideband noise. After this, the signal is band limited to 300 MHz, centered on 350 MHz. After band limiting, the noise signal modulates an FMCW signal with a center frequency of 350 MHz.

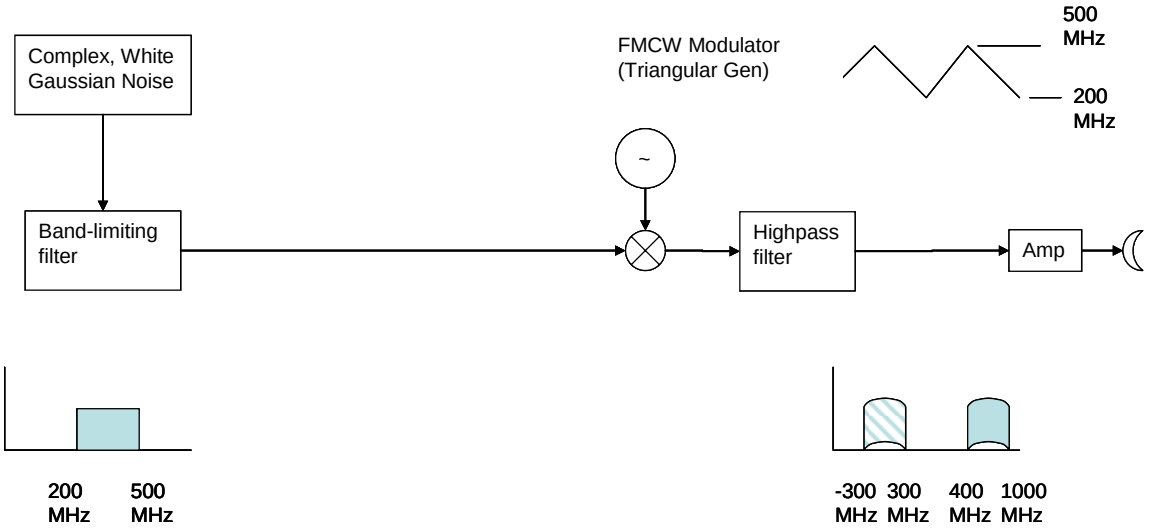

Figure 11. Block Diagram – Transmitter of the Noise FMCW Radar.

After noise modulation, the resultant signal is high pass filtered to remove the complex lower sideband modulation leaving the transmitted signal with a *B* = 600 MHz centered at $f_c = 700\,\text{MHz}$. Finally, the modulated signal is amplified before transmission. In the actual model by Guosui, the received signal is correlated to a time-delayed version of this emission. For the scope of this thesis, the transmitted signal is the one of interest, since the potential to intercept this signal is the goal.

3. Mathematical Description

In [16], Guosui characterizes transmission of the Noise FMCW as:

$$e(t) = E\cos\left[\omega_o t + \theta(t)\right] \tag{13}$$

where

$$\theta(t) = \int_0^t D_f \xi(t_1) dt_1 \tag{14}$$

The variable D_f is the angular frequency per volt and $\xi(t_1)$ is the noise voltage of a stationary process with zero mean. The return (echo) signal is lower in

amplitude, time delayed, and shifted in frequency (for a moving target). The mathematical expressions for the complete Noise FMCW are found in [16].

4. Model Development and Results

This code was built to model the RSR designed by Dr. Lui Guosui [1] except a triangular FMCW waveform is used. The design approach in this model is the use of a random, white Gaussian noise signal, to modulate the FMCW signal, which is then bandlimited. The primary excursion here from the RNR model is the use of an FMCW signal. A key performance element is the bandwidth. For good range resolution for clutter discrimination and LPI, the FMCW signal spreads the energy over a large modulation bandwidth ΔF. In this thesis, the ΔF was chosen to be 300 MHz to provide a range resolution of 0.5 meters, following:

$$\Delta R = \frac{c}{2\Delta F} \tag{15}$$

which is consistent with the range resolution equation used in the RNR section.

After the quadrature components of the triangular FMCW waveform are prepared, the in-phase and quadrature components are pulled from the real and imaginary portions of the intercepted signal for time-frequency processing. Various plots were produced along the path shown in the block diagram. The white Gaussian noise production and the bandlimiting of this noise are nearly identical from the RNR model and therefore not shown. Next along the path of the block diagram is the FMCW signal, shown in the frequency domain in Figure 12 below.

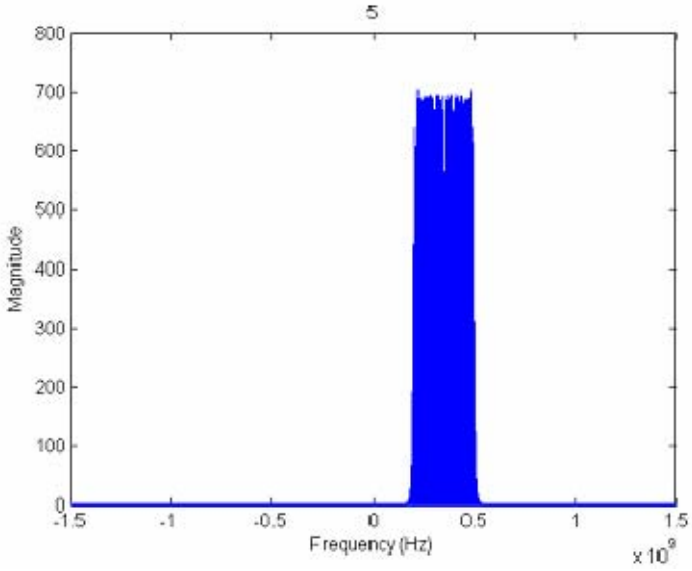

Figure 12. Magnitude of the FMCW Signal, ΔF = 300 MHz, f_c = 350 MHz.

The modulation bandwidth between 200-500 MHz is readily observed ($\Delta F = 300$ MHz and is centered at 350 MHz). The next two points along the path of the block diagram illustrate the noise modulation and bandlimiting after noise modulation, as shown in Figure 13 below.

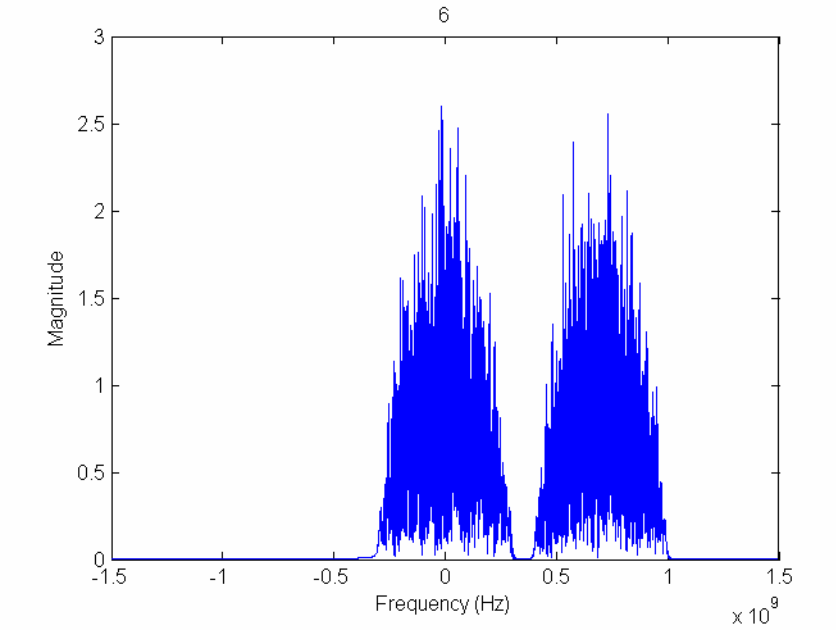

Figure 13. Noise Modulated FMCW Signal, ΔF = 300 MHz, f_c = 350 MHz.

The modulation of the FMCW signal by the 350 MHz noise signal is readily observed. For the upper sideband product, this modulation results in the new center frequency of 700 MHz as in Figure 13 above. Realistically, the transmitted portion of the Noise FMCW signal is shown in Figure 14 below, and is an illustration of the magnitude spectrum after filtering with the high pass filter.

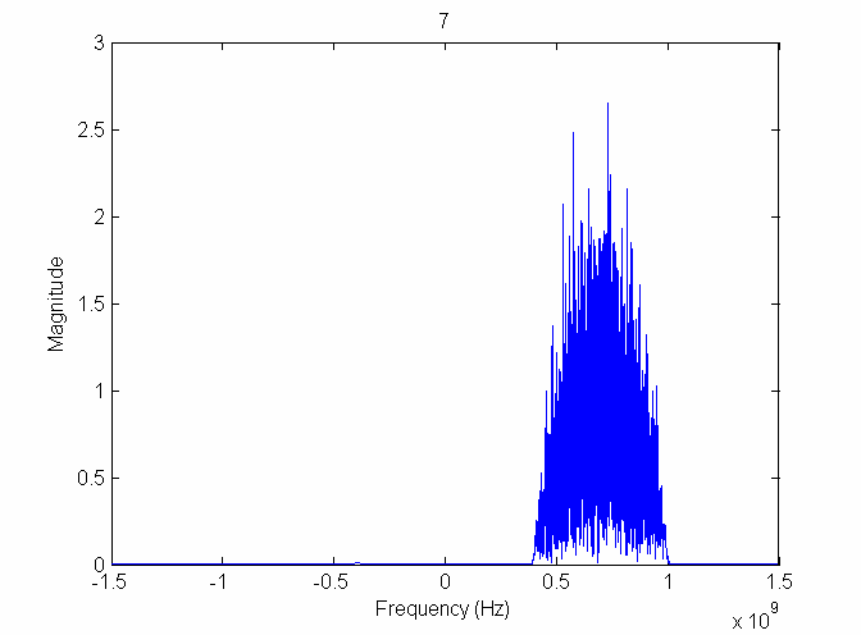

Figure 14. Noise FMCW Signal, ΔF = 300 MHz, f_c = 700 MHz – high passed.

This would be the signal produced by the LPI emitter and captured by the intercept receiver. Since emission conservation is key for LPI considerations, the lower sideband modulation product was chosen to be the emitted signal. This also takes advantage of the less expensive hardware involved in building a lower frequency receiver. The next section describes the Doppler processing fidelity and other signal characteristics from the emitter.

5. Receiver Periodic Ambiguity Results

The emitter's Doppler processing fidelity, range resolution, and response to clutter can be identified with the PACF and the PAF [8]. To begin the

processing, certain inputs were made to the PAF generation process described in Appendix B [8]. Pre-processing parameters chosen for the PAF generation are shown in Table 2 below.

Frequency-modulated signal	Option 2
Periods used to include N:	1
Sampling frequency used f_s (Hz):	3×10^{9}
Carrier frequency f_c (Hz):	350×10^{6}
Modulation period (s):	1×10^{-6}

Table 2. PAF Pre-processing Parameters – Noise FMCW.

Examining the basic characteristics, the noise FMCW RSR model produced the following parameters about the transmitted noise signal. Figure 15 shows the amplitude and phase versus the delay offset axis normalized by the subcode period (the sampling period in this case). The noise bandwidth of the signal was 300 MHz.

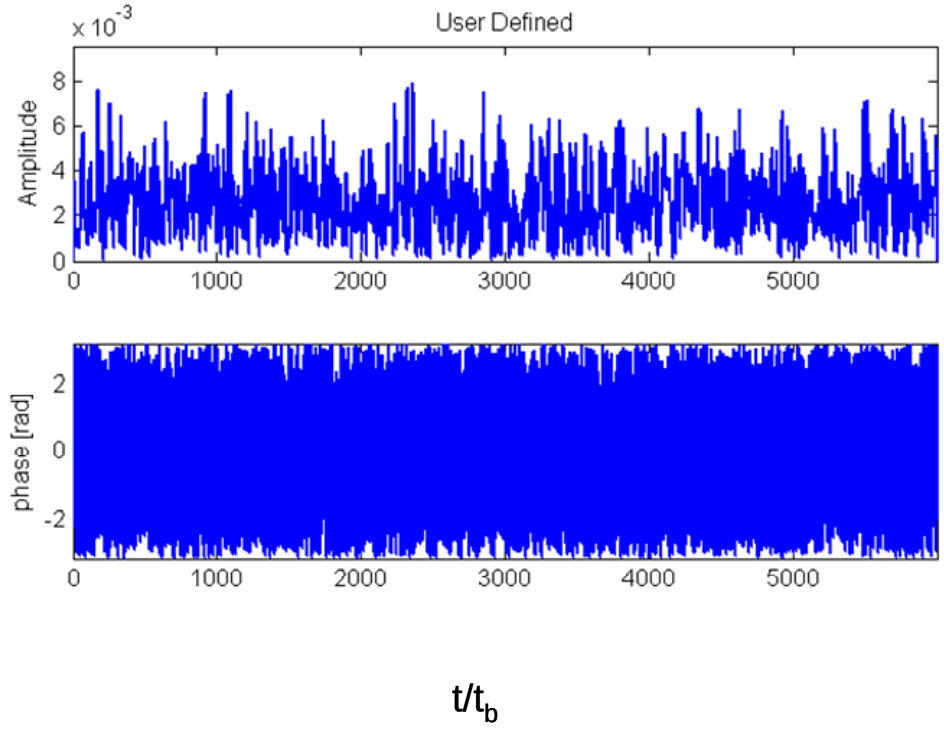

Figure 15. Noise FMCW – Transmitted Signal Parameters.

By observation, the signal appears as random noise in both amplitude and phase. The ACF and PACF of the transmitted signal are shown in Figure 16. Discernable from the ACF (top), the peak sidelobes appear at approximately –20 dB down from the main lobe. On the PACF (bottom), the side lobes are also –20 dB.

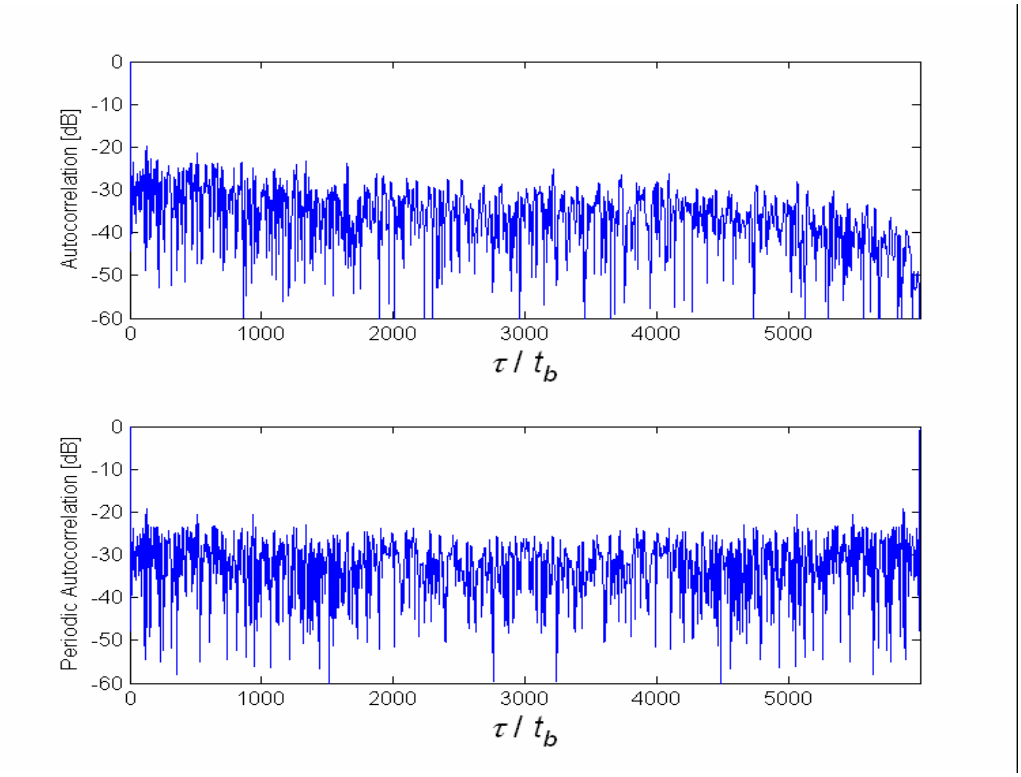

Figure 16. Noise FMCW – ACF & PACF Parameters.

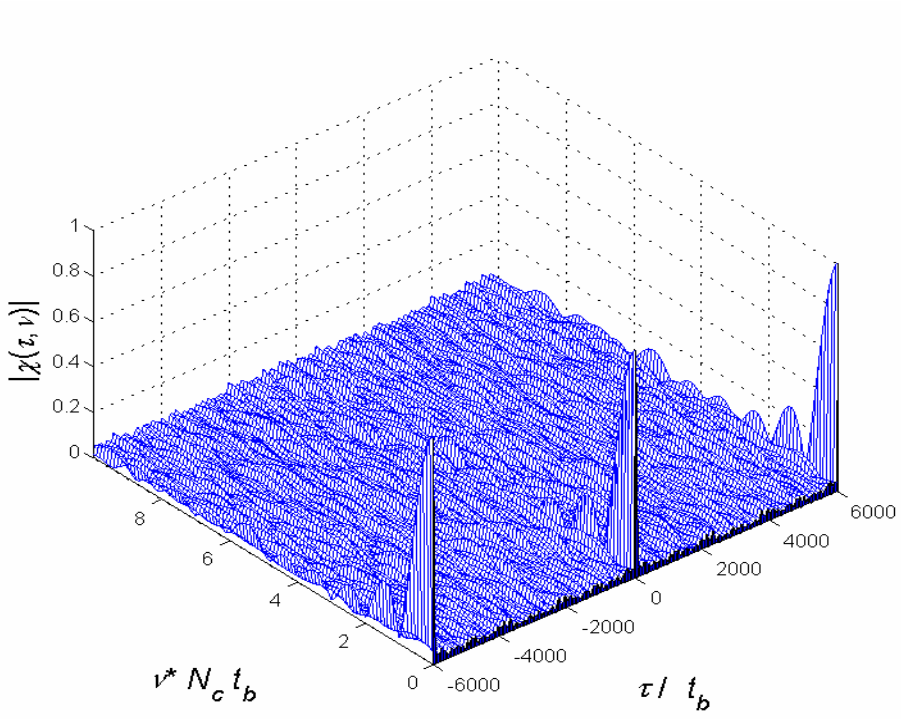

Figure 17. Noise FMCW – Periodic Ambiguity Function.

The PAF repeats at integer multiples of the code period multiplied by the sampling frequency. In this case, the PAF repeats at every 6000 points (2 μsec * 3 GHz). The peak sidelobes in the normalized Doppler axis are noticeable (0.25). This radar is expected to have challenges with the range resolution, Doppler, and response to clutter.

E. RANDOM SIGNAL RADAR – SINE PLUS NOISE FMCW

1. Theory of Operation

The Sine Plus Noise FMCW RSR uses an additional sine signal added to the noise source. A block diagram of the transmitter is shown in Figure 18 [1]. To account for the injected sine wave, the receiver uses two bandpass filters to expand the receiver's frequency range for the Doppler plus noncorrelation signal and for the noncorrelation signal only. The major difference between the noise FMCW and the Sine Plus Noise FMCW is the filters have bandwidths expanded to include multiples of the added sine signal within the return signal.

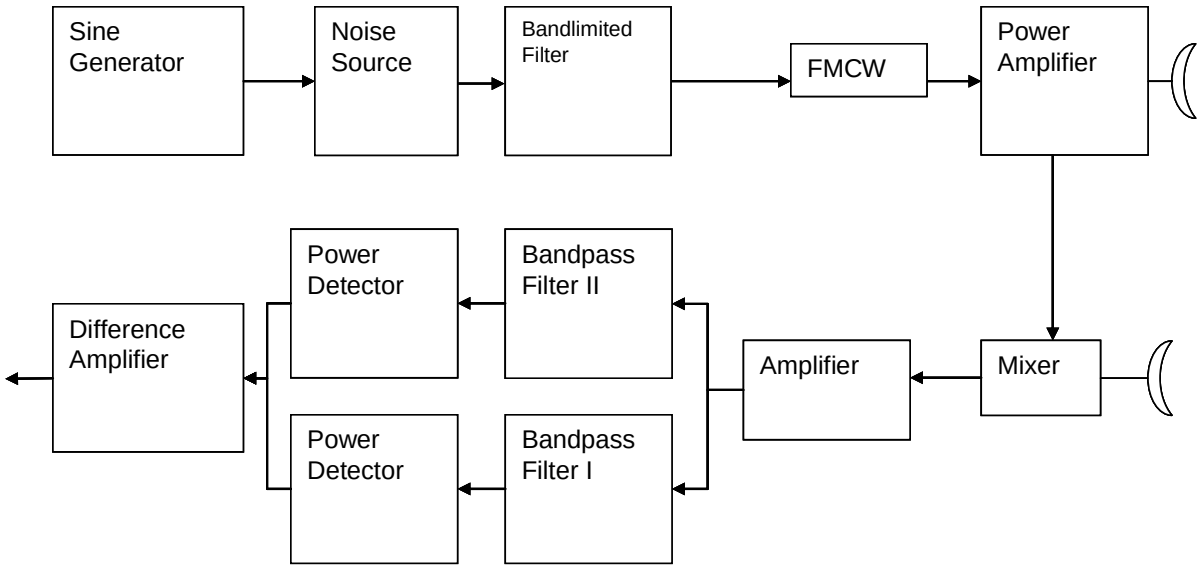

Figure 18. Block Diagram – Complete Sine Plus Noise FMCW Radar [After 1].

Although the Sine Plus Noise FMCW as implemented in [1] mitigates the CW leakage sidelobes more effectively than the Noise FMCW, their implementation cannot determine the speed of a moving target or detect a long range target (due mostly to their implementation using a sawtooth FMCW waveform as opposed to a triangular waveform such as modeled in this thesis). Thus, their research looks towards a more competitive form of RSR, the Random Binary Phase-Coded CW Radar to overcome the limitations of target velocity and long-range detection.

2. Overview and Transmitter Block Diagram

This form of noise technology employs an additional tone signal that is modulated by the white Gaussian noise which further modulates the FMCW waveform. Figure 19 shows a detailed block diagram of the transmitter modeled in this thesis.

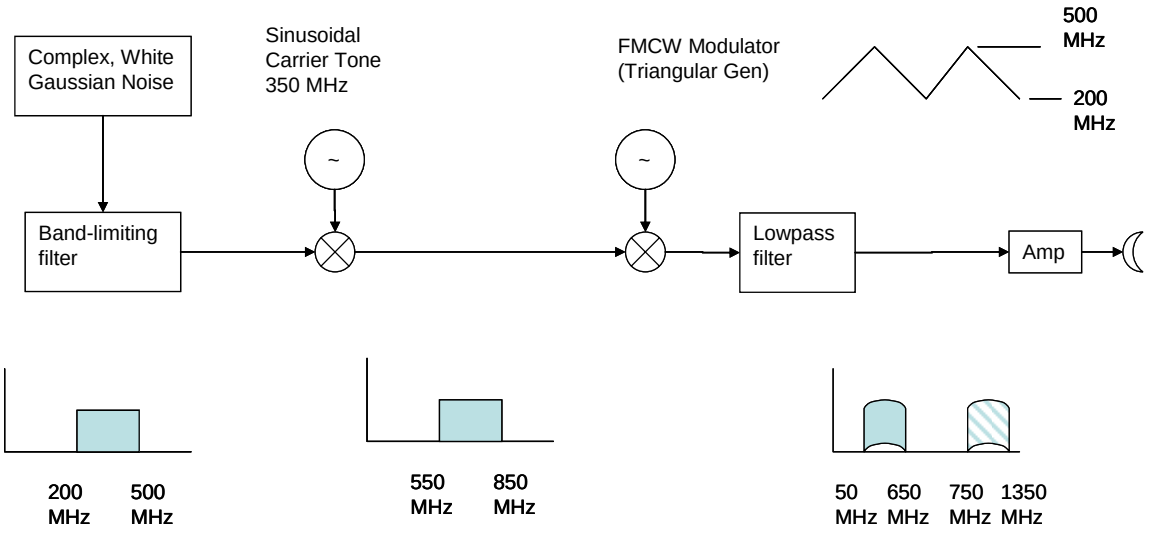

Figure 19. Block Diagram – Transmitter of the Sine Plus Noise FMCW Radar.

In this approach, a microwave noise generator produces noise to the desired range of operation. After this, the signal is bandlimited to 300 MHz, centered on 350 MHz. After the bandlimiting, the noise signal is added (added in

frequency, multiplied in time) to a single tone with a frequency of $f_T = 350$ MHz. The upper band is centered at 700 MHz from the modulation product and this new signal modulates an FMCW signal with a center frequency of 350 MHz. After noise modulation, the resultant signal is low pass filtered to remove the lower sideband modulation products. Duplicate signals are unnecessary and counterproductive to LPI principles; therefore the upper sideband is eliminated (and also keeps the hardware complexity low). Finally, the 600 MHz bandwidth signal with center frequency of 350 MHz is amplified before transmission. In the model built by Guosui, the received signal is correlated to a time-delayed version of the emission. For the scope of this thesis, the transmitted source is the one of interest, since the potential to intercept this signal is the goal.

3. Mathematical Description

In [16], Guosui characterizes transmission of the Sine Plus Noise FMCW similarly to the Noise FMCW, but adds the additional signal as:

$$e(t) = E\cos\left[\omega_o t + \theta_1(t) + \theta_2(t)\right] \tag{16}$$

where

$$\theta_1(t) = D_1 \sin \omega_m t \tag{17}$$

$$\theta_2(t) = \int_0^t D_f V(t_2) dt_2 \tag{18}$$

where the variable D_f is the angular frequency per volt and $V(t_2)$ is the modulated noise voltage of a normal stationary process with zero mean. Also ω_m is the additional tone frequency.

4. Model Development and Results

The primary excursion here from the RSR-Noise FMCW model is the use of an additional tone to the noise before modulating the FMCW signal. This second tone frequency was added to the noise for leakage, or isolation between transmit and receive antennas [1, 17]. Although not explained in Guosui's

literature, it is presumed the isolation is accomplished with the same frequency simply 180 degrees out in phase for hardware implementation [18]. This is observable in the code for the Sine Plus Noise-FMCW model. To explore the phase impact, both 0 and π phases were experimented, resulting in no effect to the output. Additional variables have been added to characterize the added sine signal, as an arbitrary 350 MHz for the frequency and a normalized value of 1 for the signal amplitude. The white Gaussian noise power is –40 dB.

A key performance element is the bandwidth. For good range resolution, clutter discrimination and LPI, the FMCW signal spreads the energy over a large modulation bandwidth ΔF. In this thesis, the ΔF of the FMCW signal was chosen to be 300 MHz (centered at 350 MHz) to provide a range resolution of 0.5 meters, following:

$$\Delta R = \frac{c}{2\Delta F} \tag{19}$$

which is consistent with the range resolution equation used in earlier sections.

After the quadrature components of the triangular FMCW waveform are prepared, the in-phase and quadrature components are pulled from the real and imaginary portions of the intercepted signal for time-frequency processing. Various plots were produced along the path shown in the block diagram.

Examining now the output of the noise generator with the added tone, the effect on modulation is clear with the shifting of noise by 350 MHz, as shown in Figure 20:

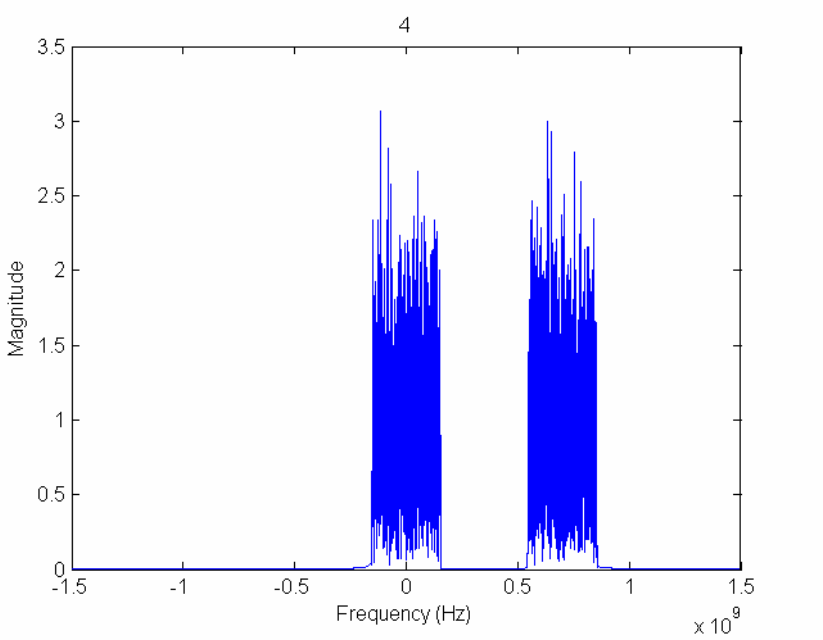

Figure 20. Sine Plus Noise FMCW, Tone Modulation of Noise, f_c = 700 MHz.

This tone is modulated by the white Gaussian noise. Thus, the frequency shift due to modulation is observed and expected. The final center frequency of the Sine Plus Noise FMCW is now at 700 MHz. Next along the path of the block diagram, the magnitude spectrum plot of the Sine Plus Noise FMCW signal is shown in the frequency domain in Figure 21. The bandlimiting between 200-500 MHz is readily observed. The next two points along the emitter path are shown in Figure 22 and illustrate the compound noise modulation of the Sine Plus Noise FMCW signal.

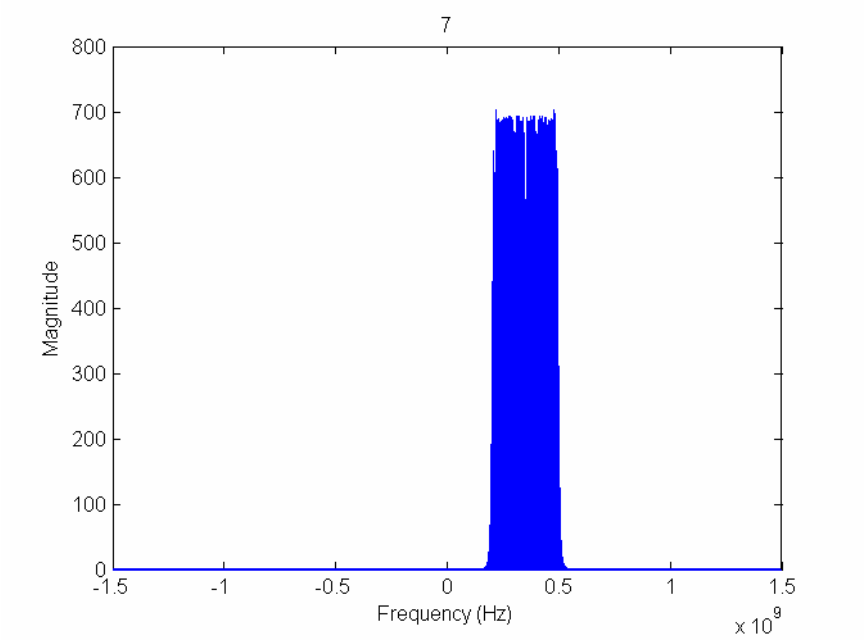

Figure 21. Magnitude of the Sine Plus Noise FMCW Signal, f_c = 350 MHz.

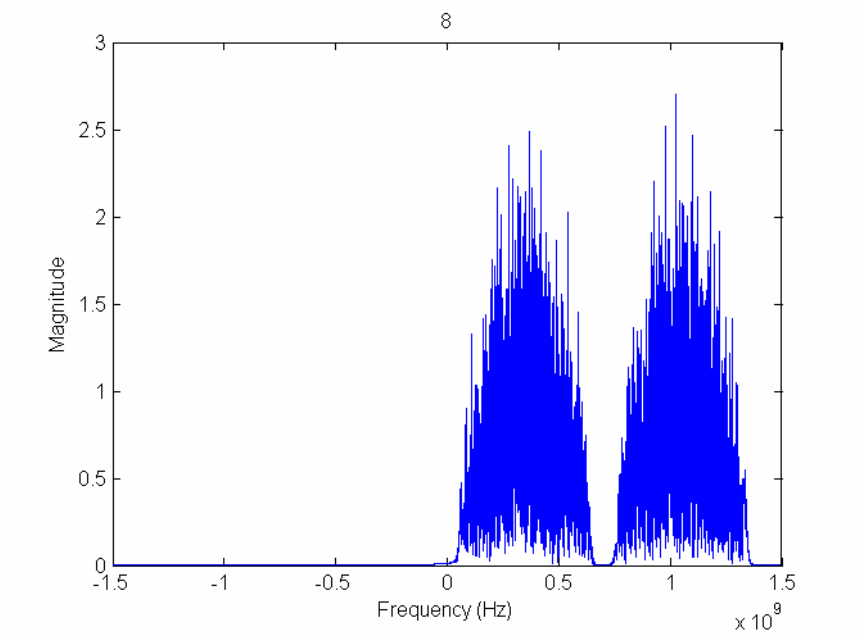

Figure 22. Sine Plus Noise FMCW Signal, f_c = 350 MHz.

The modulation of the 350 MHz FMCW signal by the compound signal is readily observed. The compound signal is comprised of a 350 MHz noise signal

and the 350 MHz tone. The resultant, modulated signal has a new center frequency of 1050 MHz. Since this upper sideband product is not necessary, the lowpass portion is transmitted and shown in Figure 23 as:

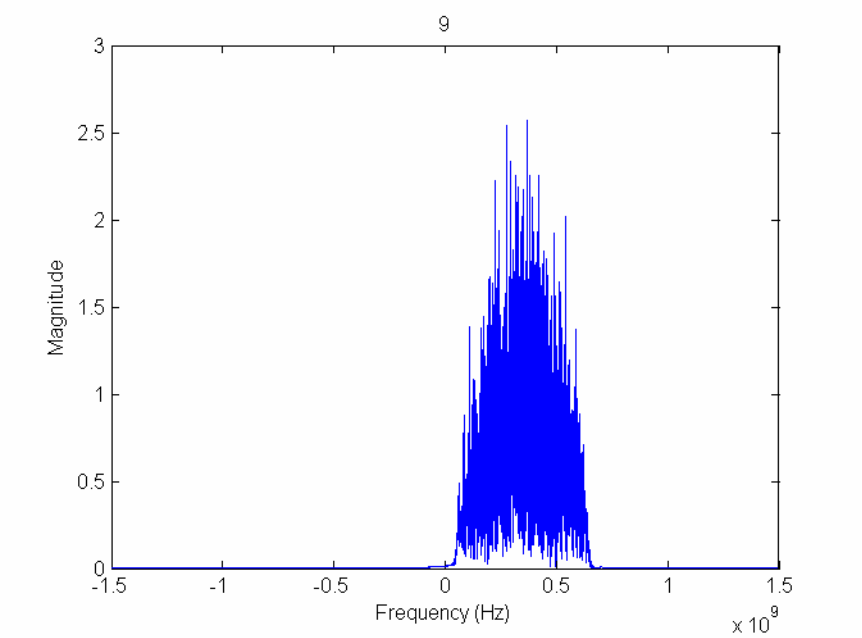

Figure 23. Sine Plus Noise FMCW Signal, f_c = 350 MHz – low passed.

This is the signal produced by the emitter and captured by the intercept receiver. Since conservation of emissions is key for LPI considerations, the lower sideband modulation product was chosen to take advantage of the less expensive hardware involved in building a lower frequency receiver. The next section describes the Doppler processing fidelity and other receiver characteristics using the PACF and PAF.

5. Receiver Periodic Ambiguity Results

The emitter's Doppler processing fidelity, range resolution, and response to clutter can be identified with the PACF and the PAF [8]. To begin the

processing, certain inputs were made to the PAF generation process described in Appendix B [8]. Pre-processing parameters chosen for the PAF generation are shown in Table 3 below:

Frequency-modulated signal	Option 2
Periods used to include N :	1
Sampling frequency used f_s (Hz):	3×10^{9}
Carrier frequency f_c (Hz):	350×10^{6}
Modulation period (s):	1×10^{-6}

Table 3. PAF Pre-processing Parameters – Sine Plus Noise FMCW.

Figure 24 shows the amplitude and phase of the Sine Plus Noise FMCW emitter versus the delay offset normalized by the subcode period. The noise bandwidth of the signal is 300 MHz.

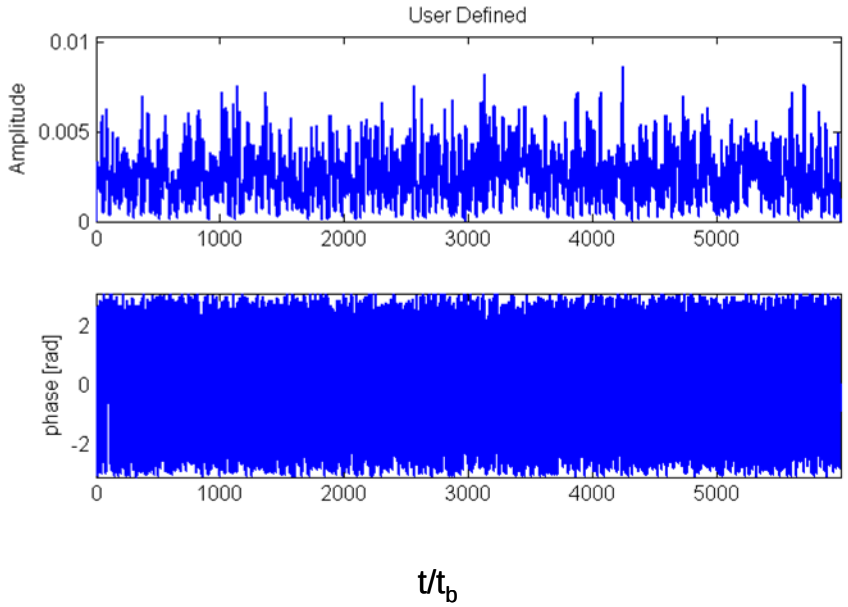

Figure 24. Sine Plus Noise FMCW – Transmitted Signal Parameters.

The signal appears as random noise in amplitude and phase. The ACF and the PACF of the Sine Plus Noise FMCW waveform are shown in Figure 25.

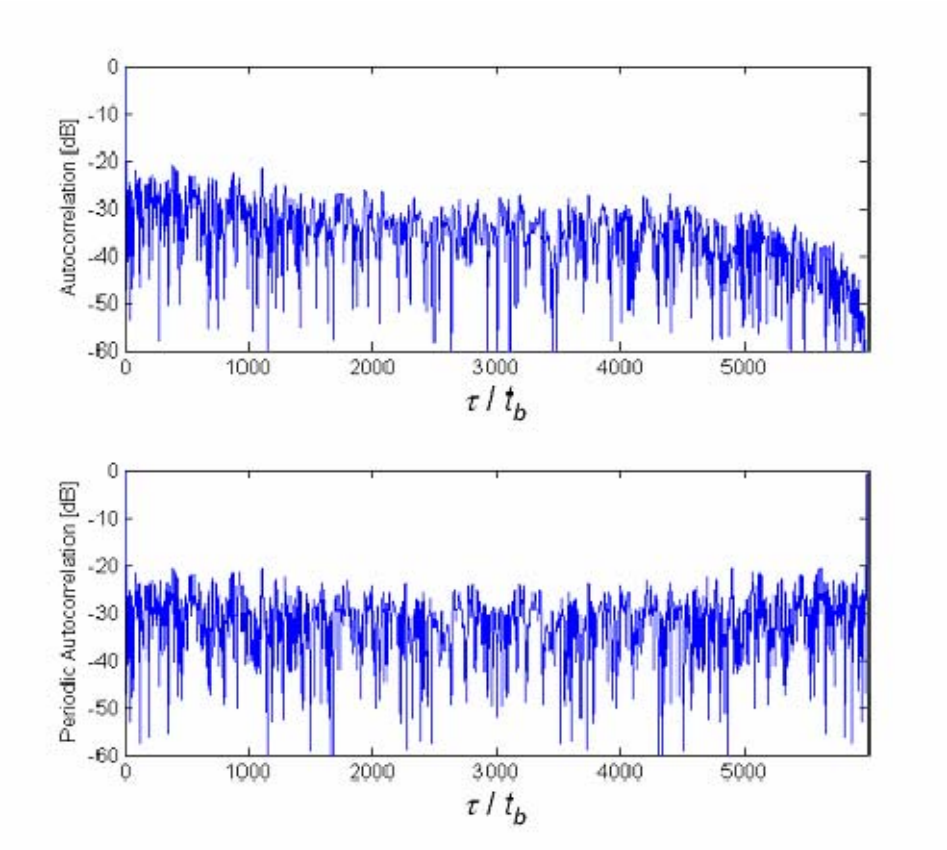

Figure 25. Sine Plus Noise FMCW – ACF & PACF Parameters.

Discernable from the ACF (top), the peak sidelobes appear at approximately –22 dB down from the main lobe. On the PACF (bottom), the peak side lobes are also about –22 dB. The PAF of the Sine Plus Noise FMCW waveform are shown in Figure 26.

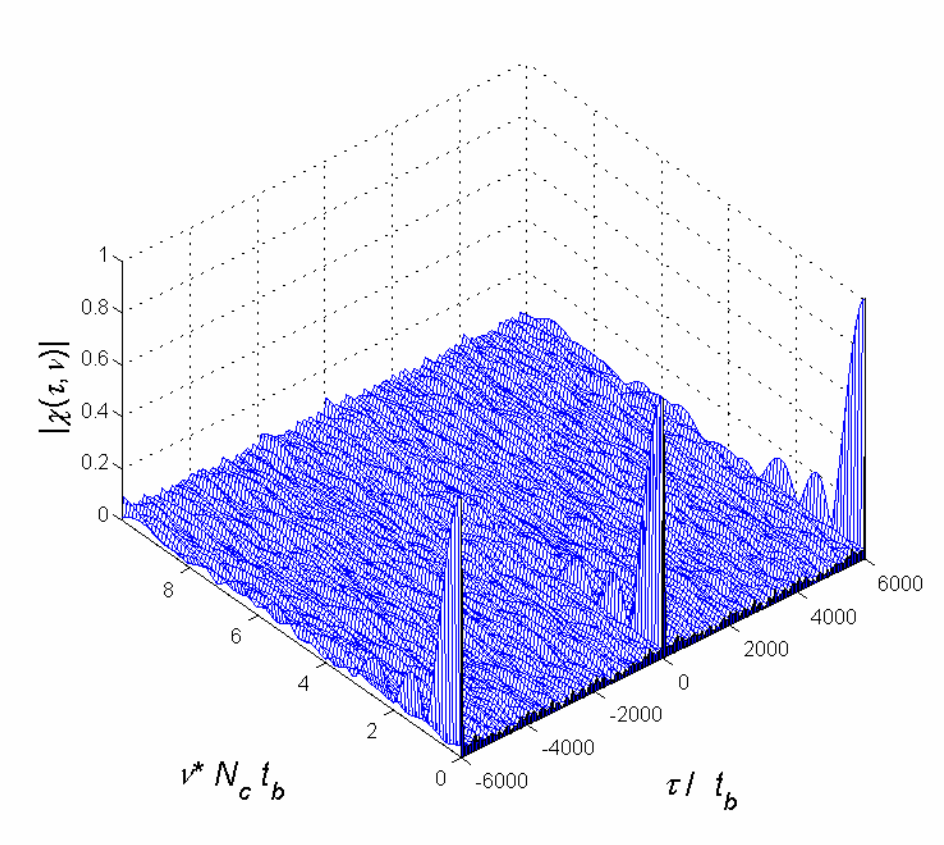

Figure 26. Sine Plus Noise FMCW – Periodic Ambiguity Function.

The delay offset axis, is normalized by the subcode period t_b and the code repeats at intervals of the code period multiplied by the ADC sampling frequency. In this case, the main lobe repeats at integer multiples of 6000 points (2 μsec * 3 GHz). Note that the zero Doppler cut of the PAF is the PACF shown in Figure 25 above. Also note the presence of significant sidelobes along the Doppler offset axis (~0.2). The PACF and PAF illustrate the sidelobe structure of a matched filter receiver when the Sine Plus Noise FMCW waveform is used. Thus, this radar waveform is expected to have challenges with the range resolution, Doppler, and response to clutter. The sidelobes can be reduced by including additional periods of the reference waveform $N>1$ in the receiver correlation

process. Also, the use of a window function (mismatched receiver) can help reduce the sidelobes at the expense of increasing the width of the PAF correlation peak.

F. RANDOM SIGNAL RADAR – RANDOM BINARY PHASE-CODED CW

1. Theory of Operation

The last RSR emitter waveform to be examined is the random binary phase coding of a CW carrier signal. The random binary phase-coded (RBPC) CW radar uses a signal that is randomly phase modulated by either 0 or π. The random phase code modulation results in a transmitted spectrum that is similar to a random Gaussian white noise source. Some later improvements were made to enhance the isolation between transmit and receive channels. One primary improvement is intermittent emissions of the transmit radar. The illumination is as long as needed for long-range target acquisition. A block diagram of the emitter is presented in Figure 27 [1].

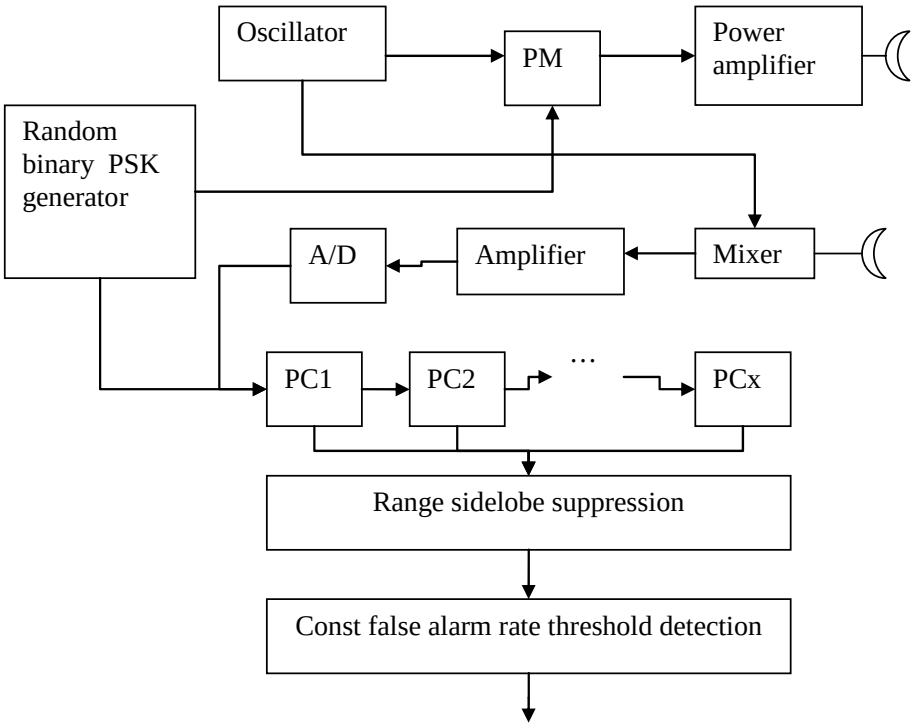

Figure 27. Block Diagram – Complete Random Binary Phase-Coded CW Radar [After 1].

2. Overview and Transmitter Block Diagram

The random binary phase modulation emitter technology employs random phases on a single tone signal. For example, with a subcode period of $t_b = 0.001$ μsec, the transmitted signal appears as wideband noise with $B = 1$ GHz to the intercept receiver. A detailed model of the transmitter is shown in Figure 28.

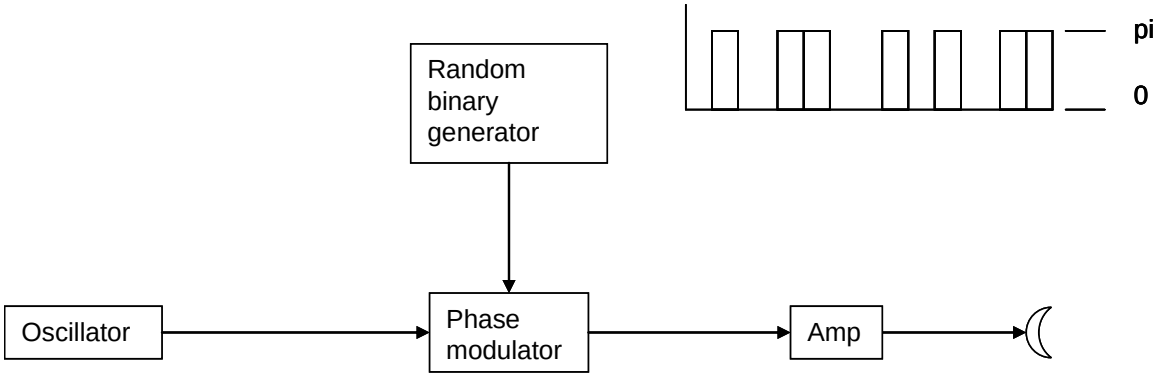

Figure 28. Block Diagram – Transmitter of the Random Binary Phase-Coded CW Radar.

With this approach, an oscillator produces a single tone at f_c = 300 MHz. This value is chosen to compare the results with the previous three models after the intercept receiver processing. A Bernoulli number generator randomly produces the phase values 0 or π for use in phase modulating the tone signal [19]. Finally, the phase modulated signal is amplified before transmission.

3. Mathematical Description

This phase values are random and created by Bernoulli trials [1, 19]. The sequence can be represented by variable S with a probability distribution of:

$$P[S = \pm 1] = 0.5 \tag{20}$$

where the mean value of S is equal to 0 [19].

4. Model Development and Results

A model was built to simulate the RSR designed by Guosui [1]. The design approach in this model is the use of a random binary phase (0 or π) on a tone frequency. Note that no noise source is used in this approach. Consequently, no bandlimiting or filtering needs to be included in the hardware. The bandwidth of the random binary phase modulation is

$$B = \frac{f_c}{cpp} = \frac{1}{t_b} \tag{21}$$

where cpp is the number of cycles of the carrier frequency in a subcode, and t_b is the subcode period. The carrier frequency used is $f_c = 300$ MHz to compare detection results with the other three software models.

In later designs, the isolation issue was addressed with intermittent interruption of the CW waveform [7]. This gave the operator improved LPI performance and ability to detect long-range targets. To address this concept in future work, the assumption would be to use the smallest number of phase codes in order to obtain the required SNR for target detection.

Waveforms with two different bandwidths were generated. The first waveform used $cpp = 1$ and the second waveform used $cpp = 3$. The number of phase codes was set to N_c = 16. Figure 29 illustrates the power spectral density (PSD) of the tone signal that is used. Figure 30 illustrates the PSD for the waveforms after the phase modulation. In Figure 30, the plot on the left is with $cpp = 1$ ($B = 300$ MHz) and the plot on the right is for $cpp = 3$ ($B = 100$ MHz).

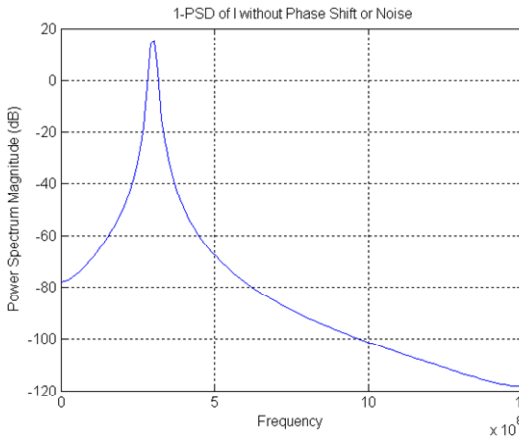

Figure 29. RBPC – PSD of Tone Signal $f_c = 300$ MHz.

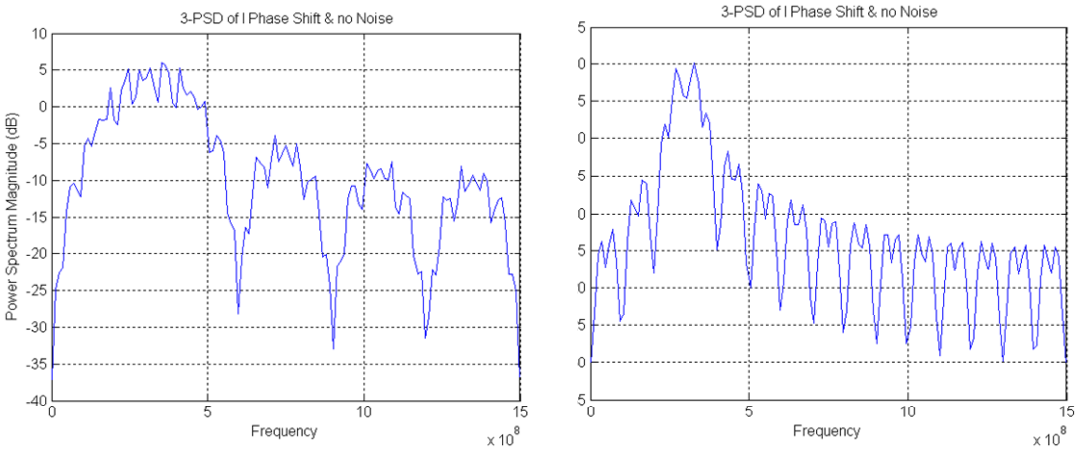

Figure 30. RBPC – PSD after Phase Modulation (left $cpp = 1$, right $cpp = 3$).

The PSD gives the appearance of a noise waveform and the two bandwidths appear as expected. Although some periodic structure is noticeable this quickly diminishes when the code period *T* contains a larger number of subcodes ($N_c \gg 16$). Figure 31 illustrates the 16 subcode (random) phase values used to generate the example waveforms shown in Figure 30.

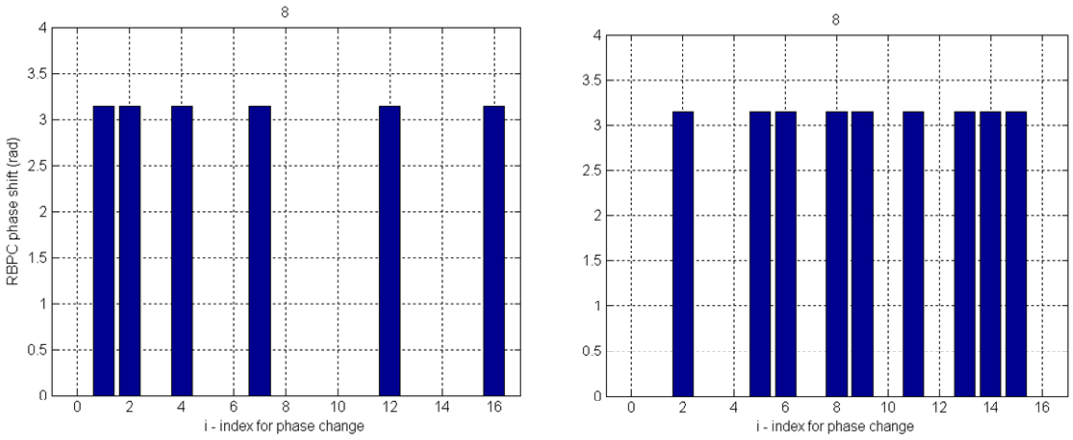

Figure 31. RBPC – N_c = 16 Random Phase Values for the Two Examples Shown in Figure 30.

5. Receiver Periodic Ambiguity Results

The emitter's Doppler processing fidelity, range resolution, and response to clutter can be identified with the PACF, PAF, and the PSD [8]. The RBPC waveform that is received is correlated to a time-delayed version of the emission. To begin processing, certain inputs were made to the PAF generation process described in Appendix B [8]. Pre-processing parameters chosen for the PAF generation are shown in Table 4 below:

Phase-modulated signal	Option 1
Periods used to include N:	1
Sampling frequency used f_s (Hz):	3×10^9
Carrier frequency f_c (Hz):	3×10^8
Cycles per phase cpp:	1 or 3
Number of phase codes, N_c:	16

Table 4. PAF Pre-processing Parameters – RBPC.

The RBPC model output is illustrated in Figure 32 and shows the amplitude and phase versus the delay offset axis normalized by the subcode period. For the cpp=1 case, $t_b = cpp / f_c = 3.33$ ns. For the cpp=3 case, $t_b = cpp / f_c = 10$ ns.

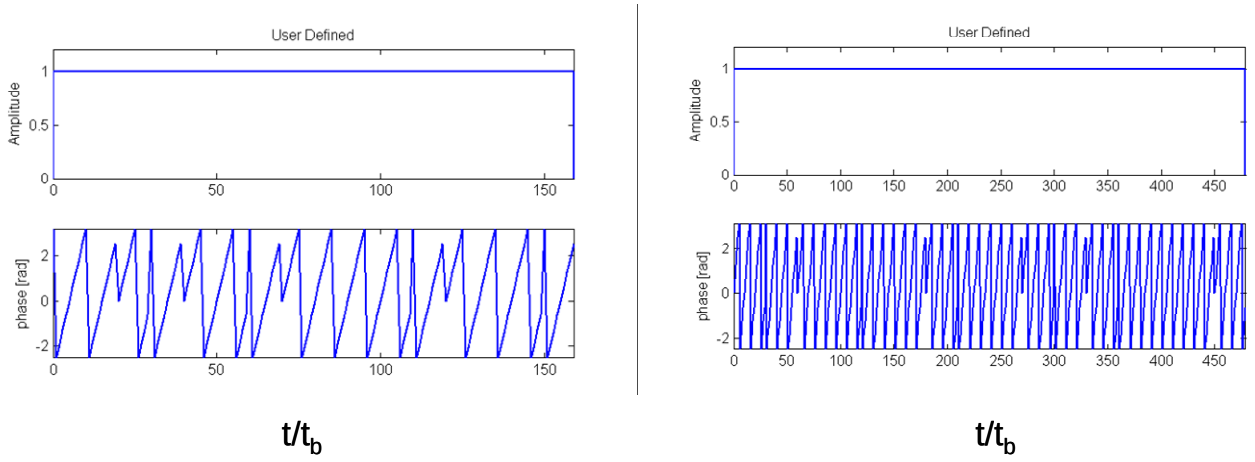

Figure 32. RBPC – Amplitude and Phase Values for cpp=1 (left) and cpp=3 (right).

The number of samples within the code period is determined by

$$N_{samples} = \frac{cpp}{f_c} * N_c * f_s \tag{22}$$

resulting in 160 ($cpp = 1$) or 480 ($cpp = 3$).

The ACF and the PACF are shown in Figure 33. The peak sidelobes appear at approximately –10 dB down from the main lobe. Also note the mainlobe width is much larger than the other RSR and RNR emitters. The PAF is shown in Figure 34 and illustrates the large sidelobes that occur with $N_c = 16$. Note again that the zero-Doppler cut of the PAF is the PACF.

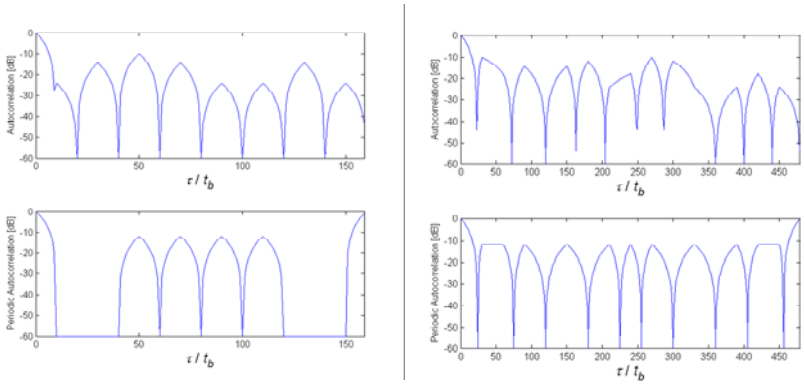

Figure 33. RBPC – ACF & PACF Parameters.

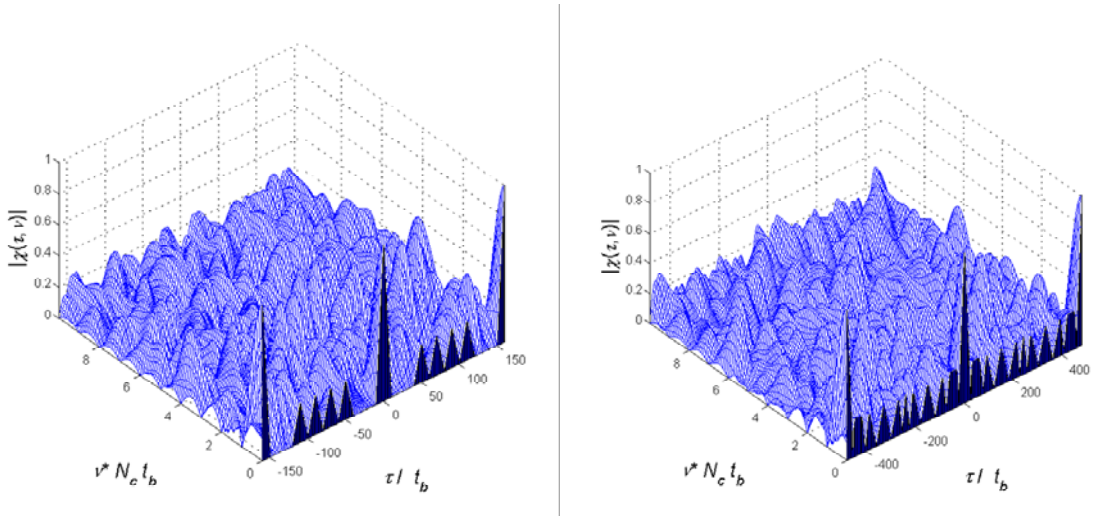

Figure 34. RBPC – Periodic Ambiguity Function $N_c = 16$.

The PACF and PAF illustrate high sidelobes with this RSR model. Thus, this radar is expected to have challenges with the range resolution, Doppler, and response to clutter.

III. INTERCEPT RECEIVER SIGNAL PROCESSING AND DETECTION RESULTS

A. ANALYSIS TOOLS FOR SIGNAL DETECTION PROCESSING

This section presents the time-frequency and bi-frequency signal processing methods used to analyzed the RSR and RNR waveforms discussed in the previous section.

1. Quadrature Mirror Filter Banks

Quadrature mirror filter bank (QMFB) techniques perform a wavelet decomposition of the input signal and have good capability to extract the time-frequency characteristics of the intercepted waveform such as the carrier frequency, code rate, bandwidth, modulation period, and phase changes [8]. The non-cooperative intercept receiver uses the QMFB to analyze the signal in layers. As the signal propagates through the layers, a tradeoff in time and frequency resolution is obtained [8]. That is, at the first layer, the resolution is large in frequency but small in time. As the number of layers increases, the frequency resolution gets smaller as the time resolution gets larger. Figure 35 below illustrates the layer structure within the QMFB and the tradeoff in time and frequency resolution that occurs. Each wavelet pair of filters consist of one highpass filter (G) and one lowpass filter (H) as shown within the tree structure.

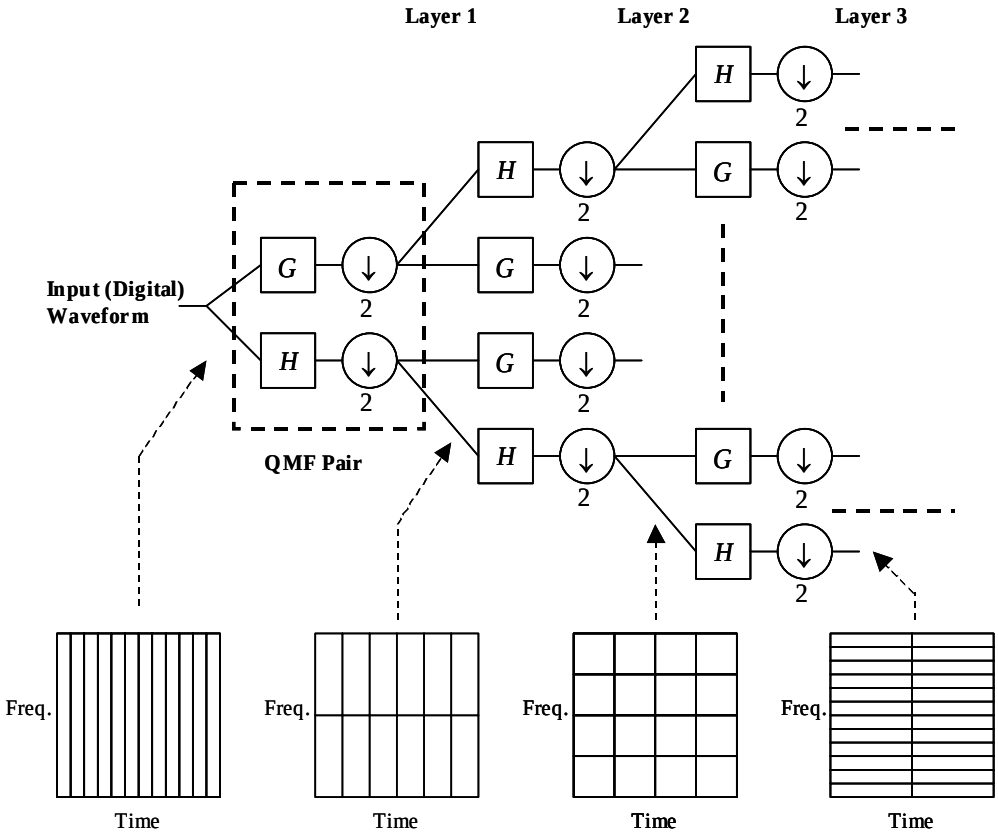

Figure 35. QMFB Filter Bank Tree.

The frequency resolution for any layer *l* is [8]

$$\Delta f = \frac{f_s}{2\left(2^l - 1\right)} = \frac{f_s}{N_F} \tag{23}$$

where L is total number of layers, N_F is the number of tiles displayed in frequency, and f_s is the sampling frequency. The time resolution for any layer *l* is [8]

$$\Delta t = \frac{2^L}{f_s\left(2^{L-l} - 1\right)} = \frac{f_s}{N_T} \tag{24}$$

where N_T is the number of tiles in time. By selecting the correct layer, the observer can identify the waveform parameters of interest. To determine the total number of layers, the QMFB MATLAB code displays the number of layers

necessary to process the signal. The number of layers depends upon the record length (2^L). Zero padding is used if the number of samples within the intercepted signal is not a power of 2.

Getting started with the QMFB time-frequency tool, the GUI in Figure 36 below shows what data was needed for execution:

Figure 36. QMFB Implementation GUI.

The emitter model produced a data file, which was used for the input signal; along with the proper directory. Of particular importance was the ADC sampling frequency (3 GHz), which carried over from the emitter model. The layer selection was consistently chosen at 6, as this provided a good trade off in time and frequency resolution to illustrate detection results. One exception

however, was realized in the RBPC model analysis, where layer 2 was chosen for accurate time resolution. This resolution was necessary to correlate the peaks and valleys of the QMFB results with the phase changes from the intercepted signal. Other signal characteristics, such as bandwidth and carrier frequency, were also observed and are available in Layer 9 or 11. Layer 11 is the highest odd numbered layer displaying the signal characteristics with high frequency resolution.

2. Cyclostationary Signal Analysis

Since all digital signals have some parameters that vary with time, better spectral analysis results can be obtained if signals are modeled as a cyclostationary process. Classifying digitally modulated signals as cyclostationary means their characteristics fall into two general definitions. First, their probabilistic parameters, mean and correlation, vary in time with single or multiple periodicity. Second, there is a non-zero correlation exhibited between certain frequency components when their frequency separation is related to the periodicity of interest (e.g., symbol rate, carrier frequency). That is, the signals have spectral correlation, where the signal is correlated with frequency shifted versions of itself, at certain frequency shifts**.** For example, a signal *x*(*t*) is cyclostationary with cycle frequency α if and only if, some of its delay product waveforms $z(t) = x\left(t-\tau\right)x^{*}(t)$ (for some delays) exhibit a spectral line at a frequency α. In the spectral domain, cyclostationarity is evident as a spectral correlation. The spectral correlation properties of the signal are evident in cyclic autocorrelation function $R_x^{\alpha}(\tau)$ and the spectral correlation density (SCD) function $S_x^{\alpha}(f)$.

The cyclic spectral density or cyclic spectrum is given as

$$S_x^{\alpha}(f) = \Im\left\{R_x^{\alpha}(\tau)\right\} = \lim_{T\to\infty}\frac{1}{T}X_T\left(f+\frac{\alpha}{2}\right)X_T^*\left(f-\frac{\alpha}{2}\right) \tag{25}$$

where α is the cycle frequency and

$$X_T(f) = \int_{\frac{-T}{2}}^{\frac{T}{2}} x(u)e^{-2j\pi fu}du$$

is the Fourier transform of the time-domain signal $x(u)$. The cyclic spectral density exists on the two-dimensional bi-frequency plane with frequency f and cycle frequency α [8].

Two methods to estimate the cyclic spectral density are the time-smoothing FFT accumulation method and the direct frequency-smoothing method. For this work, the time smoothing FFT accumulation method (TFAM) is used. Figure 37 below shows a block diagram of the TFAM.

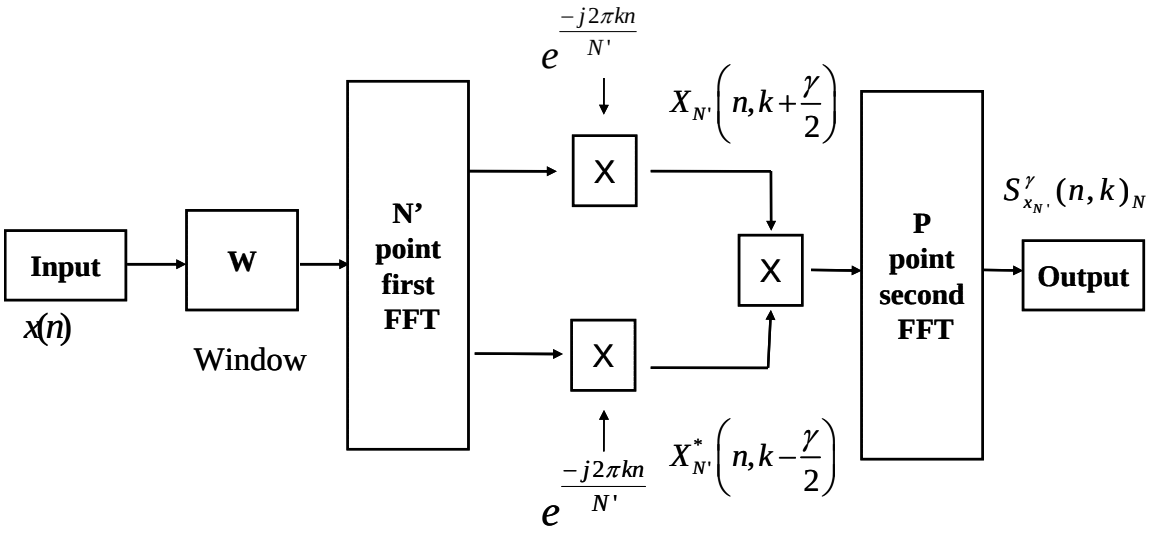

Figure 37. Block Diagram – Cyclostationary TFAM.

The TFAM divides the frequency plane into smaller channel pair regions and FFTs one block at a time in an effort to reduce the number of computations required to estimate the SCD. The signal is first windowed with e.g., a Hamming window. Then a sliding *N*' point short FFT is generated followed by a baseband

frequency translation. The correlation product is then formed and the output is smoothed with a second *P* point FFT to generate the SCD $S_{x_N}^{\gamma}(n,k)$. Here γ is the cycle-frequency and *k* is the frequency (change of variables due to a discrete version of the SCD).

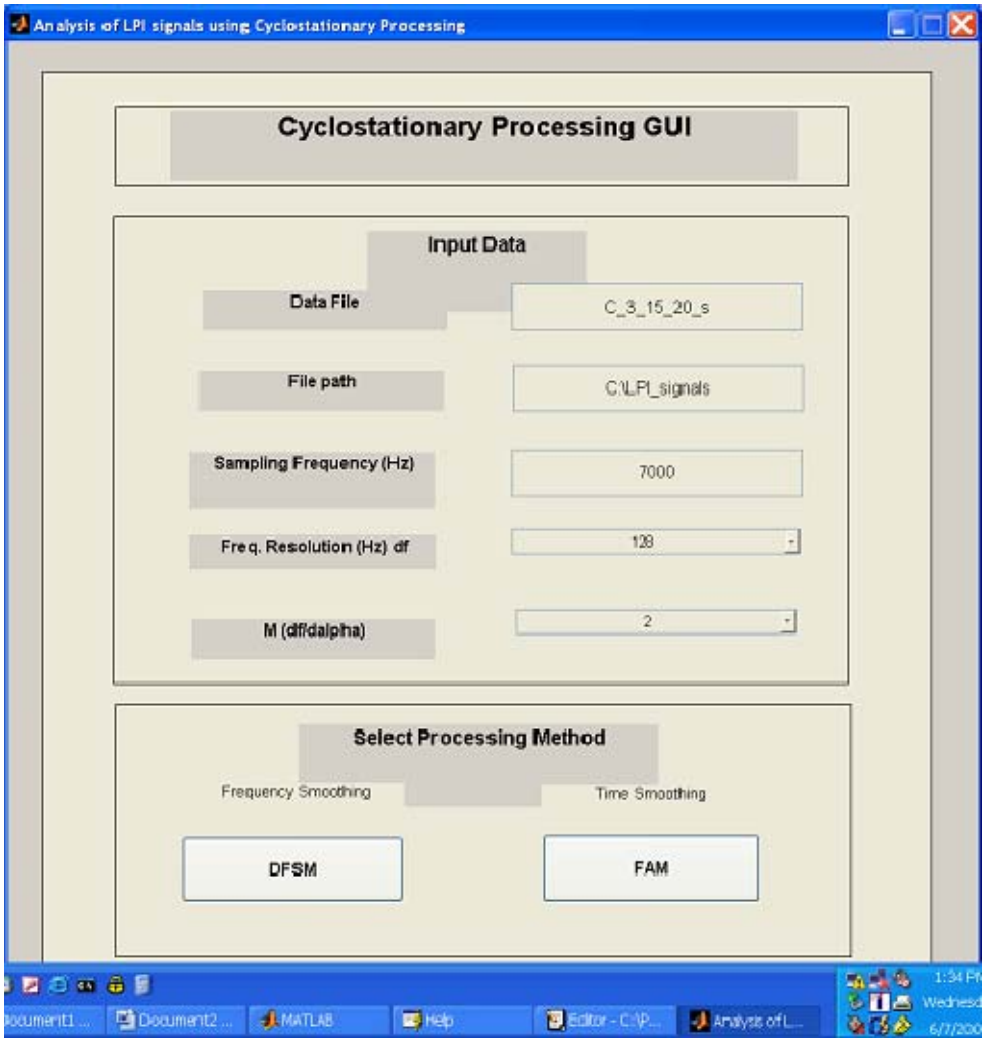

Figure 38. Cyclostationary GUI.

Software computation of the SCD using the TFAM was done using MATLAB and the GUI shown in Figure 38. Parameters needed include the ADC sampling frequency used (3 GHz) the frequency resolution *df* (10 MHz) and the Grenander's uncertainty value *M* (*M* = 2). The setup also requires the file name, and file directory.

B. RANDOM NOISE RADAR MODEL

1. QMFB

The QMFB detection results for the RNR are shown in Figure 39 for layer 6. As observed in layer 6 the noise bandwidth of 300 MHz and duration of signal (4 μsec) are evident on the time frequency plane. The signal is centered at a frequency of $f_c = 350$ MHz.

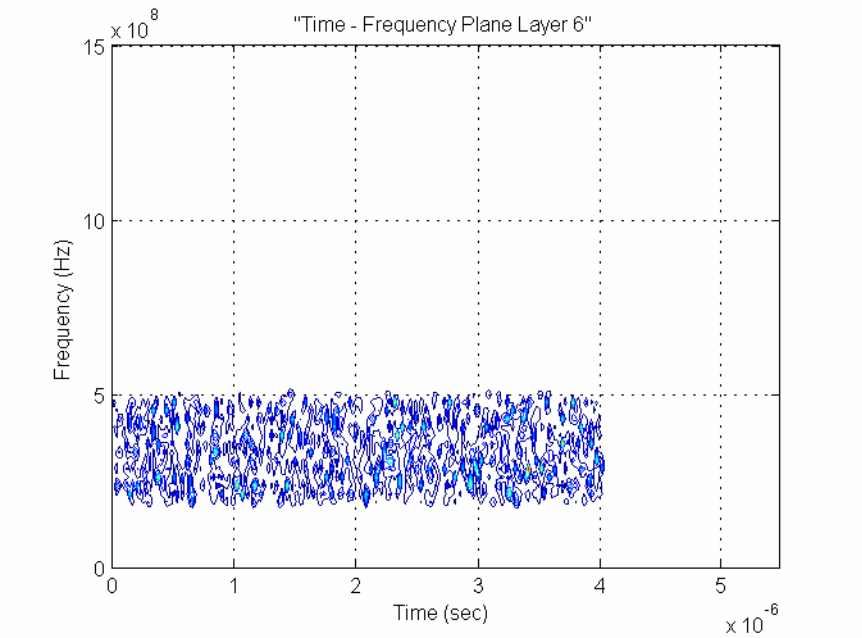

Figure 39. QMFB for RNR, f_c = 350 MHz, Noise *B* = 300 MHz.

Note determining the distribution of the noise is a subject beyond the scope of this thesis and a subject of future study. The 100 MHz noise bandwidth waveform (not shown) revealed similar results, with the bandwidth 1/3 the size observed in Figure 39 above.

Concluding these results, it would be obvious to the trained operator that an artificial noise signal with no modulation has been intercepted. It could be reasoned the QMFB is an effective tool against the Narayanan model of RNR.

2. Cyclostationary

In this application, the TFAM technique is used to estimate the SCD for the RNR signal. From the plot shown in Figure 40 below, one can observe the signal appearing in four separate locations on the bi-frequency plane. This is due to the quadrant symmetry of the SCD.

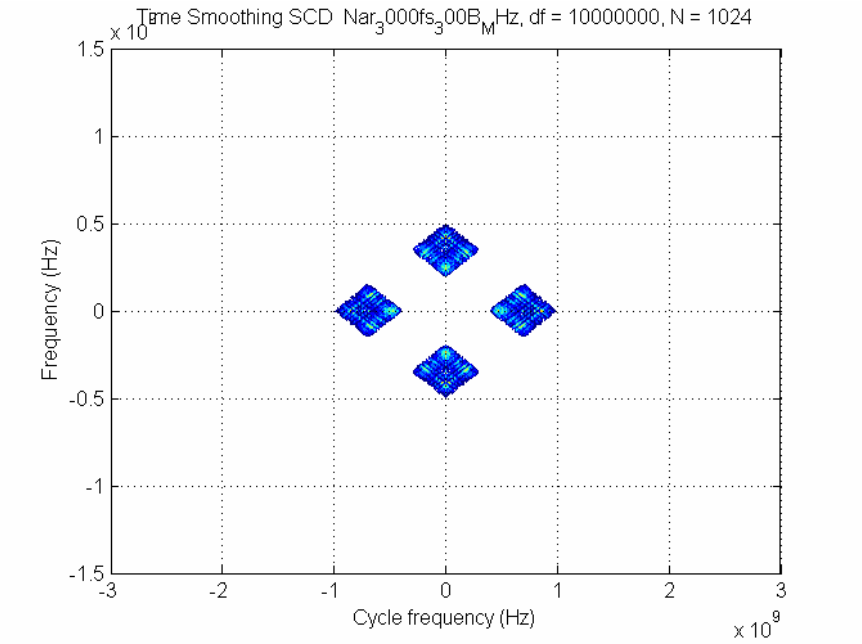

Figure 40. CSA for RNR, f_c = 350 MHz, Noise *B* = 300 MHz.

Looking closely at the right-most quadrant, Figure 41 shows several distinctive features. As expected, the noise is centered at twice the carrier frequency (700 MHz) along the cycle frequency (x) axis. Also, the noise bandwidth of 300 MHz can be identified on both the cycle frequency axis (from midpoint to either end of the diamond) or the frequency axis (diamond tip to diamond tip).

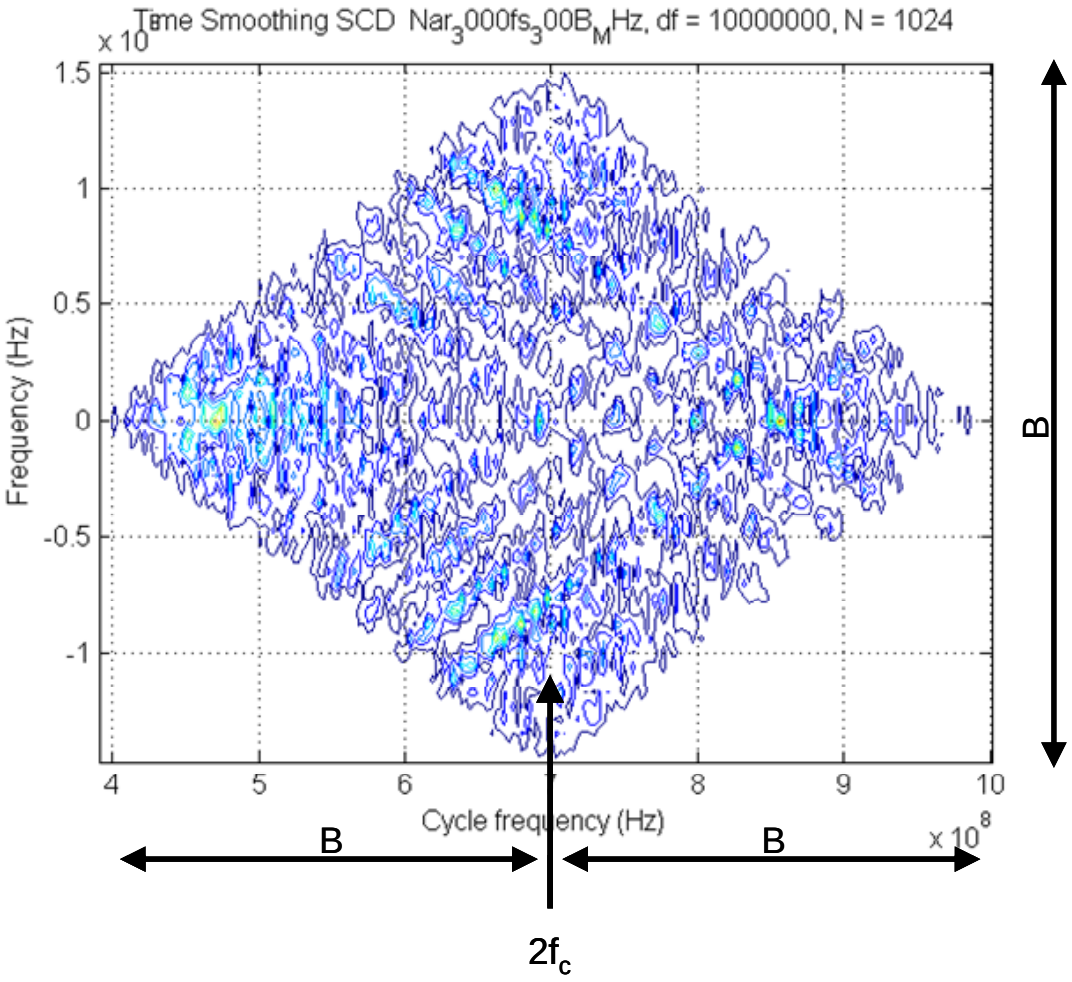

Figure 41. CSA for RNR, f_c = 350 MHz, Noise *B* = 300 MHz – zoomed.

Summarizing, the cyclostationary results on the RNR signal gives a significant indication of the noise emitter in the SCD. It could be reasoned this bi-frequency tool is effective against RNR signals. With experience, the operator can use the bi-frequency results not only to measure the waveform parameters but to also identify which type of emitter is present.

C. RANDOM SIGNAL RADAR – NOISE FMCW RADAR

In this section, the time-frequency and bi-frequency analysis tools are used to examine the characteristics of the noise FMCW radar. The signal intercepted is a noise modulated triangular FMCW signal centered at $f_c = 350$

MHz with modulation bandwidth $\Delta F = 300$ MHz (200 MHz to 500 MHz). For this emitter, two modulation cycles are transmitted and intercepted. The noise bandwidth examined the SCD with the QMFB and is *B* = 300 MHz (200 MHz to 500 MHz). The ADC sampling frequency is $f_s = 3$ GHz.

1. QMFB

In this example, the noise bandwidth is *B* = 300 MHz. Within the QMFB *L* = 12 layers, layer 6 is used to identify the significant information about the intercepted signal since this layer presents a good trade-off in identifying the waveform parameters in both time and frequency. Figure 42 shows the QMFB layer 6 for the intercepted waveform. Note the triangular shape of the linear FMCW signal is observed. Also revealed is the modulation bandwidth $\Delta F = 300$ MHz as well as the noise bandwidth of *B* = 300 MHz.

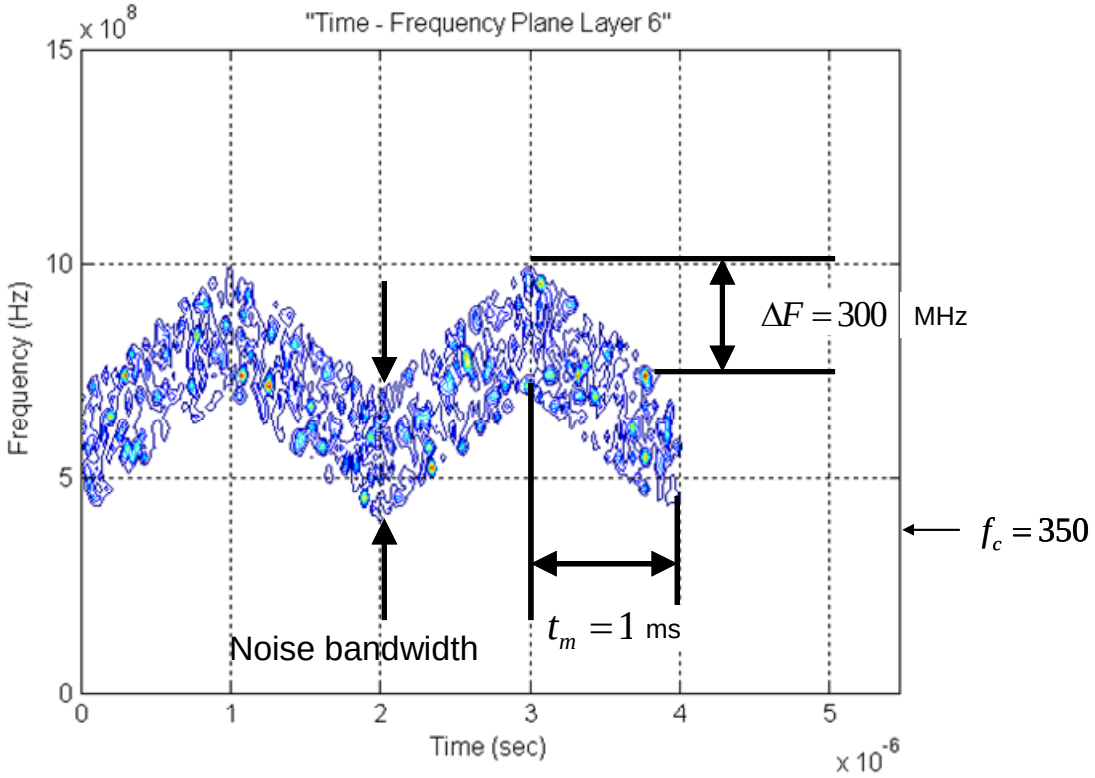

Figure 42. QMFB for Noise FMCW Radar, Noise *B* = 300 MHz.

Note from Figure 13, the total noise modulated FMCW waveform bandwidth extends from 400 MHz (200 MHz + 200 MHz) to 1000 MHz (500 MHz + 500 MHz) centered at 700 MHz. The modulation period of $t_m = 1$ μsec is also observable. In summary, the QMFB analysis can extract the important parameters of the RSR noise FMCW waveform exactly. Note that this information is not available using PSD techniques (since the phase information is not preserved in the autocorrelation function).

2. Cyclostationary

In this example, the noise bandwidth within the noise FMCW emitter is set to *B* = 300 MHz. Since in this case the noise bandwidth and the modulation bandwidth overlap, the total noise FMCW bandwidth transmitted *B* = 300 MHz. The time-smoothing technique was chosen to estimate the SCD. From Figure 43, one can observe the signal appearing in four separate quadrants on the bi-frequency plane.

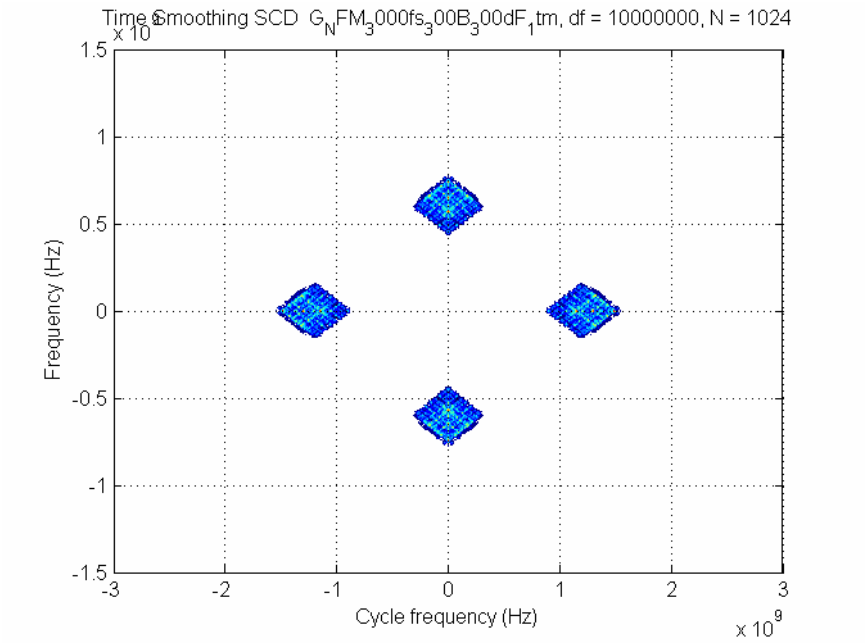

Figure 43. CSA for Noise FMCW, f_c = 350 MHz, $\Delta F = 300$ MHz, Noise *B* = 300 MHz.

Examining the right most quadrant, as shown in Figure 44 below, the diamond is centered at 1200 MHz, which is twice the center frequency of the modulated signal. Theoretically, the center frequency is expected at 1400 MHz, from twice the center frequency of the two modulated signals (350 MHz for the noise and 350 MHz for the FMCW signal). The difference of 200 MHz is observed as an offset through several scenarios changing the FMCW modulation bandwidth as shown in Table 5 below.

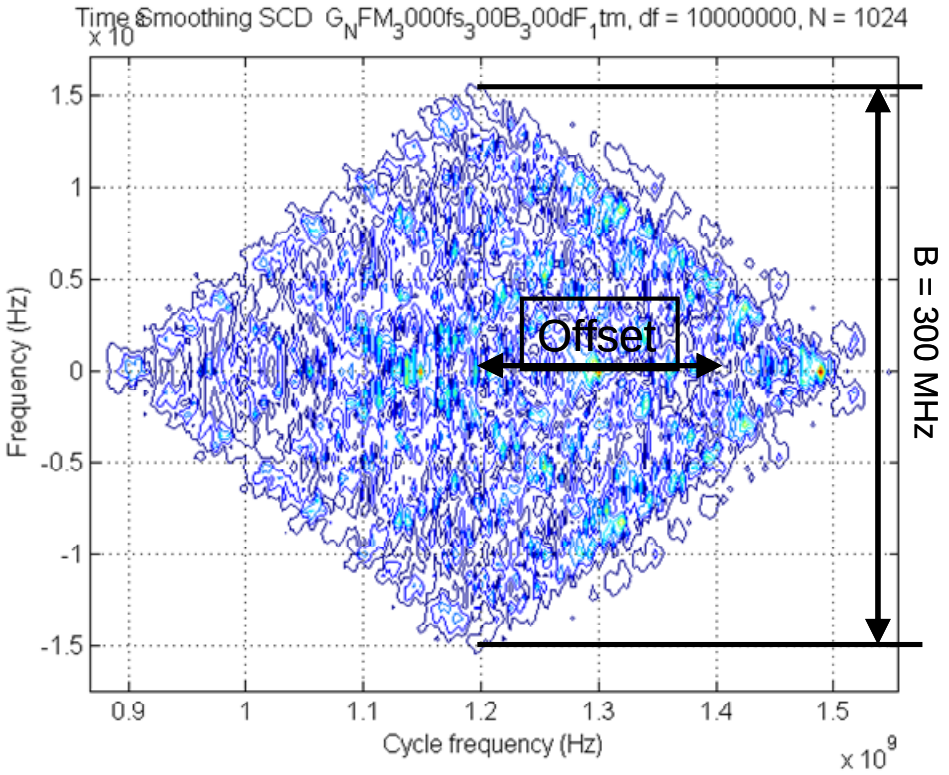

Figure 44. CSA for Noise FMCW, f_c = 350 MHz, $\Delta F = 300$ MHz, Noise *B* = 300 MHz.

ΔF (MHz)	Offset (MHz)	Center frequency observed (MHz)
500	250	1150
300	200	1200
200	100	1300
100	50	1350
1	0	1400

Table 5. Noise FMCW Modulation Bandwidth Effects.

Other signal characteristics, such as the signal bandwidth of $\Delta F = 300$ MHz can be measured along the cycle frequency axis, as expected. The bandwidth can also be measured along the frequency axis as well. This sweep bandwidth shows nicely in the QMFB results. Thus, there is enough information for the trained operator to notice an unnatural signal is the captured emission.

In summary for the cyclostationary results on the RSR signal, there is significant indication of a source signal. It could be reasoned the time-frequency and bi-frequency tools are effective against the Noise FMCW signal.

D. RANDOM SIGNAL RADAR – SINE PLUS NOISE FMCW RADAR

In this section the time-frequency QMFB and the bi-frequency CSA are applied to the Sine Plus Noise FMCW intercepted waveform. The transmitted signal is the same noise modulated triangular FMCW signal as in Section C, however there is an additional tone signal at ($f_T = 350$ MHz) modulation that is present. To review, the noise bandwidth extends from 200 MHz to 500 MHz and the FMCW modulation bandwidth extends from 200 MHz to 500 MHz. Modulation by the tone signal at 350 MHz creates the noise in two bands. The upper band extends from 750 MHz to 1350 MHz while the lower band extends from 50 MHz

to 650 MHz. As shown in Figure 22, the lowpass filter retains the lower side band for transmission (50 MHz to 650 MHz).

1. QMFB

Layer 6 is again chosen to extract the parameters of the intercepted waveform. Figure 45 below shows the results of the two triangular waveforms that are intercepted. Note that the total waveform bandwidth is 600 MHz (50 Hz to 650 Hz) centered at 350 MHz as expected. Also shown is the noise bandwidth of *B* = 300 MHz evident about the FMCW waveform. The modulation period of the triangular waveform is also easily determined as $t_m = 1\,\mu$ s.

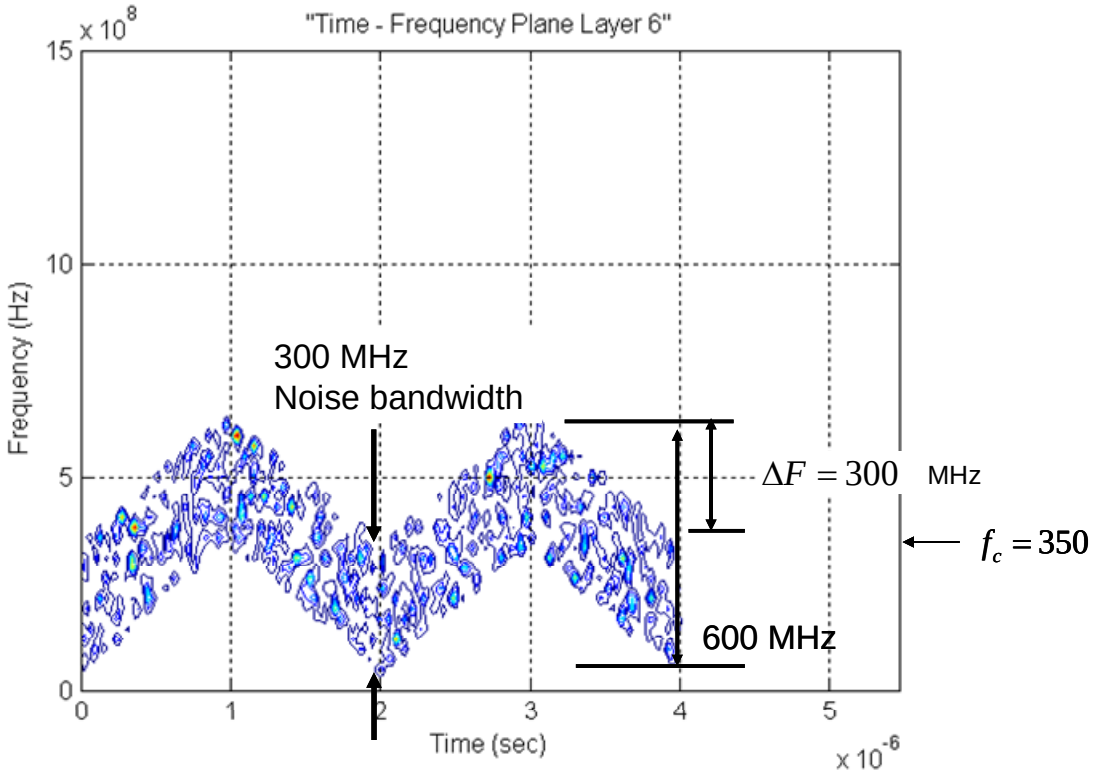

Figure 45. QMFB for Sine Plus Noise FMCW, f_c = 350 MHz, Noise *B* = 300 MHz.

In summary, to the trained operator the QMFB can correctly extract the parameters of the noise FMCW plus sine waveform demonstrating that the QMFB represents an effective tool against this form of RSR.

2. Cyclostationary

In this application, the time smoothing technique was chosen to estimate the SCD. As in other results, the signal appears in four separate locations. In addition, the signal in Figure 46 below is modulated by a noise signal with 300 MHz wide bandwidth.

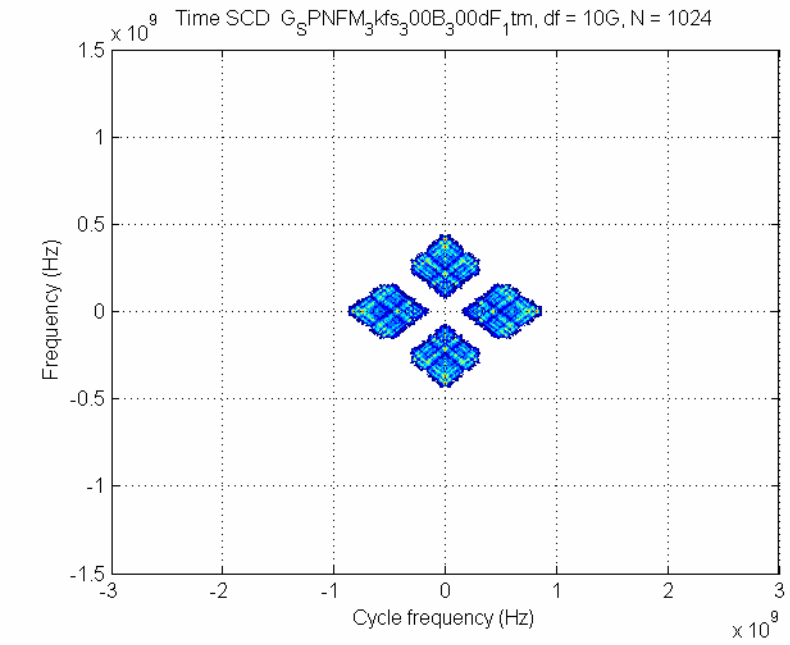

Figure 46. CSA for Sine Plus Noise FMCW, f_c & f_{noise} = 350 MHz, Noise *B* = 300 MHz.

Examining the right most quadrant, as shown in Figure 47, the diamond is centered at 525 MHz, which is twice the center frequency of the modulated signal. Theoretically, the center frequency is expected at 1400 MHz, from twice the center frequency of the two modulated signals (350 MHz for the noise and

350 MHz for the FMCW signal). The difference of 200 MHz is observed as an offset through several scenarios changing the FMCW modulation bandwidth as shown in Table 5.

For the carrier frequency, the signal frequency intercepted is that of the low-passed, compound Sine Plus Noise FMCW signal, centered at 350 MHz, and is 180 degrees out of phase. This phase shift effectively pulls the noise modulation from the cyclostationary results. Although the shape is expected to be centered at twice this frequency, it appears to be centered 200 MHz to the left of the expected value of 700 MHz (twice the 350 MHz FMCW center frequency). Again the offset shows as in the Noise FMCW model in Table 5. The results of Figure 47 below still provide the trained operator enough information to flag the signal of interest.

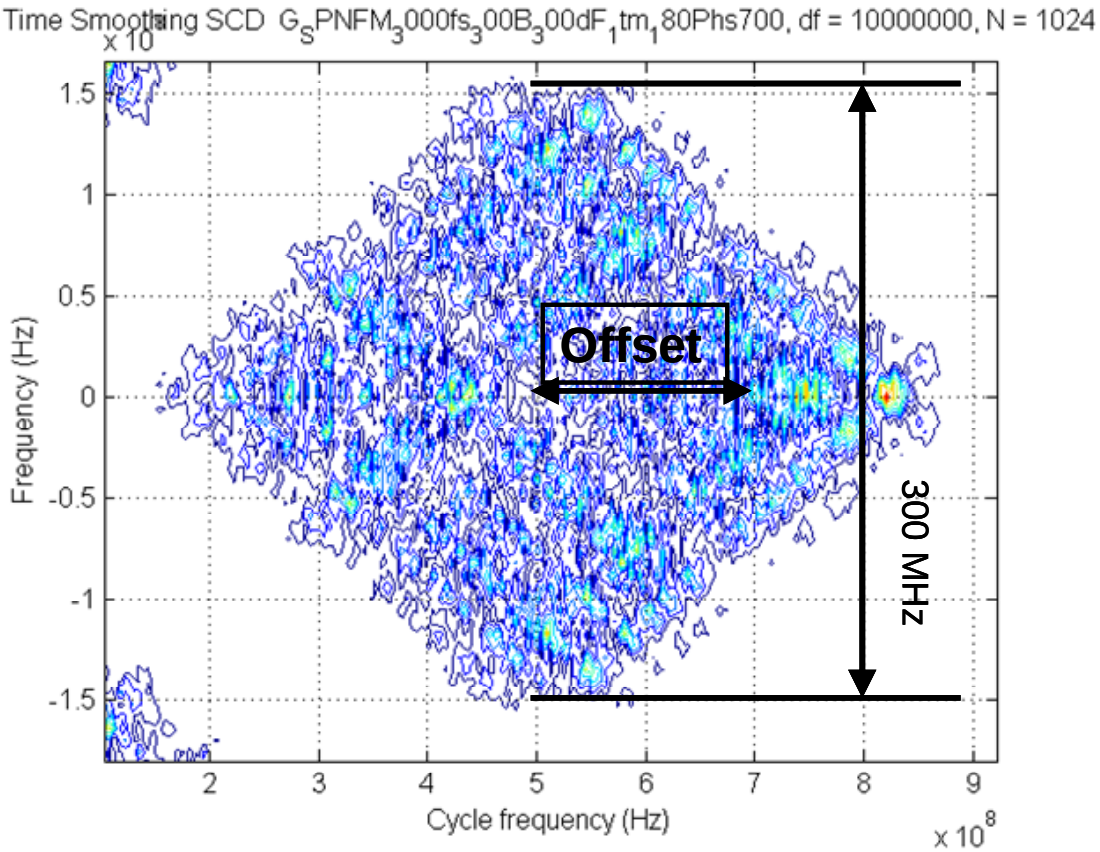

Figure 47. CSA for Sine Plus Noise FMCW, f_c & f_{noise} = 350 MHz, Noise *B* = 300 MHz – zoomed.

Examining the zoomed view in Figure 47 above, the cycle frequency (x) axis length of this shape displays twice the bandwidth, or 600 MHz wide (200-800 MHz on the figure), as expected. Along the frequency (y) axis, the bandwidth of 300 MHz is observed, as expected. One interesting point however is the centering of the shape. For any signal, the resultant shape is expected at twice the center frequency. Therefore, the signal is expected at 700 MHz, but with compounded noise modulation, the centering is at 500 MHz. Thus, there is enough information for the trained operator to notice an unnatural signal in the intercepted emission.

In summary for the cyclostationary results on the RSR signal, there is significant indication of a source signal. It could be reasoned the time-frequency and bi-frequency tools are effective against the Sine Plus Noise FMCW model of RSR.

E. RANDOM SIGNAL RADAR – RANDOM BINARY PHASE-CODED CW RADAR

The RBPC radar uses a random phase modulation to achieve LPI characteristics. The tone signal used is $f_T = 300$ MHz. This tone frequency was chosen to later compare QMFB and cyclostationary results with the previous two RSR models. The phase change for each subcode is randomly selected as either 0 or π. Both *cpp* = 1 (*B* = 300 MHz) and *cpp* = 3 (*B* = 100 MHz) are investigated. The ADC sampling frequency is $f_s = 3$ GHz.

1. QMFB

To extract signal characteristics with the QMFB, a range of layers were explored. Twelve layers were generated for the RBPC waveform. For fine time resolution Layer 2 is shown in order to examine the phase information of the intercepted signal. Correlation of the layer 2 phase change with that of the transmitted signal illustrates the unique capabilities of the QMFB. For fine frequency detail the middle QMFB layers are most useful (e.g., layer 5 or 6).

Details such as the bandwidth and carrier frequency can be easily observed since the middle layers represent a good tradeoff between time and frequency resolutions.

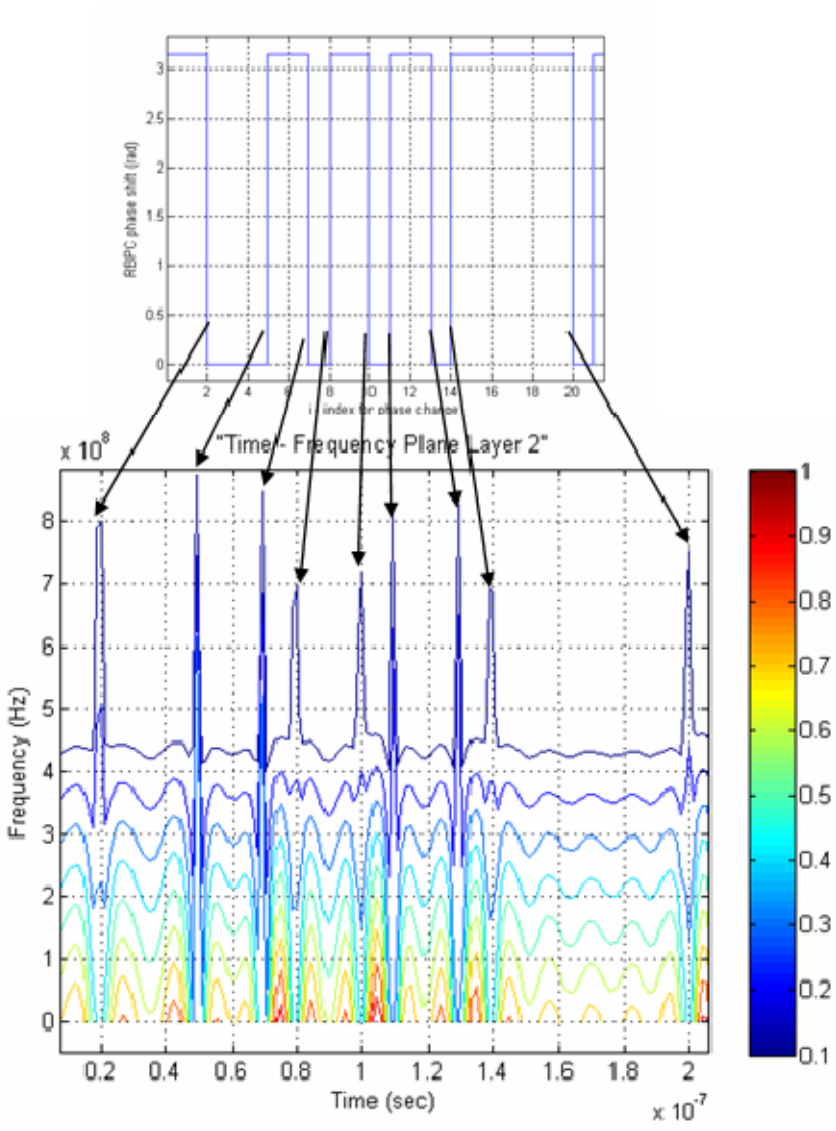

Figure 48. QMFB for RBPC and Correlation to Phase Change.

To demonstrate the capability of the lower layers in determining the exact structure of the intercepted waveform, Figure 48 (top) shows the random phase values that were used to generate an RBPC LPI waveform with $f_c = 300$ MHz

and *cpp* = 3 (*B* = 100 MHz). Each subcode width is $t_b = 10$ ns. In Figure 48 (bottom), the layer 2 results for this waveform are shown. Note that the positions of the phase change are readily noticed within the layer 2 results and correlate well with the random phase values that were used. In Figure 49, layer 5 is examined for cpp=1 (*B* = 300 MHz) and layer 6 for cpp=3 (*B* = 100 MHz). The carrier frequency and bandwidth are both observable to the operator.

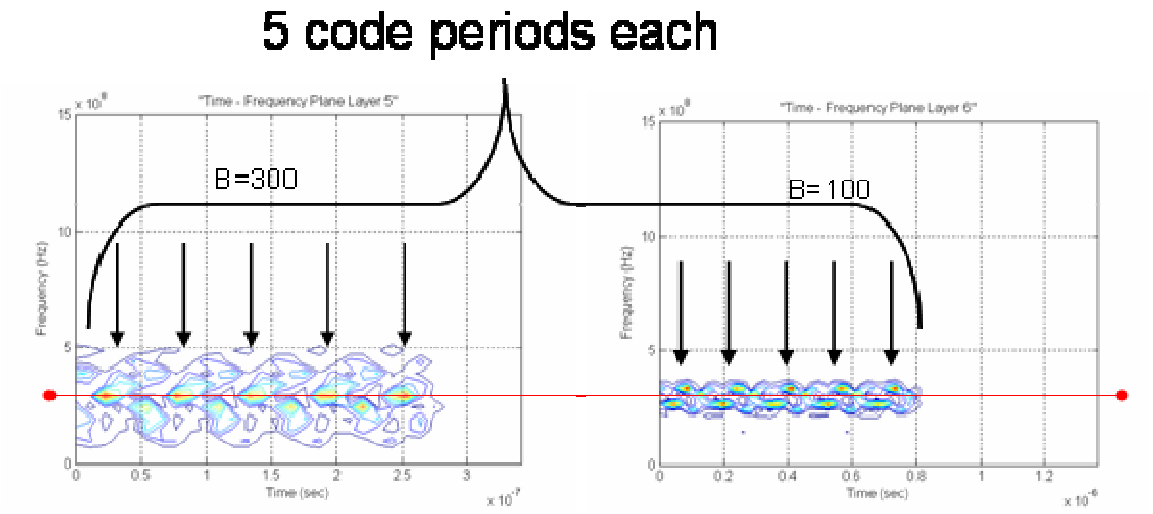

Figure 49. QMFB for RBPC, f_c = 300 MHz, cpp Disparity.

For fine frequency information, the higher order layers can be examined. For example, Figure 50 below shows layer 9 for a *cpp* = 1 and layer 11 for a *cpp* = 3 (center frequency of 300 MHz). Note that the duration of the signal cannot be determined due to the large (coarse) resolution in time that occurs with the upper layers.

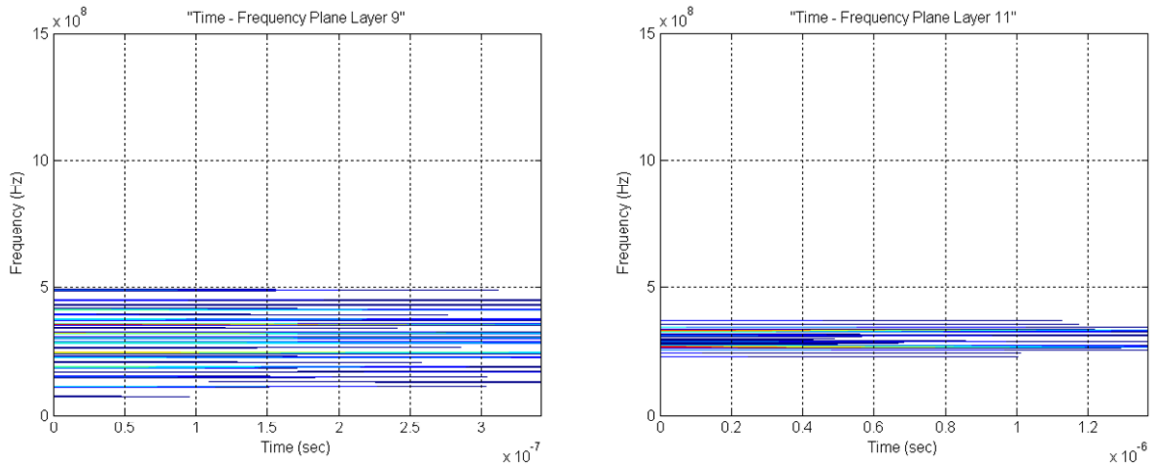

Figure 50. QMFB for RBPC – Frequency Resolution.

In summary, the QMFB is highly effective for determining the presence of the random binary phase modulation waveform. The layer that is used is dependent on the type of information being extracted. Detailed phase analysis can be conducted using the lower layers however the presence of noise can degrade this capability. To the trained operator the QMFB represents an effective tool against the RBPC CW model of RSR.

2. Cyclostationary

The cyclostationary tools applied to the RBPC model of RSR is examined below. The signal shown is a common 300 MHz tone. For computational simplicity, the cyclostationary frequency resolution (df) was 10 MHz and the Grenander's uncertainty value *M* = 2. The first set of results will illustrate the $cpp = 1$ waveform as shown in Figure 51 below. Note the four quadrant symmetry that is present as well as the difference in signal texture. Figure 51 shows the zoom view into the right-most quadrant,

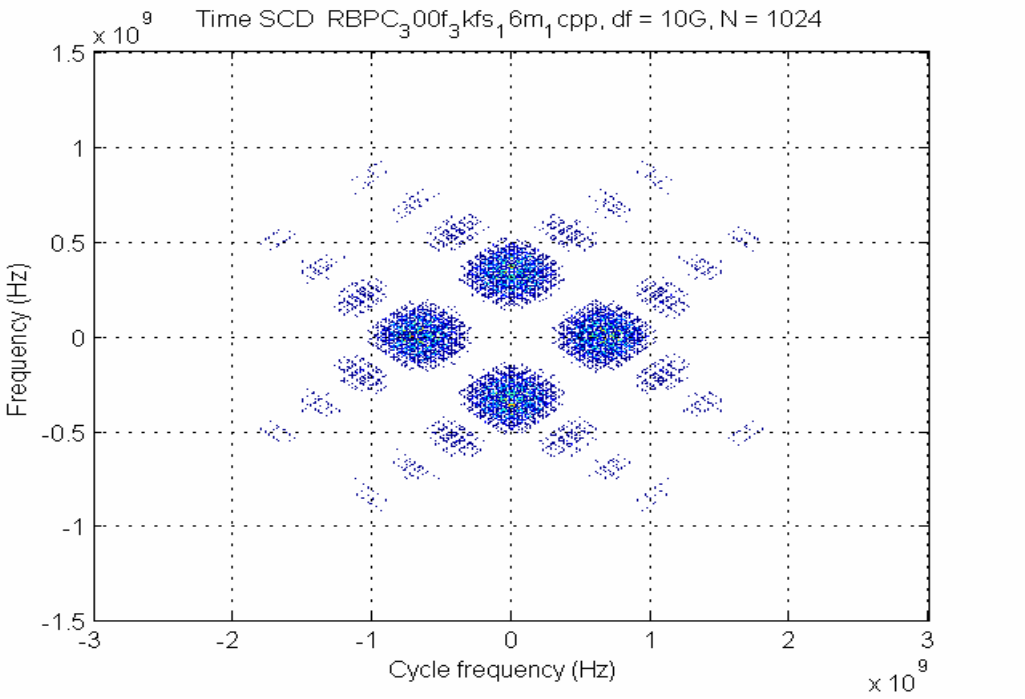

Figure 51. CSA for RBPC, f_c = 300 MHz, cpp=1.

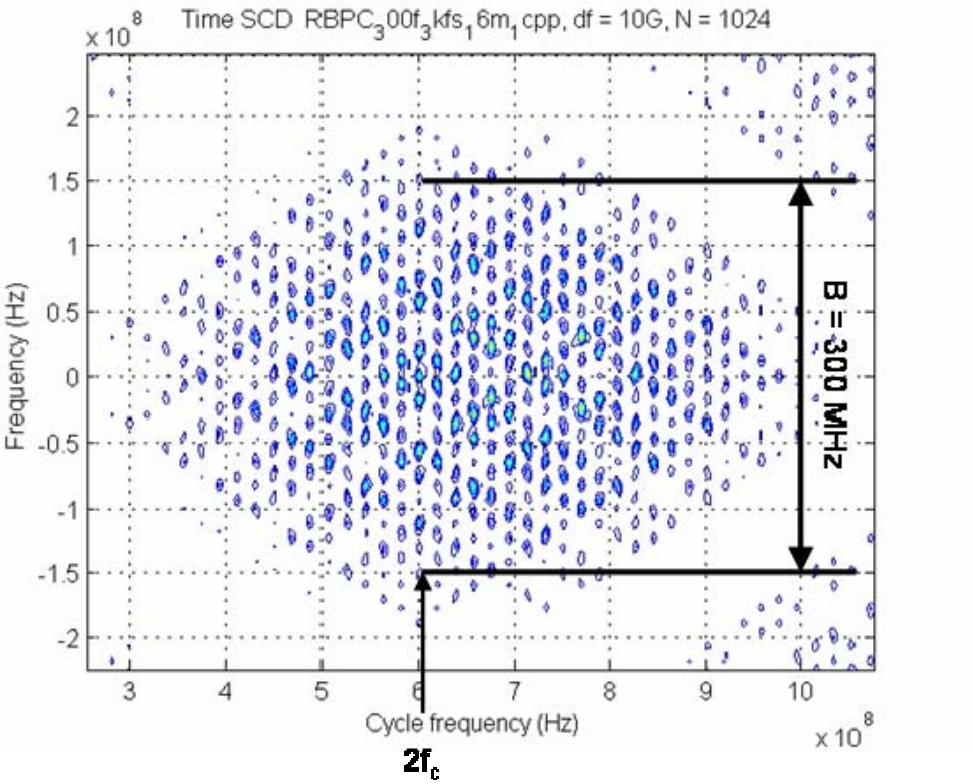

Figure 52. CSA for RBPC, f_c = 300 MHz, cpp=1 – zoomed.

The waveform is centered upon twice the carrier frequency or $2f_c = 600$ MHz along the cycle frequency axis. The bandwidth can also be measured along the cycle frequency axis from the midpoint of 600 MHz to the right edge of the diamond or from the midpoint to the left edge of the diamond as shown. The bandwidth can also be measured along the frequency axis as shown.

Figure 53 examines the case with for *cpp* = 3 (*B* = 100 MHz). Note the difference in bandwidth is immediately apparent on the bi-frequency plane.

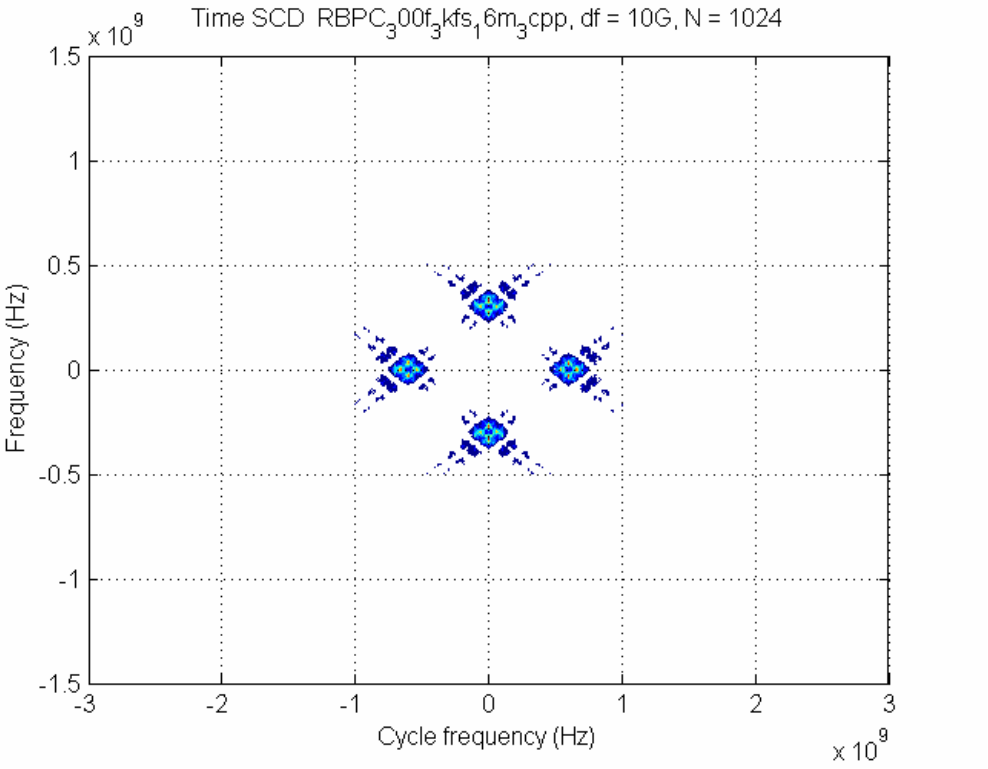

Figure 53. CSA for RBPC, f_c = 300 MHz, cpp =3.

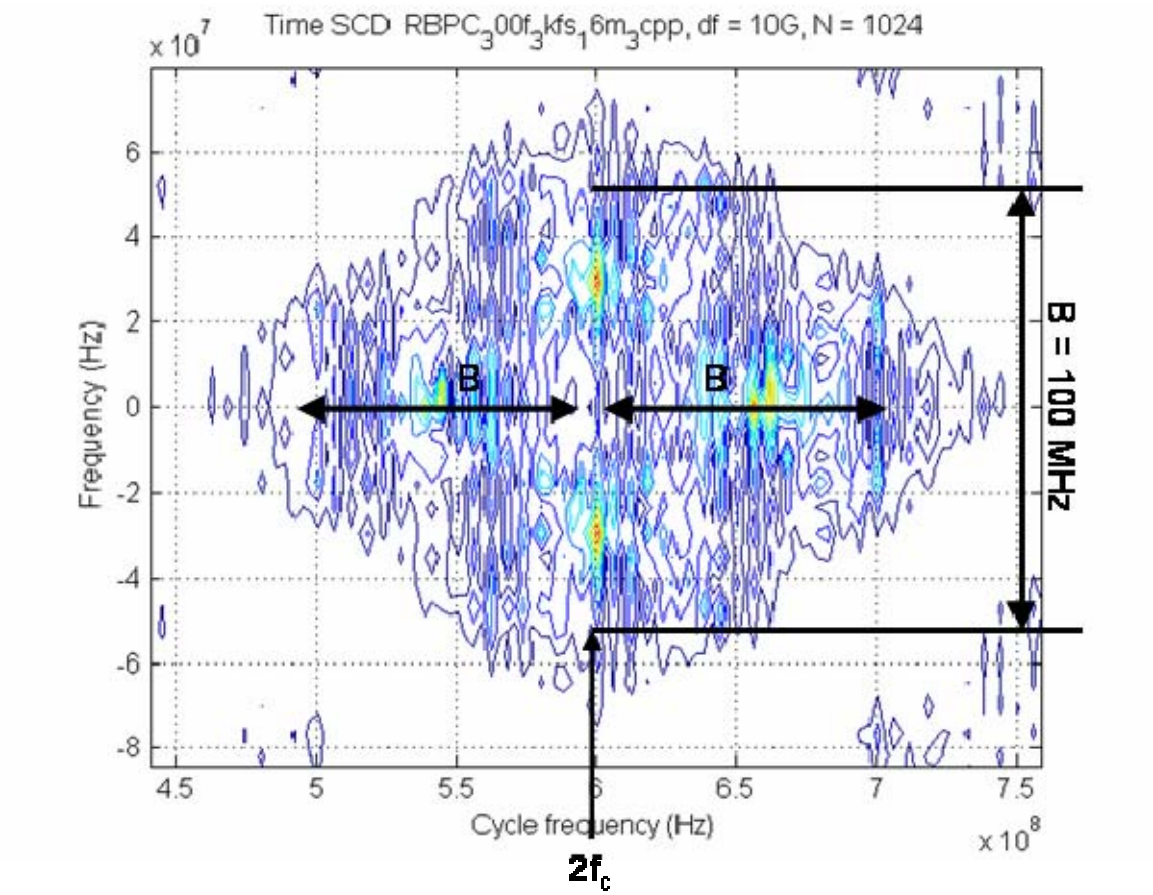

Figure 54. CSA for RBPC, f_c = 300 MHz, cpp=3 – zoomed.

Zooming into the right most quadrant, the waveform is again centered at 600 MHz or twice the carrier frequency of 300 MHz. The bandwidth also can be measured as shown along the cycle frequency axis and frequency axis.

In summary, the cyclostationary results on RBPC signal show good waveform details in both the cycle frequency axis and frequency axis and represents an effective tool against the RBPC CW model of RSR.

THIS PAGE INTENTIONALLY LEFT BLANK

IV. CONCLUSION

A. FINDINGS ON NOISE TECHNOLOGY RADAR

The basic approach taken in this research was to model the noise technology radar transmitter techniques found in the literature. Both the RSR and RNR LPI techniques were modeled. From the non-cooperative intercept receiver's perspective, the LPI waveform was digitized (in-phase and quadrature components) and both time-frequency and bi-frequency signal processing techniques were used to identify the waveforms as well as extract the signal parameters. From the preliminary analysis in this thesis, the conclusion is that these techniques are highly effective against the RSR and RNR noise technology emitters.

Significant other research was reviewed and contributed to the understanding of the noise technology concepts being examined. These references (23–41) are listed in the Reference section at the end of this thesis. They range from alternate research paths and application by the leading authors, to modifications by other researchers worldwide seeking to improve on the leading architectures of RNR and RSR. Further research into aspects of noise technology radar would benefit by review of these references.

1. Random Noise Radar

Observing the time-frequency tools shows the QMFB can clearly extract the bandwidth and center frequency from the intercepted RNR signal. The cyclostationary analysis also gives us solid frequency and bandwidth information. Concluding these results, it would be obvious to the trained operator that an artificial signal is in the noise.

2. Random Signal Radar

Regarding the Noise FMCW radar, the transmitted signal characteristics such as the ramp frequency, FMCW modulation bandwidths, and a modulation

period of 1 μsec clearly come forward in the QMFB time-frequency tool. This applies for all noise bandwidth cases as well, with appropriate frequency shifts due to modulation.

An interesting discovery comes from the cyclostationary results of the Noise FMCW architecture. The noise modulation shifts the center of the shape by the lower range of the sweep (ramp) bandwidth ΔF (200 MHz). This was unexpected and a significant discovery of another signal characteristic. Further investigation may take place in follow-on study with this discovery. Standard signal characteristics were observable, such as bandwidth and modulation frequency.

Regarding the Sine Plus Noise FMCW radar, the transmitted signal characteristics show explicitly from the QMFB tool. For example, intermodulation products show explicitly, centered at 350 and 1050 MHz respectively; along with the range of FMCW modulation bandwidths (200-500 MHz). For realistic application, the upper sideband product was filtered out for increased LPI and a lack of advantage from this repeated signal. Three noise bandwidth cases were studied to reveal the ability to capture signal characteristics despite the LPI noise bandwidth variations from an emitter.

Again the cyclostationary results showed exciting results with the indication of the modulation bandwidth frequency range. This is found with close-up views of the four-shape, SCD. Results also showed the centering of the shape off by 200 MHz, coincident with the lower sweep (ramp) bandwidth frequency, for both noise modulated and non-noise modulated cases.

Regarding the Random Binary Phase-Coded CW radar, the analysis shows the QMFB to be a highly effective tool. Generic bandwidth and center frequency characteristics are identifiable in the higher layers (7-11). Looking at Layer 2, the analyst can pick out phase changes by the peaks and valleys of the QMFB. As an additional signal characteristic, distinct code repetitions in the middle (5-7) layers can be observed by a discerning operator.

Concluding with the cyclostationary results on RBPC signal, the original 300 MHz tone appears nicely even for the untrained operator for the time-smoothing approach, as expected. As with non-noise-modulated results, the signal is centered at twice the center frequency and the bandwidth is observable along the frequency (y) axis; and twice the bandwidth along the cycle frequency (x) axis. It could be reasoned the time-smoothing approach to the cyclostationary analysis is an effective tool against the RBPC CW model of RSR.

In comparison of the sidelobe performance, each noise technology architecture utilized the same analysis – examining the PAF for the highest peak sidelobe. The resultant decibel level provided insight into the estimated periodic ambiguity of the transmitting radar. Table 6 summarizes the noise radar side lobe performances.

ARCHITECTURE	**OBSERVED HIGHEST SIDELOBE LEVEL (dB)**
RNR	–12
RSR – Noise FMCW	–20
RSR – Sine Plus Noise FMCW	–22
RSR – RBPC	–10 (cpp=1) –12 (cpp=3)

Table 6. Observed Sidelobe Comparison among Noise Technology Architectures.

Considering the resolution of the charts and variability in the detection algorithms, it is concluded the observed levels to be relevant and a good predictor of ambiguity. Further investigation may take place in follow on study.

Concluding these results, the time-frequency and bi-frequency tools are effect against noise technology radar.

B. POTENTIAL APPLICATION

1. Intelligence Surveillance and Reconnaissance

Future work would find a way to realize these techniques in hardware for the global emergence of noise technology radar. Coincidental to this evolution is the emergence and increased capability for unmanned aerial systems. In this application, the physical size, speed, and mission length form a natural stealth operating scenario. Adding traditional radar on this platform would negate much of this progress. Therefore, addition of noise technology radar is a natural fit and evolutionary step to surveillance or anti-terrorism applications.

2. Model Enhancements

There were several areas in this thesis which could be the foundation for future work. One point involves Doppler. This capability is not produced in this thesis, but may be a straightforward addition by modeling the entire receiver. Early efforts in this thesis included more of the receiver, but were abandoned for the interest in intercept capability.

Another opportunity for future work may lie in examining the effect of variable observation intervals (pulse widths). There is no relationship in the model between the observation interval and sampling frequency, except to determine the number of samples used. However, this would be an interesting section in a future book on the topic, or a conference paper.

Although filtering and LO selection can help focus the bandwidth of interest, a busy signal environment would be another endeavor for future work. This analysis was conducted with one intercept receiver against one emitter signal. Future research may be more realistic considering an operating environment.

To confirm the assumption about intermittency with the RBPC radar, a future researcher could add random zeroing to the long numbers of phase codes to research any unforeseen behavior with random intermittency effects on the data. It is unexpected at this point, but not confirmed. Whatever the future holds for this technology, there is room to explore both military and civilian applications.

THIS PAGE INTENTIONALLY LEFT BLANK

APPENDIX A – OTHER WORLDWIDE EFFORTS IN RNR

A. CONTRIBUTIONS OF AXELSSON – SWEDEN

1. Approach

Mr. Sune Axelsson has research interests in sensors, modeling of terrain background, noise radar, and high-resolution (synthetic aperture) radar. He is currently working in Sweden. Mr. Axelsson's work suggests using random noise to phase or frequency modulate a sine wave as an alternative to the random signal generated by a microwave source. Several advantages emerge in this approach to noise technology radar. Initially, a higher transmitted mean power can be achieved. This can offer the radar operator improved range resolution by increasing the noise bandwidth of the modulated carrier beyond that of the modulating signal. As an additional advantage, the range sidelobes are suppressed beyond the 4 dB improvement seen through simple random biphase modulation. These distinct advantages seem attractive for applications in synthetic aperture radar mapping, altimetry, and scatterometry. For improved range correlation, Axelsson suggests an additional technique reintroducing noise before a fast, but simple analog-to-digital converter (ADC) in the return channel. This seeks to overcome the substantial integration time needed for Doppler processing [14]. This approach is extremely close to that proposed by Narayanan; therefore it is not studied in detail. As an example in Equation 9 in Axelsson [14], the sine wave modulated by noise can be written in the complex form as:

$$S(t) = A\exp\left[j\omega_o t + j\phi(t)\right] \tag{26}$$

where the amplitude A is constant and the phase $\phi(t)$ varies with time. In contrast, Narayanan allows the amplitude to be a random function of time, as described in Equation 2 in the paper, "Radar Penetration Imaging Using Ultra-wideband Random Noise Waveforms" [20]. Otherwise the logic flow and principles are the same [4]. Axelsson's approach is highlighted here because of the extensive open literature sources and the improvements, such as enhanced ADC processing.

2. Model of Transmitted Waveform

Axelsson in [3] proposes an alternative solution to the delay line idea used by other researchers. Instead of using a variable delay line applied to the reference signal, this approach variably delays the I/Q output components of the digital source signal and correlates them with the target (receive) signal I/Q components. Figure 55 below illustrates the complete receiver as:

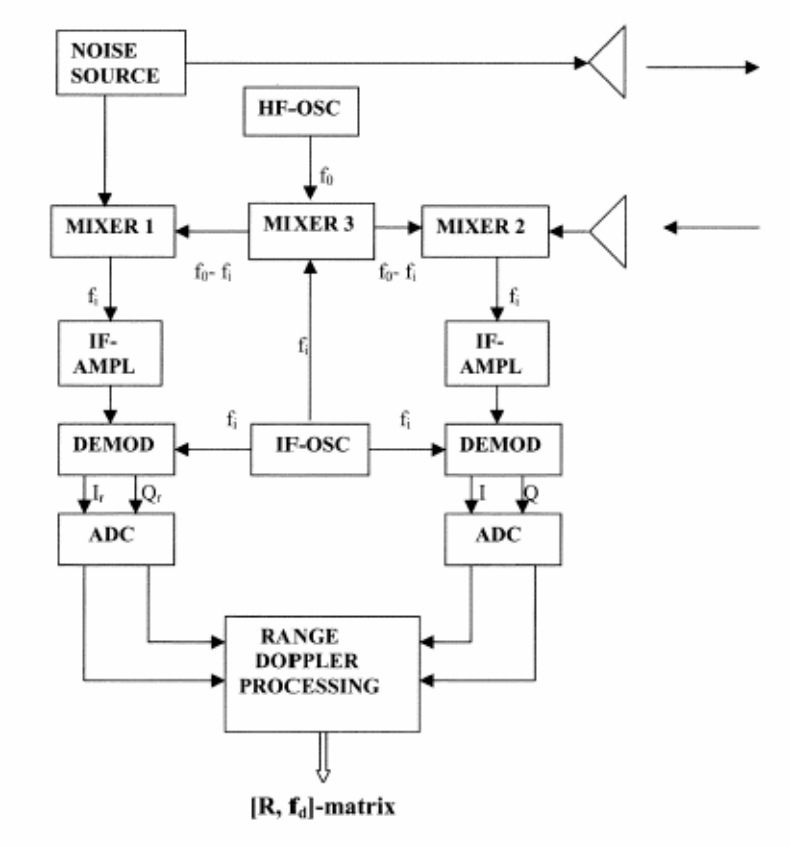

Figure 55. Block Diagram – Digital Range and Doppler Processing [From 2].

In Figure 55 above, Axelsson shows the digital delay introduced *after* the signal processing takes place to meet the speed requirements of real-time processing. After the noise source transmits the signal to the antenna, the carrier frequency (f_0) is mixed and used to offset the intermediate frequency (f_i) in MIXER3. Looking closer, the reference (transmitted) signal is variably delayed

(in the ADCs) after the signal is downconverted from the intermediate frequency (f_i) and the I_r/Q_r components are extracted (DEMOD block in Figure 55 above). The return signal also sees the down conversion and I/Q demodulation. The two signals are then correlated for range Doppler processing.

For long noise sequences, Axelsson proposes modifying the velocity/range processing into two separate steps. First step is forming N range cells with integration time shorter than the Doppler shifts of the received signals. Then, the second step is repeating this processing for M time steps. From this, a signal vector for each range cell that varies the time phase by the Doppler shift is produced. Each signal vector then goes through an FFT giving the range/Doppler matrix as the output, as shown in Figure 55 above. This FFT is where the speed is gained in the processing computations.

3. Receive Signal Correlation Using Binary and Low-bit ADC

Although the benefit of real-time processing may be realized, naturally, there is a cost. The binary or low-bit analog-to-digital converter (ADC) has limitations manifested in degraded sidelobe suppression. Therefore to mitigate this phenomenon, Axelsson in [3] adds random noise into the down-conversion process. By introducing additional noise before or after the down-conversion, there is no effect on the correlation function, as follows. Nominally, the average peak-to-sidelobe ratio (PSR) is:

$$PSR = \frac{S^2}{\sigma_S^2} = N \tag{27}$$

where S is the correlation sum of the received and transmitted signals, σ_s is the variance of this sum, and N is the time-bandwidth product ($N = 2 * B * T$) defined by the number of independent noise samples during measurement (T). As another illustration, the high-resolution ADC has the following PSR:

$$PSR = \frac{N\sigma_x^4}{\left[N\sigma_x^4 + N\sigma_x^2\sigma_z^2 \right]} = \frac{N}{\left(1 - SNR^{-1}\right)} \tag{28}$$

where x is the signal sequence of independent random numbers (noise) with zero mean and variance. As an example with N =10^4 and SNR= –10 dB, the PSR is 30 dB. For the case of the *binary and low-bit* ADC, the effect of adding noise back into processing before the ADC, produces the PSR as:

$$PSR = N\left(\frac{2}{\pi}\right)^2 \arcsin^2\left[\left\{\frac{SNR}{(1+SNR)}\right\}^{\frac{1}{2}}\right] \tag{29}$$

where N is the time-bandwidth product ($N = 2 * B * T$) defined by the number of independent noise samples during measurement (T).

With a large SNR, the binary ADC approaches the performance of the high-resolution ADC. With a small SNR, the PSR approaches $N * \left(\frac{2}{\pi}\right)^2 * SNR$, which gives an improvement factor of 4 dB. Therefore, an inexpensive, low-bit ADC overcomes the limitation of low sidelobe suppression. However, the question arises about where to add the noise. Axelsson suggests adding noise to both reference and receive channels is not necessary. Through the equations in [3], adding noise to the reference side has little effect due to the averaging that takes place in the correlation. Therefore, Axelsson's model efficiently adds noise only to the receive channel for ADC processing.

In conclusion, the addition of small levels of noise (–10 dB) before the ADC in the receive channel reduces sidelobes and improves performance. Fortunately, these levels of noise are easy to find on the electronic battlefield, thus may be used as an asset rather than "noise."

B. CONTRIBUTIONS OF OTHERS

This section is a brief survey of other RNR generation and/or correlation techniques found in the open literature. Many other researchers and their work are described; including the mathematics involved with signal processing and LPI signals.

1. Logistic-Map Based Binary Phase Code

Mr. Xin Wu and the staff of the Radar Laboratory of the Nanyang Technological University in Singapore have devised a way of using binary phase coding for radar pulse compression [21]. Using the pulse compression approach to LPI radar, the researchers found the performance of their Logistic-Map based Binary Phase Code (LMBPC) generation is similar to that of the random binary codes used in RSR. However, the generation is much simpler and not limited by the length of the code. Mr. Wu proposes a binary phase code with a low peak side lobe without tradeoffs to Doppler tolerance. To generate this technique, the logistics map follows the equation below and is sensitive to initial conditions, thereby allowing for an almost infinite number of LMBPC waveforms. This is much simpler, faster, and reproducible over the creation using Bernoulli trials.

$$x_{n+1} = f\left(x_n\right) = r x_n \left(1 - x_n\right) \tag{30}$$

where $r \in [0,4]$ and $x_n \in [0,1]$. The variable r is the bifurcation (dividing by two) parameter. In trials, the logistics map exhibits chaotic behavior between 0 and 1, when r=4.

In exploring the periodic ambiguity function, the researchers suggest the response of the matched filter to the Doppler shifted return, sheds light onto the performance of the radar. Their response resembles the ideal thumbtack, indicating the accuracy of the ability to measure the range and velocity of the target. For reference, the LMBPC periodic ambiguity function follows:

$$\mathrm{X}\left(t_x, f_d\right) = \int_{-\infty}^{\infty} u(t) u^*\left(t + T_x\right) \exp\left(j 2\pi f_d t\right) dt \tag{31}$$

where $u(t)$ is the envelope of the LMBPC waveform, u^* is the complex conjugate, T_x is the time delay, and f_d is the Doppler frequency.

For further separation between detection range and Doppler tolerance, the team proposed replacing the single matched filter in traditional pulse compression with a bank of shorter matched filters. Thus by increasing the number of parallel correlators, they saw an increase in the maximum detection range, range resolution, and maximum Doppler tolerance, respectively:

$$R_{\max} = \frac{cnBT_B}{2} \tag{32}$$

$$\Delta R = \frac{cT_B}{2} \tag{33}$$

$$f_{d\max} = \frac{1}{2BT_B} \tag{34}$$

where c is the speed of light, n is the number of pulses, B is the total length of the correlators, and T_B is the bit duration of the pulse. For example, modifying a few parameters makes way for strong performance characteristics accordingly:

If:	Performance results in:
T_B is 0.05 µsec	ΔR = 7.5m
B is 256	$f_{d\max}$ = 39062.5 Hz
$R_{\max}$ is 30 km	n becomes 16

Table 7. LMBPC Pulse Compression Improvement Factors.

Although, this approach is beneficial, it still relies on expensive hardware, often a limiting factor for many organizations.

2. Random Phase Code for Pulse Compression

Ralf Stephan and Heinrich Loele and the staff of the Radio Frequency and Microwave Technology Institute at the Technical University of Ilmenau, Germany were working on an analog version of RNR for medical applications [2]. They were focusing on a variable delay line to achieve a suitable bandwidth. They needed a variable delay to change the range bins and could not quite get what they were looking for in the hardware used. Most of the effort was in hardware and some components were modeled in Simulink [22].

C. OTHER NARAYANAN CONTRIBUTIONS

Professor Narayanan has explored many variations of RNR with various individuals over the years. In the research for this thesis, these exploratory steps became fundamental to the research and growth of understanding this new noise radar technology. The information is presented here for background on the field.

1. Random Pulse Modulation

Working with Mr. Yan Zhang in [5], Dr. Ram Narayanan considered the RNR receiver as an estimator of the correlation function. From this statistical point of reference, they explain the mean squared error (MSE) and show how a fielded system should arrive at the lowest variance of range resolution in the shortest time. To overcome the extensive processing time and signal smoothing requirements, they propose architecture with the monopulse RNR and find it to behave as traditional monopulse radar to give decent angle tracking capability. The focus here will propose using the interferometer and RNR monopulse as receiver architecture for real-time angle estimation.

As an estimator of correlation, the notional receiver is depicted in Figure 56 below, with key design elements. First, the bandpass filter selects the frequency range of interest and boosts the signal-to-noise ratio (SNR). Second, the low pass filter (LPF) further reduces the mixed receive/transmit signal and the digital signal processor (DSP) averages the result to extract a “smoothed” resultant signal.

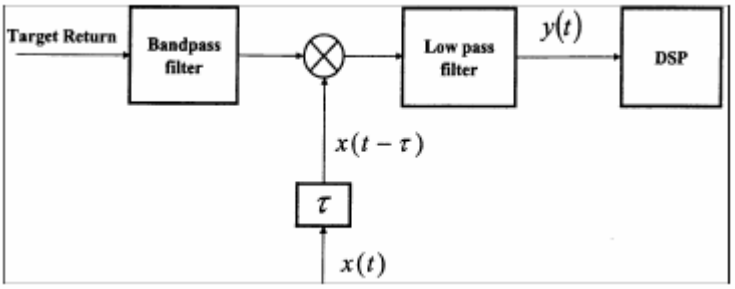

Figure 56. Block Diagram – RNR Monopulse Correlation Receiver [From 5].

Two of the major design considerations were the integration time and the LPF bandwidth. With an increase in observation time, an increase in velocity resolution and a reduction in sidelobes of the correlation between the transmitted and received signals are also observed. For example, an observation time of 50 μsec results in an elongated periodic ambiguity function of the dc components, while an observation time of 50 msec results in a clean spike in the periodic ambiguity function [5]. The LPF extracts the dc component from the correlation output and must maintain a short rise time to allow for quick estimates from a fast moving target:

$$t_{rise} \propto \frac{1}{\omega_{pass}} \tag{35}$$

where ω_{pass} is the LPF cutoff frequency. For the advantage of quick rise time, a design cost of additional frequency components at the output must be budgeted.

2. Random Noise Monopulse Radar

Again working with Mr. Yan Zhang in [5], Dr. Ram Narayanan considered the random noise monopulse radar as an alternative. Figure 57 below illustrates the overall layout of this design concept. Each of the two receive channels correlates the sum and difference channels with a delayed transmitted signal replica. Then the dc components are extracted before calculating the complex correlation between the sum and difference channels overall.

With the assumptions the target speed is much smaller than the speed of light and the separation distance between the two receive horn antennas is very small compared with the target range. This equation mirrors that of the output of standard single frequency monopulse radar. Illustrating the alternative design concept, Figure 57 below highlights the effort on the sum and difference channels:

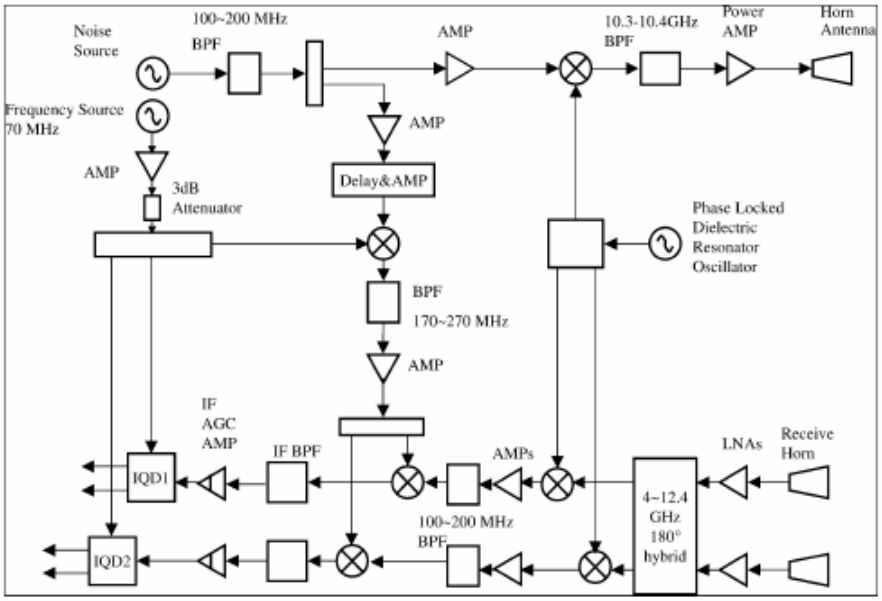

Figure 57. Block Diagram – Monopulse RNR [From 5].

After running several simulations, Narayanan and Zhang found this Monopulse RNR to perform similarly to the traditional monopulse radar. Their emphasis for design considerations is on integration time, LPF bandwidth, and signal propagation in receivers.

3. Advantages of the Variable Delay Line

Working with Mr. Muhammad Dawood in [15], Dr. Ram Narayanan generated RNR, constant PSD, and average power output of 0 dBm (1 mW) in the 1-2 GHz range. The variable delay line work is different from the standard RNR model through the addition of a variable delay line just before the Upconverter mixer running to the receive signal mixer. The major advantage of this model is to improve coherence between a target among interference and the receiver. Theoretical statistics on clutter performance were verified through experimentation and found in [14].

THIS PAGE INTENTIONALLY LEFT BLANK

APPENDIX B – DETAILS OF THE FDA TOOL

A. PARAMETER SELECTION

Filtering the signal in this thesis was accomplished with use of the Filter Design and Analysis (FDA) tool as part of the Signal Processing toolbox in MATLAB. Filtering applications take place in all models. Initially, the RNR and RSR designs call for bandlimiting the reference source during the echo correlation in the transmitting receiver. In this thesis, bandlimiting the noise was accomplished by passing the white Gaussian noise through filters created in the FDA tool. The 100 MHz filter band passed the signal from 300-400 MHz, while the 300 MHz filter bandpassed the signal from 200-500 MHz. To minimize the maximum ripple in the pass bands, the Equiripple type of a finite-duration impulse response (FIR) filter was chosen. This FIR was chosen as an effort to consider practical applications at every design option. Experiments with the Butterworth type of infinite-duration impulse response (IIR) filter showed dispersed results in the time-frequency processing, and thus dismissed. To illustrate this description, an example of the FDA tool is shown in Figure 58 below:

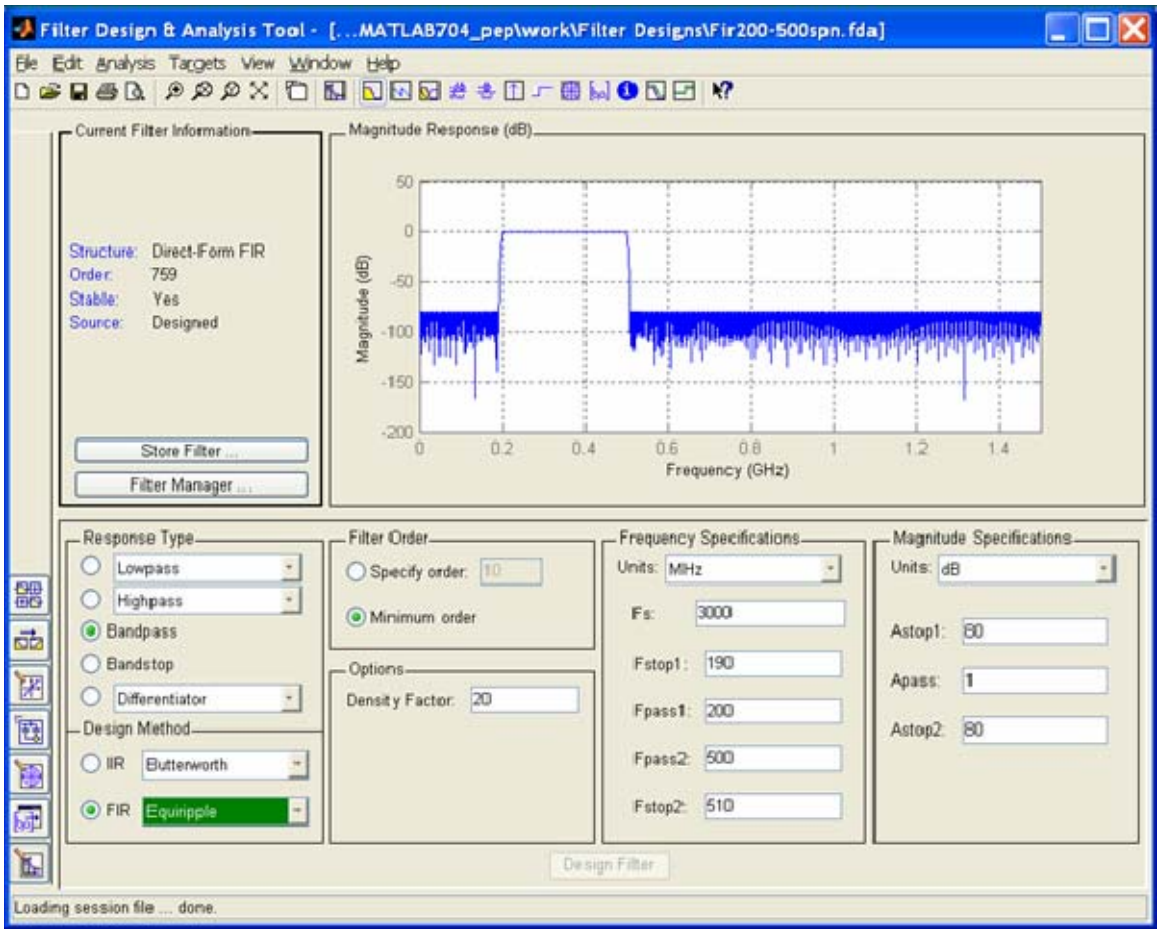

Figure 58. FDA Tool GUI.

Upon opening the FDA tool, specifying the filter began with the Response Type options, which the designer can intuitively select. The bandpass, lowpass, and highpass filters used in this thesis followed the naming convention: local-*pass type-frequency*. Each filter requirement was mentioned in the respective section. Back on the FDA tool, the Design Method section provides further specification, depending on the application. The Equiripple filter was chosen to minimize ringing in all filter designs. The Filter Order was minimized to approach realistic conditions. Selecting the Frequency Specifications was intuitive with sharper stop bands increasing the filter order, as preferred. The Magnitude Specifications were chosen to be –80 dB in the stop bands to focus on the cutoff values. Realistic values for hardware may be selected here depending on the

fiscal budget for the applied design. After specifications were made, the Design Filter button on the bottom of the GUI was selected to display the magnitude response and produce the filter order.

B. OUTPUT UTILIZATION

The designer is not finished here. To convert the filter coefficients into a usable format, the designer must use the Export feature under the File menu. Several options to saving location become available, but the ".mat" file option was chosen for files to be located in the respective directory. The name for the coefficients was chosen in this thesis as, "nps." Ending the effort was naming convention for the file, which used the pass type and the frequency described above.

Using the FDA tool saved large amounts of time, increased confidence in accuracy, and was highly intuitive. As a desirable feature of heterodyne correlation, the return signal should be at the intermediate frequency (IF). Ideally, the Doppler return will show in a few Hz around the IF (usually +/- 50 Hz for a slower aircraft target). So, narrow band filters with sharp cutoffs are needed to pass only the desired information (5-10 MHz around IF). Also, sharp cutoffs are preferred to reduce extraneous noise from getting into the detector and degrading the SNR. In Narayanan's original work [4] to suppress the high-frequency IF harmonics produced from the I/Q Detector, lowpass filters are designed for 200 MHz. A key point to note is the I/Q detector generates the in-phase and quadrature lowpass equivalent frequencies of the original bandpass signal; and both the I and Q signals are lowpass signals at the Doppler frequency [4]. One point on Doppler, the capability is not produced in this model, but may be an easy addition for future work. For this modeling, the received signal is simulated.

THIS PAGE INTENTIONALLY LEFT BLANK

LIST OF REFERENCES

[1] Guosui, L., Hong, G., and Weimin, S., “Development of random signal radars,” *IEEE Transactions on Aerospace and Electronic Systems*, Vol. 35, No. 3, pp. 770-777, July 1999.

[2] Stephan, R. & Loele, H., “Theoretical and Practical Characterization of a Broadband Random Noise Radar”.

[3] Axelsson, Sune R.J., “Noise Radar for Range/Doppler Processing and Digital Beamforming using Low-bit ADC,“ *IEEE Transactions on Geoscience and Remote Sensing*, Vol. 41, No. 12, pp 2703-2720, December 2003.

[4] Interview between R. Narayanan, Professor of Electrical Engineering, The Pennsylvania State University, University Park, Pennsylvania, and the author, 17 March 2006.

[5] Zhang, Y., and Narayanan, R. M., “Design Considerations for a Real-Time Random-Noise Tracking Radar,” *IEEE Transactions on Aerospace and Electronic Systems*, Vol. 40, No. 2, pp. 434-445, April 2004.

[6] Dawood, M., and Narayanan, R. M., “Receiver Operating Characteristics for the Coherent UWB Random Noise Radar,” *IEEE Transactions on Aerospace and Electronic Systems*, Vol. 37, No. 2, pp. 586-594, April 2001.

[7] Guosui, L., Hong, G., and Weimin, S., Hongbo, S., Jianhui, Z., “Random Signal Radar – A Winner in Both the Military and Civilian Operating Environments,” *IEEE Transactions on Aerospace and Electronic Systems*, Vol. 39, No. 2, pp. 489-498, April 2003.

[8] Pace, P. E., *Detecting and Classifying Low Probability of Intercept Radar*, p. 183, 214-216, Artech House, Boston, 2004.

[9] Dawood, M., and Narayanan, R. M., “Generalised wideband ambiguity function of a coherent Ultrawideband random noise radar,” *IEE Proceedings – Radar Sonar Navigation*, Vol. 150, No. 5, pp. 379-386, October 2003.

[10] Narayanan, R. M., and Dawood, M., “Doppler Estimation Using a Coherent Ultrawide-Band Random Noise Radar,” *IEE Proceedings-Radar, Sonar, and Navigation*, Vol. 151, No. 3, pp. 143-148, June 2004.

[11] Pace, P. E., *Advanced Techniques for Digital Receivers*, p. 254, Artech House, Boston, 2000.

[12] Hongbo, S., Yilong, L., and Guosui, L., "Ultra-Wideband Technology and Random Signal Radar: An Ideal Combination," *IEEE AES Systems Magazine*, pp. 3-7, November 2003.

[13] D. K. Barton, C. E. Cook, P. Hamilton, *Radar Evaluation Handbook*, pp. K-2, Artech House, Norwood, MA, 1991.

[14] Axelsson, Sune R.J., "Noise Radar Using Random Phase and Frequency Modulation," *SAR Image Analysis, Modeling, and Techniques VI, Proceedings of SPIE*, Vol. 5236, pp 60-71, 2004.

[15] Dawood, M., and Narayanan, R. M., "Multipath and Ground Clutter Analysis for a UWB Noise Radar," *IEEE Transactions on Aerospace and Electronic Systems*, Vol. 38, No. 3, pp. 838-853, July 2002.

[16] Guosui, L., Xiangquan, S., Jinhui, L., Guoyu, Y., and Yaoliang, S., "Design of noise FM-CW radar and its implementation," *IEE Proceedings-F*, Vol. 138, No. 5, pp. 420-426, October 1991.

[17] Guosui, L., Hong, G. Xiaohua, Z. and Weimin, S., "The Present and Future of Random Signal Radars," *IEEE AES Systems Magazine*, pp. 35-40, October 1997.

[18] Booker, G. M., "Understanding Millimetre Wave FMCW Radars," Australian Centre for Field Robotics, University of Sydney, Sydney, Australia, gbrooker@acfr.usyd.edu.au, August 2006.

[19] Hong, G., Guosui, L., Xiaohua, Z., Weimin, S., and Xi, L., "A New Kind of Noise Radar – Random Binary Phase Coded CW Radar," *IEEE National Radar Conference, Syracuse, NY, May 1997,* pp. 202-206, 1999.

[20] Narayanan, R. M., and Dawood, M., "Radar Penetration Imaging Using Ultra-wideband Random Noise Waveforms," *IEEE Transactions on Antennas and Propagation, Vol. 48, No. 6, pp. 868-878, June 2000.*

[21] Wu, X., Liu, W., Zhao, L. and Fu, J., "Chaotic Phase Code for Radar Pulse Compression," pp. 279-283, 2001.

[22] Stephan, R., Re: RNR Generation Modeling, Available email correspondence, Technical University of Ilmenau, 23 November 2005.

[23] Garmatyuk, D. S., and Narayanan, R. M., "Ultra-Wideband Continuous-Wave Random Arc-SAR," *IEEE Transactions on Geoscience and Remote Sensing*, Vol. 40, No. 12, pp. 2543-2552, December 2002.

[24] Xu, X., and Narayanan, R. M., “FOPEN SAR Imaging Using UWB Step-Frequency and Random Noise Waveforms,” *IEEE Transactions on Aerospace and Electronic Systems*, Vol. 37, No. 4, pp. 1287-1300, October 2001.

[25] Stove, A. G., Hume, A. L., and Baker, C. J., “Low probability of intercept radar strategies,” *IEE Proceedings – Radar Sonar Navigation*, Vol. 151, No. 5, pp. 249-260, October 2004.

[26] Mills, R. F., and Prescott, G. E., “A Comparison of Various Radiometer Detection Models,” *IEEE Transactions on Aerospace and Electronic Systems*, Vol. 32, No. 1, pp. 467-473, January 1996.

[27] Maier, M. W., and Weber, C. L., “Airborne Clutter Performance of Randomized Radar Waveforms,” *IEEE Transactions on Aerospace and Electronic Systems*, Vol. 31, No. 3, pp. 951-959, July 1995.

[28] Mills, R. F., and Prescott, G. E., “A Comparison of Various Radiometer Detection Models,” *IEEE Transactions on Aerospace and Electronic Systems*, Vol. 32, No. 1, pp. 467-473, January 1996.

[29] Hogberg, S. W., and Si, J., “Decimating Pseudorandom Noise Receiver,” *IEEE Transactions on Aerospace and Electronic Systems*, Vol. 35, No. 1, pp. 338-343, January 1999.

[30] Greiner, C., Mossberg, T. W., and Iazikov, D., “Bandpass engineering of lithographically scribed channel-waveguide Bragg gratings,” *Optical Society of America, Optics Letters*, Vol. 29, No. 8, pp. 806-808, April 2004.

[31] Stewart, C. H., *Spread Spectrum Coherent Processor*, U. S. Paten 5265121, 23 November 1993.

[32] Xu, Y., and Narayanan, R. M., “Polarimetric Processing of Coherent Random Noise Radar Data for Buried Object Detection,” *IEEE Transactions on Geoscience and Remote Sensing*, Vol. 39, No. 3, pp. 467-478, March 2001.

[33] M. I. Skolnik, *Introduction to Radar Systems*, 2nd Edition, pp. 399-438, McGraw-Hill, New York, 1980.

[34] Xu, X., and Narayanan, R. M., “Rangel Sidelobe Suppression Technique for Coherent Ultra Wide-Band Random Noise Radar Imaging,” *IEEE Transactions on Antennas and Propagation*, Vol. 49, No. 12, pp. 1836-1842, December 2001.

[35] Narayanan, R. M., Zhou, W., Wagner, K. H., and Kim, S., “Acoustooptic Correlation Processing in Random Noise Radar,” *IEEE Geoscience and Remote Sensing Letters*, Vol. 1, No. 3, pp. 166-170, July 2004.

[36] Bell, D. C., and Narayanan, R. M., “Inverse synthetic aperture radar imaging using a coherent Ultrawideband random noise radar system,” *Optical Engineering*, Vol. 40, No. 11, pp. 2612-2623, November 2001.

[37] Staderini, R., Re: UWB Generation Modeling, Available email correspondence, Medical University of Rome, 24 November 2005.

[38] Fu, J., Re: RNR Generation Modeling, Available email correspondence, National Technical University of Nanyang, 23 November 2005.

[39] Lush, D. and Hudson, D., “Ambiguity Function Analysis of Wideband Radars,” *IEEE*, pp. 16-20, 1991.

[40] Ying, S., Weihua, S., and Guosui, L., “Ambiguity Function of Chaotic Phase Modulated Radar Signals,” *IEEE Proceedings of the ICSP, 1998,* pp. 1574-1577, 1999.

[41] Garmatyuk, D. S., and Narayanan, R. M., “ECCM Capabilities of an Ultrawideband Bandlimited Random Noise Imaging Radar,” *IEEE Transactions on Aerospace and Electronic Systems*, Vol. 38, No. 4, pp. 1243-1255, October 2002.

INITIAL DISTRIBUTION LIST

1. Defense Technical Information Center
   Ft. Belvoir, Virginia

2. Dudley Knox Library
   Naval Postgraduate School
   Monterey, California

3. Prof. Phillip E. Pace
   Department of Electrical and Computer Engineering
   Naval Postgraduate School
   Monterey, California

4. Prof. David C. Jenn
   Department of Electrical and Computer Engineering
   Naval Postgraduate School
   Monterey, California

5. Colonel Stephen D. Hargis
   MILSATCOM Systems Wing
   Space & Missile Systems Center
   El Segundo, California

6. Ms. Susan Braun
   The Charles C. Lauritsen Library
   The Aerospace Corporation
   El Segundo, California

7. Commander
   Unmanned Aerial Vehicle Battlelab
   Air Combat Command
   Creech Air Force Base, Nevada

8. Mr. Alfred DiMatessa
   U.S. Naval Research Laboratory
   Code 5700
   Washington, D.C.

9. Dr. Frank Klemm
   Naval Research Laboratory
   Code 5700
   Washington DC

10. Dr. Ted Roberts
U.S. Naval Research Laboratory
Code 5700
Washington, D.C.

11. Dr. Peter Craig
U. S. Office of Naval Research
Code-313
Arlington, Virginia

12. Dr. Chip Grounds
U. S. Office of Naval Research
Code-313
Arlington, Virginia

13. Dr. Ram M. Narayanan
Department of Electrical Engineering
The Pennsylvania State University
University Park, Pennsylvania

14. Dr. Ben G. Fitzpatrick
Department of Mathematics
The Loyola Marymount University
Los Angeles, California

15. Commander
National Air & Space Intelligence Center
Air Intelligence Agency
Wright-Patterson Air Force Base, Ohio